Localization in Complex networks

Ph.D. Thesis

By

Ankit Mishra

DISCIPLINE OF PHYSICS
INDIAN INSTITUTE OF TECHNOLOGY, INDORE, INDIA
July 2022

Localization in Complex networks

A THESIS

Submitted in partial fulfilment of the requirements
for the award of the degree
of

DOCTOR OF PHILOSOPHY

by

Ankit Mishra

DISCIPLINE OF PHYSICS
INDIAN INSTITUTE OF TECHNOLOGY, INDORE, INDIA

July 2022

INDIAN INSTITUTE OF TECHNOLOGY INDORE

I hereby certify that the work which is being presented in the thesis entitled "**Localization in complex networks**" in the partial fulfillment of the requirements for the award of the degree of DOCTOR OF PHILOSOPHY and submitted in the DEPARTMENT OF PHYSICS, Indian Institute of Technology Indore, is an authentic record of my own work carried out during the time period from June 2017 to July 2022 under the supervision of Dr. Sarika Jalan, Professor, IIT Indore.

The matter presented in this thesis has not been submitted by me for the award of any other degree of this or any other institute.

Ankit Mishra
15/02/2023

Signature of the student with date

(**Ankit Mishra**)

This is to certify that the above statement made by the candidate is correct to the best of my/our knowledge.

Signature of Thesis Supervisor with date

(**Prof. Sarika Jalan**)

16/02/2023

Ankit Mishra has successfully given his/her Ph.D. Oral Examination held on 15/02/2023.

Signature of Thesis Supervisor with date

(**Prof. Sarika Jalan**)

16/02/2023

Acknowledgements

Countless people supported my effort on this long journey of my Ph.D. Words cannot express my gratitude to my supervisor Prof. Sarika Jalan, for guiding and supporting me through this thesis journey at Indian Institute of Technology (IIT) Indore. I have benefited greatly from your wealth of knowledge and punctilious editing. I am extremely grateful that you took me on as a student and continued to have faith in me over the years.

My sincere regards to the PSPC committee members, Dr. Manavendra Mahto, Dr. Debasis Nayak, and Dr. Ranveer Singh for several vital suggestions and feedback during the entire journey of Ph.D. I would also like to extend my thank to the Director, IIT Indore, DPGC convener, Head (Physics), and all the faculty members and staff members of Discipline of Physics, IIT Indore for their timely help and support throughout. I also like to thank my collaborator Jayendra N. Bandyopadhyay with whom my first paper got published. I humbly acknowledge the sincere efforts of all the staff members of the Academic Office, Accounts Section, R&D Section, IT Section, and Central Library, Medical Team, Hostel Team, IIT Indore whose constant support ascertained the smooth functioning of my research work.

I am feeling very much blessed and from the bottom of my heart, I would like to say thanks to all my present and past research scholars at Complex Systems Lab, Dr. Aradhana Singh, Dr. Sanjiv K. Diwedi, Dr. Camellia Sarkar, Dr. Aparna Rai, Dr. Ajaydeep, Dr. Alok, Dr. Pramod, Dr. Saptarshi, Dr. Priodyuti, Dr. Anil, Rahul, Vasundhara, Tanu, Sanket, Jerry and Ayushi for their love, care, support, and guidance.

Words fall short for expressing my gratitude towards the most important people of my life, my family! My loving mother, my caring father, my elder sister, and my brother-in-law. Without them, I would not have been able to embark on this journey. Finally, I thank Almighty God for sending all these wonderful people to my life. Thank you!!

Ankit Mishra

Dedicated

to

My Family

Synopsis

Introduction

Since the pioneering work of Anderson on localization of electronic wave function in disordered media, eigenvector localization has become a fascinating and active area of research [1]. In his original paper, Anderson argued that disorder introduced in the diagonal elements of a Hamiltonian matrix will lead to localization of the electronic wave function. Later this theory successfully explained the phenomenon of metal-insulator transition. Then after, the phenomenon of localization has been studied in various systems such as random regular graph (RRG) [8], Cayley tree [9], and random networks [10] [11] and it still remains an active field of research. Moreover, there exist systems with many interacting units that behave very unusually, and it becomes difficult to control or predict the system, such as the human brain and the world economy. These systems can be better understood in the framework of networks. A network consists of *nodes* and *links*. The *nodes* correspond to the elements of a system and links represent the interactions between these elements. Eigenvector localization serves well in understanding and getting insight into various structural and dynamical properties of networks. For instance, it was found that if the eigenvector corresponding to the largest eigenvalue is localized and the infection rate is slightly higher than the threshold, then the disease will be localized on only a finite set of vertices [19]. In [20], it was shown that perturbation propagation in ecological networks weakened due to the localization behavior of principal eigenvectors. Further, [21] it was postulated that the stability of the system from the external shock would depend upon the localization behavior of the eigenvector corresponding to the lowest eigenvalue of the connectivity matrix.

Though most of the work on localization in networks focuses on the localization properties of the principal eigenvector. However, sporadic investigations indicate that non-principal eigenvalues and associated eigenvectors of the adjacency matrices of networks contribute to the transient dynamics [24, 25]. Moreover, localization properties of non-principal eigenvectors have also found its application in characterizing or identifying community [26, 27]. Thus, it is equally important to know about the localization properties of non-principal eigenvectors. In fact, few attempts have already been made to study the localization properties of non-principal eigenvectors. Quantum diffusion of a particle localized at an initial site on small-world networks was demonstrated to have its diffusion time being associated with the participation ratio and it is higher for the case of regular networks than that of the networks with the shorter path length [15]. In [28], it was shown that Anderson-like transition could be obtained in complex networks without a diagonal disorder and one just has to tune the clustering coefficient. Also, using spectral statistics, localization transition was studied for ER random network, Cayley tree, and Barabasi-Albert scale-free networks [29].

In this thesis, we explored the localization properties of the eigenvectors of small-world networks constructed using the Watts and Strogatz algorithm [35] as follows. Starting from a regular network where each node is connected with its k nearest neighbors, the connections are rewired randomly with a probability p_r. For the intermediate rewiring probability, the network undergoes the small-world transition characterized by high clustering and low path-length. We select the small-world model networks as the rewiring parameter quantifying randomness allows us to investigate localization arising due to increasing disorder in topology. By disorder in topology, we mean heterogeneity in the connections among nodes. Further, this setup also allows us to investigate the effect of the interplay of diagonal disorder and randomness quantified by p_r on localization. In the last part of the thesis, we study the origin of localization in hypergraphs. The motivation to include the hypergraph in the study is due to the fact that networks are restricted to pair-wise interactions but many real-world systems entail simultaneous interactions between more than two nodes popularly known as higher-order interactions [112]. These systems can be better understood in the framework of hypergraphs which consists of hyperedges accounting for the multi-body interactions.

Objectives

- To understand localization induced due to topological disorder.
- To study the interplay of diagonal disorder and randomness on localization.
- To find out the origin of localization in hypergraph.

Theoretical Framework

A network denoted by $G = \{\mathrm{V}, \mathrm{E}\}$ consists of set of *nodes* and interaction *links*. The set of *nodes* are represented by $\mathrm{V} = \{v_1, v_2, v_3, \ldots, v_N\}$ and *links* by $\mathrm{E} = \{e_1, e_2, e_3, \ldots, e_M\}$ where N and M are size of V and E respectively. Mathematically, a network can be represented by its adjacency matrix A whose elements are defined as $A_{ij} = 1$ if node i and j are connected and 0 otherwise. The eigenvalues of the adjacency matrix A are denoted by $\{\lambda_1, \lambda_2, \lambda_3, \ldots, \lambda_N\}$ where $\lambda_1 \geq \lambda_2 \geq \ldots \geq \lambda_N$ and the corresponding orthonormal eigenvectors as $\{\boldsymbol{x}_1, \boldsymbol{x}_2, \boldsymbol{x}_3, \ldots, \boldsymbol{x}_N\}$. Localization of an eigenvector means that a few entries of the eigenvector have much higher values compared to the others. We quantify localization of the $\boldsymbol{x}_j$ eigenvectors by measuring the inverse participation ratio (IPR) denoted as $Y_{\boldsymbol{x}_j}$. The IPR of an eigenvector $\boldsymbol{x}_j$ is defined as [19]

$$Y_{\boldsymbol{x}_j} = \sum_{i=1}^{N} (x_i)_j^4, \tag{1}$$

where $(x_i)_j$ is the i^{th} component of the normalized eigenvectors $\boldsymbol{x}_j$ with $j \in \{1, 2, 3 \ldots, N\}$. The most delocalized eigenvector $\boldsymbol{x}_j$ will have all its components equal, i.e., $(x_i)_j = \frac{1}{\sqrt{N}}$, with IPR value being $1/N$. Whereas, for the most localized eigenvector, only one component of the eigenvector will be non-zero, and the normalization condition of the eigenvectors ensures that the non-zero component should be equal to unity. Thus the value of IPR for the most localized eigenvector is equal to 1. It is also worth noting that there may exist fluctuations in the IPR values for a given state $\boldsymbol{x}_j$ for different realizations of the network for a given rewiring probability. However, it is not possible that λ_j remain the same for all the random realizations of network,

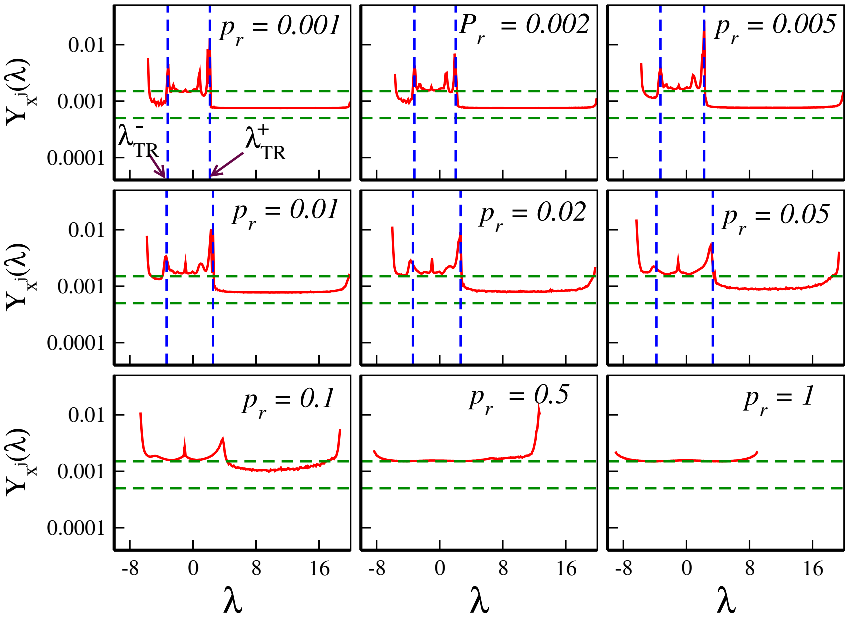

Figure 1: IPR of the eigenvectors plotted as a function of the corresponding eigenvalues for various values of the rewiring probability. The dashed green lines plotted at 0.0005 and 0.0015 correspond to the minimum possible value of the IPR $(1/N)$ and the random matrix predicted value for the maximum delocalized state $(3/N)$. Here, $N = 2000$ and $\langle k \rangle = 20$ are kept fixed for all the networks.

as in that case we would have simply added all the IPR's for λ_j for the different realizations and divided it by the number of realizations which would have been an ideal case. However, in absence of that, for the robustness of the results, we consider a small width $d\lambda$ around λ and average all the IPR values corresponding to those λ values which fall inside this small width denoted by $(Y_{\boldsymbol{x}_j}(\lambda))$.

Further, we hire the distribution of ratio of consecutive eigenvalue spacing (eigenvalue ratio statistics) from Random matrix theory (RMT) to study localization properties of eigenvectors. Following Ref. [44], the ratio of consecutive eigenvalue spacing is defined here as

$$r_i = \frac{min(s_{i+1}, s_i)}{max(s_{i+1}, s_i)} \tag{2}$$

where $s_i = \lambda_{i+1} - \lambda_i$ is the spacing between eigenvalues λ_{i+1} and λ_i with $i \in (1, 2, 3 \ldots N - 1)$. Also, one can verify that $0 < r_i < 1$. The distribution func-

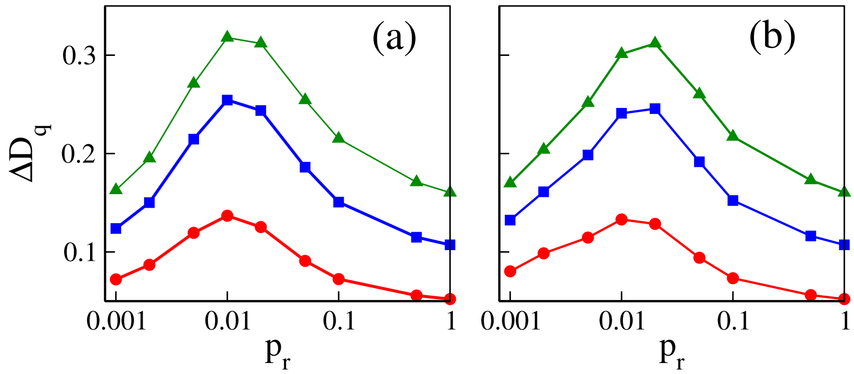

Figure 2: Plot of ΔD_q as a function of rewiring probability p_r for q = 2 (●) , 5 (■) and 10 (▲) respectively. (a) $\lambda \approx 1.271$ (b) $\lambda \approx 1.371$. These are the eigenvalues from the central regime.

tion ($P(r)$) approximating GOE statistics is given as

$$P(r) \sim \frac{54/8 \times (r + r^2)}{(1 + r + r^2)^{5/2}} \tag{3}$$

and the theoretical average value of r for GOE and Poisson statistics has been estimated to be equal to 0.53 and 0.38, respectively, with the distribution function for Poisson statistics is given by

$$P(r) \sim \frac{2}{(1 + r)^2} \tag{4}$$

Summary of work done

Localization induced due to topological disorder

This chapter explores the localization properties of eigenvectors induced due to topological disorder. First, we characterize the eigenvalue spectrum into different regimes as shown in Fig. 1. he central part ($\lambda_{TR}^{-} \leq \lambda \leq \lambda_{TR}^{+}$) of the spectrum consists of critical eigenvectors having IPR of the order of 10^{-3}. This is the most localized part of the eigenvalue spectrum. Further, $Y_{x_j}(\lambda)$ has U-shape for the smaller eigenvalues ($\lambda < \lambda_{TR}^{-}$) while it remains almost constant for the higher

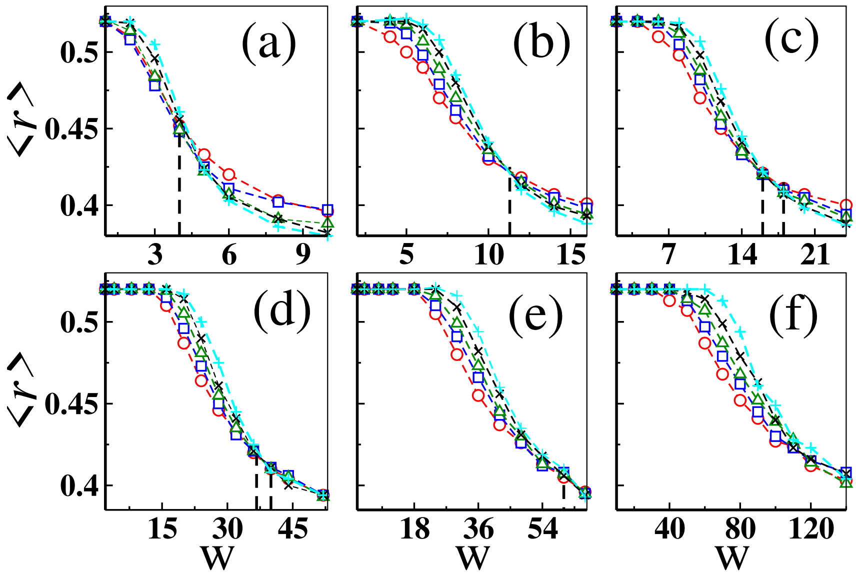

Figure 3: Plot of $\langle r \rangle$ as a function of diagonal disorder (w) for various rewiring probabilities. $\circ$, $\square$, $\triangle$, $*$ and $+$ symbols are used for $N = 2000, 4000, 8000, 16000$ and 32000 respectively with $\langle k \rangle = 20$. (a) $p_r = 0.001$ (b) $p_r = 0.005$ (c) $p_r = 0.01$ (d) $p_r = 0.05$ (e) $p_r = 0.1$ (f) $p_r = 1$. Vertical lines represent the crossing point of $\langle r \rangle$ for different N.

eigenvalues($\lambda > \lambda_{TR}^{+}$) forming the tail part of the spectra. Using the multifractal analysis, we find that there exists no significant change in the eigenvalue (λ_{TR}^{+}) separating the central regime and the mixed regime. Additionally, we notice no significant change in λ_{TR}^{+} with an increase in N, i.e. for $N \to \infty$, $\lambda_{TR}^{+}(N) \sim \mathcal{O}(1)$. Further, we demonstrated that the rewiring procedure can be divided into two domains. For small rewiring, $p_r \leq 0.01$, with an increase in the random connections, there exists a continuous enhancement in the localization of the eigenvectors corresponding to the central regime, while for the higher rewiring probability $p_r \geq 0.01$, eigenvectors gradually lose their degree of localization (Fig. 2). Interestingly, this change in the behavior of the eigenvectors takes place at the onset of the small-world transition possibly arising due to the fact that for $p_r \leq 0.01$, there exists a decrease in the characteristics path length (r) co-existing with a high clustering coefficient (CC = 3/4). It is well known that a higher clustering drives localization of the eigenvectors. On the other hand, for $p_r \geq 0.01$, there exists a significant decrease in CC with r being small, eigenvectors undergo a continuous decrease in the degree

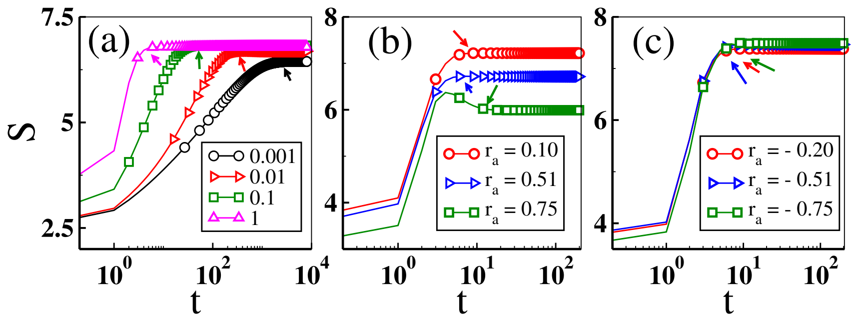

Figure 4: (Color online) S as a function of t for various model networks when random walker starts from a randomly chosen node with probability 1; (a) small-world networks, (b) assortative ER networks, and (c) disassortative ER networks. Here, (a) $N = 1000$ and $\langle k \rangle = 10$ and (b)-(c) $N = 2000$ and $\langle k \rangle = 8$. Arrow indicate position where S hits the steady state.

of localization with an increase in randomness in connections.

Interplay of diagonal disorder and randomness on localization

In this chapter, we introduce diagonal disorder in the adjacency matrix of the small-world networks. Thus, we study the effect of interplay of diagonal disorder and randomness on localization. Diagonal disorders in complex networks, i.e self-loops in the graph representation, may represent various intrinsic properties of the nodes, and depending upon the system under consideration, they may carry different physical meanings. In this part of the thesis, we adopt Random matrix theory (RMT), first originated in nuclear physics and later found its application in different areas of Physics. We found that upon increasing diagonal disorder, eigenvectors go from the delocalized to a localized state captured by the gradual transition of eigenvalue ratio statistics from GOE to Poisson statistics (Fig. 3). Moreover, the more random a network is, the more resilient it is to diagonal disorder on inducing localization. Further, we relate the localization transition to the transient dynamics of the maximal entropy random walker. The lower the w_c (for fixed N and $\langle k \rangle$), the higher time is taken by the walker to reach the steady-state (Fig. 4). We argued that when the walker has reached the steady-state, the probability of finding it on all the nodes becomes finite. For small τ, the walker would be able to access all the nodes in a

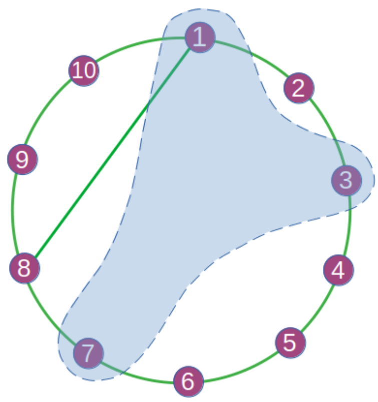

Figure 5: (Color online) Schematic diagram of hypergraph model used in the paper. One pair-wise link, $E^p = \{1, 8\}$ and One hyperedge, $E^h = \{1, 3, 7\}$ are added into the ring lattice with size $N = 10$. The pair-wise links are colored in green and hyperedge with sky-blue enclosing the involved nodes.

sufficiently shorter time, and thus it requires a high value of the diagonal disorder strength to make the network localized. On the other hand, for sufficiently longer τ, probability of finding the walker remains finite on a few nodes, and consequently, a low w_c would be enough to make it localized.

Origin of localization in hypergraph

A hypergraph is a generalization of a network which is capable of capturing higher-order interactions. It consists of nodes and hyperedges; a hyperedge connects d nodes at a time where $d \geq 2$. We generate the hypergraph in this work as follows. First, a ring lattice is constructed in which each node is connected to its nearest neighbors on both sides. We then randomly choose d nodes uniformly from all the existing nodes. If already there is no hyperedge comprising of the chosen d nodes, we add a hyperedge consisting of these d nodes. For simplicity we restrict for $d = 3$, for each iteration. Next, we add pair-wise links by choosing $d = 2$ nodes uniformly and randomly from the existing nodes as illustrated in Fig. 5 for ten nodes. A

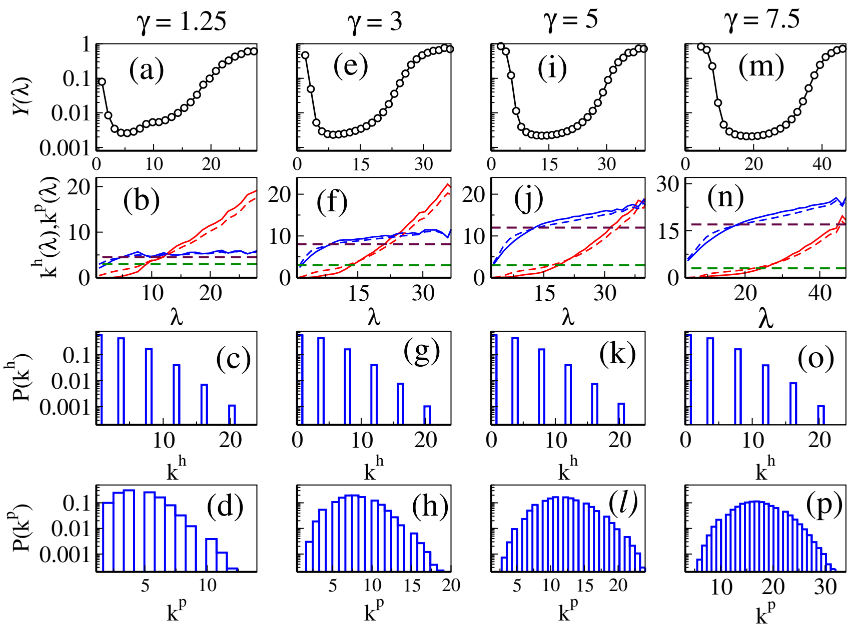

Figure 6: (Color online) Average IPR ($Y_{\boldsymbol{x}_j}(\lambda)$) (black), $k^h(\lambda)$ (red), $k^p(\lambda)$ (blue), $\hat{k}^h(\lambda)$(red-dashed), $\hat{k}^p(\lambda)$ (blue-dashed) against λ for various $\gamma > 1$. The corresponding higher-order degree distribution and pair-wise degree distribution are also plotted in last two rows. The green-dashed and brown-dashed lines are at $\langle k^h \rangle$ and $\langle k^p \rangle$ on y axis. The size of the hypergraph, $N = 2000$ and $M^h = 500$ remain fixed for all γ values with 40 random realizations.

hypergraph can be represented by its Laplacian matrix L^H. The generalized degree of a node i in the hypergraph is given by k_i^H which can be further decomposed into $k_i^H = k_i^h + k_i^p$ where k_i^h and k_i^p are the contributions from the higher-order and the pair-wise links, respectively. Similarly, the average degree, $\langle k \rangle = \frac{\sum_i k_i^H}{N}$, can be decomposed as $\langle k \rangle = \langle k \rangle^h + \langle k \rangle^p$ where $\langle k \rangle^h = \frac{\sum_i k_i^h}{N}$ and $\langle k \rangle^p = \frac{\sum_i k_i^p}{N}$. Also, it is important to note that if a node, say i, gets 1 additional pair-wise links and 1 higher-order links, its degree will be increased by 1 and 4 from the pair-wise and higher-order links, respectively. To provide an equal opportunity to the pair-wise and higher-order links for steering localization on a given node, we introduce the total number of pair-wise links 4 times greater than the higher-order links, i.e., $M^p = 4 \times M^h$ for $k_i^h = k_i^p$. Next, we define a parameter $\gamma = \frac{M^p}{4 \times M^h}$ to measure relative contribution for both the types of the links. Thus, if $\gamma > 1$ then $k_i^p < k_i^h$; if $\gamma < 1$ then $k_i^p > k_i^h$ holds.

We define following physical quantities, $k^h(\lambda)$, $k^p(\lambda)$, $\hat{k}^h(\lambda)$, $\hat{k}^p(\lambda)$. For any eigenvector $\boldsymbol{x}_j$, these quantities can be calculated as the following.

$k^h_{\boldsymbol{x}_j}$: higher-order degree of the node i_o with the maximum component in $|(x_i)_j|$, i.e., $(x_{io})_j = \max\{|(x_1)_j|, |(x_2)_j|, \ldots |(x_N)_j|\}$

$k^p_{\boldsymbol{x}_j}$: pair-wise degree of the node i_o with the maximum component in $|(x_i)_j|$ i.e. $(x_{io})_j = \max\{|(x_1)_j|, |(x_2)_j|, \ldots |(x_N)_j|\}$

$\hat{k}^h_{\boldsymbol{x}_j}$: higher-order degree expectation value of eigenvector, defined as $\sum_{i=1}^{N}(x_i)^2_j k^h_i$.

$\hat{k}^p_{\boldsymbol{x}_j}$: pair-wise degree expectation value of eigenvector, defined as $\sum_{i=1}^{N}(x_i)^2_j k^p_i$.

All these physical quantities are averaged over λ and $\lambda + d\lambda$ and we obtain $k^h(\lambda)$, $k^p(\lambda)$, $\hat{k}^h(\lambda)$ $\hat{k}^p(\lambda)$.

We have investigated the interplay of higher-order and pair-wise links in instigating the localization of the eigenvectors of the hypergraphs. We find that for $\gamma \leq 1$, there is no impact of pair-wise links on eigenvector localization. For $\gamma > 1$, we find that with increasing γ, the degree of the localization of the eigenvectors corresponding to the smaller eigenvalues increases. Also, the role of higher-order links is not significant as compared to the pair-wise links in inducing localization for smaller eigenvalues. Whereas, for larger eigenvalues, the higher-order links play a crucial role in instigating localization despite the fact that the number of nodes with high higher-order degree (k^h) remains very small for all the γ values (Fig. 6).

Conclusion

In this thesis, we have explored the localization properties of eigenvectors of complex networks. Specifically, we focus on the small-world networks and hypergraph. First, without introducing the diagonal disorder, we investigated localization arising due to disorder in topology. we argued that distorting the initial regular network topology by rewiring a few connections does not lead to localization of the eigenvectors. Instead, it drives them toward the critical states with $0.4 < D_2 < 0.90$. Further, we find that before the onset of the small-world transition, increasing the topological disorder leads to an enhancement in the eigenvectors localization, whereas just after the onset, the eigenvectors show a gradual decrease in the localization. We then introduce diagonal disorder in the adjacency matrix and found that there exists a gradual transition from delocalized to localized states captured by the eigenvalue ratio statistics. The critical disorder (w_c) required to procure the Poisson statistics increases with the randomness in the network architecture. We then relate critical disorder with the time taken by the maximum entropy random walker to reach the steady-state. Finally, we discuss the origin of localization in hypergraph.

Keywords : Network Science, complex networks, eigenvector localization.

LIST OF PUBLICATIONS

Publications from thesis

1. **Ankit Mishra**, J.N Bandyopadhyay and Sarika Jalan (2021), *Multi-fractal analyses of eigenvectors of small-world networks*, Chaos, Solitons and Fractals **144**, 110745 (DOI: 10.1016/j.chaos.2021.110745). [IF – 5.94]

2. **Ankit Mishra**, Tanu Raghav and Sarika Jalan (2022), *Eigenvalue ratio statistics of complex networks: Disorder versus randomness*, Phys. Rev. E **105**, 064307 (DOI: 10.1103/PhysRevE.105.064307). [IF – 2.53]

3. **Ankit Mishra**, Ranveer Singh and Sarika Jalan (2022), *On the second largest eigenvalue of networks*, Applied network science **7**, 47 (DOI: 10.1007/s41109-022-00484-w)

4. **Ankit Mishra** and Sarika Jalan (2022), *Eigenvector localization in hypergraphs: pair-wise vs higher-order links* (arXiv: 2207.12785)

Other publications

4. Rahul K Verma, Kalyakulina Alena, **Ankit Mishra**, Mikhail Ivanchenko and Sarika Jalan (2022) *Role of mitochondrial genetic interactions in determining adaptation to high altitude in human population around the globe*, Scientific Reports **12**, 1-12 (DOI: 10.1038/s41598-022-05719-5) [IF – 4.37]

Table of Contents

List of Figures

List of Tables

Introduction

Chapter 1

Introduction

1.1 Overview and historical perspective

The phenomena of localization is still an active area of research after its discovery in the $1950s$ by Philip Anderson [1]. In his seminal paper, Anderson showed that if the diagonal disorder of the Hamiltonian matrix of the tight-binding model ($d = 3$) exceeds some threshold then it would lead to the localization of the electronic wave function. For $d \leq 2$, any finite disorder can turn all eigenvectors into localized states. Later this theory was successful in explaining the metal-insulator transition. Then, in the subsequent years, localization was explored in many systems with disorder originating not only from the diagonal elements of the underlying matrix but also from the off-diagonal terms or both [2] [3] [4]. Furthermore, localization in systems where disorder originates from randomness in their geometry is also studied in many works leading to extensive research on localization in topologically disordered systems [5] [6]. Also, in the $1990s$, Power-law banded matrix (PLBM) was introduced [7] whose matrix elements decreased in a power-law fashion. Later almost two decades, PLBM was studied rigorously in terms of localization-delocalization transition. In the latest development, there has been a keen interest among the researcher to investigate localization transition in systems having $d \to \infty$ such as random regular graph (RRG) [8], Cayley tree [9] and random networks [10] [11].

Moreover, there exist systems with many interacting units that behave very unusually, and it becomes difficult to control or predict the system, such as the human brain and the world economy. There have been various attempts to characterize such complex systems, such as sensitivity to the initial conditions [12], involvement of non-linearity in mathematical modeling [13], pattern formation, [14], etc. The Complex network is one of the theoretical approaches or tools available in complexity science to study complex systems and has seen tremendous growth in the last two decades. Complex networks can be represented by their adjacency and laplacian matrices. Further, spectra (eigenvectors and eigenvalues) of the adjacency matrix and the laplacian matrix of networks provide important insight into several structural and dynamical processes on networks [15–18]. Most important questions concerning structural and dynamical properties include; (1) During disease spreading, which sets of nodes are more affected or how fast disease can be spread in the entire networks? [19] (2) In perturbation propagation, whether perturbation remains confined to the source node or gets to the distant nodes? [20] (3) In an external shock, how resilient or stable could a network be [21]? (4) In information spreading, it is important to know what structural properties of networks relate to the disparate temporal dynamic ? [22, 23] Eigenvector localization serves well in understanding or dealing with such questions. For instance, it was found that if the eigenvector corresponding to the largest eigenvalue is localized and the infection rate is slightly higher than the threshold, then the disease will be localized on only a finite set of vertices [19]. In [20], it was shown that perturbation propagation in ecological networks weakened due to the localization behavior of principal eigenvectors. Further, [21] it was postulated that the stability of the system from the external shock would depend upon the localization behavior of the eigenvector corresponding to the lowest eigenvalue of the connectivity matrix.

Though most of the works around spectra focus on the extremal eigenvalues and corresponding eigenvectors, sporadic investigations indicate that non-principal eigenvalues and associated eigenvectors of the adjacency matrices of networks contribute to the transient dynamics [24, 25]. Moreover, localization properties of non-principal eigenvectors have also found its application in characterizing or identifying community structures [26, 27]. Furthermore, few attempts have been made to investigate Anderson-like transition in complex networks. For example, [28], it was shown that Anderson-like transition could be obtained in complex networks without a diagonal disorder and one just has to tune the clustering coefficient. Also, using spectral statistics, localization transition was studied for ER random network, Cayley tree, and scale-free networks [29]. In this thesis, we attempt to understand three questions. (1) Localization induced due to disorder in topology, (2) Interplay of diagonal disorder and randomness on localization and (3) Origin of localization in hypergraph.

1.2 Networks and its basic properties

A network denoted by $G = \{\mathrm{V}, \mathrm{E}\}$ consists of set of *nodes* and interaction *links*. The set of *nodes* are represented by $\mathrm{V} = \{v_1, v_2, v_3, \ldots, v_N\}$ and *links* by $\mathrm{E} = \{e_1, e_2, e_3, \ldots, e_M\}$ where N and M are size of V and E respectively. Mathematically, a network can be represented by its adjacency matrix A whose elements are defined as $A_{ij} = 1$ if node i and j are connected and 0 otherwise.

1.2.1 Structural properties

Degree: The degree of a vertex v_i in a graph G is number of vertex adjacent to v_i and is denoted as $k_i = \sum_{j=1}^{n} a_{ij}$.

Degree sequence: The degree sequence of a graph G is the list of degrees of all vertices with repetition allowed.

Average degree: The average degree of the network is simply average number of edges per node and is denoted by $\langle k \rangle = \frac{1}{n} \sum_{i=1}^{n} k_i$.

Degree distribution: The degree distribution of a network, $P(k)$, is the frequency count of the occurrence of each degree.

Clustering Coefficient: The clustering coefficient [30, 31] of node i C_i is defined as the ratio of the number of edges between its neighbors and the maximum possible number of edges that could exist between the neighbors. Mathematically, it can be calculated as

$$C_i = \frac{2n_i}{k_i(k_i - 1)}$$

where k_i denotes the degree of node i, and n_i is the number of edges between the k_i neighbors of node i. The average clustering coefficient of a graph G consisting of N nodes is calculated as,

$$\langle CC \rangle = \frac{1}{N}\sum_{i=1}^{N} C_i$$

Degree-degree correlation: The degree-degree correlation capture the relationship between node's degrees and tells how nodes with different degree tend to connect with each other. It is measured by the Pearson correlation coefficient as [32]

$$r_{deg-deg} = \frac{[m^{-1}\sum_{i=1}^{m} j_i k_i] - [m^{-1}\sum_{i=1}^{m}\frac{1}{2}(j_i + k_i)]^2}{[m^{-1}\sum_{i=1}^{m}\frac{1}{2}(j_i^2 + k_i^2)] - [m^{-1}\sum_{i=1}^{m}\frac{1}{2}(j_i + k_i)]^2}$$

where m is the total number of edges in the network and j_i, k_i are the degrees of nodes with i^{th} edge and $r_{deg-deg}$ value varies in between -1 to 1. When nodes with a high degree tend to connect with similar high degree nodes, the network is known as an assortative network with $r_{deg-deg} > 0$. On the other hand, if high-degree nodes prefer to connect with low-degree nodes then the network is referred to as a disassortative network with $r_{deg-deg} < 0$.

1.2.2 Spectral properties

The eigenvalues and eigenvectors of a network is termed as spectra. The eigenvalues of the adjacency matrix A are denoted by $\{\lambda_1, \lambda_2, \lambda_3, \ldots, \lambda_N\}$ where $\lambda_1 \geq \lambda_2 \geq \ldots \geq \lambda_N$ and the corresponding orthonormal eigenvectors as $\{\boldsymbol{x}_1, \boldsymbol{x}_2, \boldsymbol{x}_3, \ldots, \boldsymbol{x}_N\}$. For an undirected network, the adjacency matrix of the network, **A** is a real symmetric matrix and thus all the eigenvalues are real. The eigenvectors of A are orthonormal to each other and forms a basis. The largest eigenvalue λ_1 satisfies $\langle k \rangle \leq \lambda_1 \leq k_{\max}$ where $k_{\max}$ is the largest degree of the networks. Also

$\lambda_1 \leq \left(\frac{2M(N-1)}{N}\right)^{\frac{1}{2}}$, where M, N are the number of edges and nodes in the graph, respectively. If G is connected, then $\chi(G) \leq 1 + \lambda_1(G)$, where $\chi(G)$ is the chromatic number of G [33]. The chromatic number $\chi(G)$ of graph G is the minimum number of colors required to color the vertices such that adjacent vertices get distinct colors. Also, along with λ_1, other eigenvalues of A implicate the following information about the structure of graph G.

1. $\lambda_1^2 + \lambda_2^2 + \cdots + \lambda_N^2 = 2M$.

2. $\sum_{i,j,i\neq j} \lambda_i \lambda_j = -M$.

3. $\lambda_1^3 + \lambda_2^3 + \cdots + \lambda_N^3 = 6|T|$,

where T is the set of all the cycles of length 3 in G (also referred as triangles). In general, the number of closed walks of length k in G equals $\sum_i^N \lambda_i^k$. A walk of length k in a graph G is a sequence of vertices $(v_1, v_2, \ldots, v_{k+1})$ such that there is an edge $v_i \sim v_{i+1}$ for $i = 1, 2, \ldots, k$. The walk is closed if $v_1 = v_{k+1}$.

1.3 Model Networks

Most real-world networks can be grouped into several classes of networks and each network is characterized by definite structural or topological properties. Most of these properties include degree distributions, clustering, assortativity, and shortest paths. The ER random network is the oldest of all the network model and was theoretically investigated by Erdős and Rényi in the late 1950s depict many fascinating phenomena including the transition to the formation of a giant cluster with an increase in the probability of connecting nodes [34]. Despite the tremendous theoretical success of the ER random network model, it was not considered to imitate real-world networks due to its limitation to capture properties like high clustering and power-law degree distribution abundantly found in a diverse range of real-world systems. Watts and Strogatz in their landmark paper [35] introduced the small-world network model which generates networks having a very high clustering coefficient, as that of a regular lattice, and average shortest path length, like that of the ER random networks, two properties readily witnessed in networks representing many real-world complex systems [36–38]. In the subsequent year, the scale-free network was discovered by Barabási that has power-law degree distribution as opposed to the Poisson degree distribution of random graphs [39]. In the following, we briefly discuss the rules to generate these model networks and their basic properties.

1.3.1 ER random networks

ER random networks are constructed using the ER model [34] as follows. Starting with N nodes, each pair of the nodes is connected with a probability $p = \langle k \rangle / N$. The degree distribution of ER random networks follows a binomial distribution.

1.3.2 Small-world networks

We construct small-world networks using the Watts and Strogatz algorithm [35] as follows. Starting with a 1D lattice in which all the nodes have an equal degree, we rewire each edge of the network with a probability p_r avoiding multiple loops and self-connections. This procedure of the rewiring allows to transform a regular network with $p_r = 0$, to random network with $p_r = 1$. In the intermediate p_r values, the network manifests the small-world behavior which is quantified by a very high clustering coefficient and a very small average shortest path length [35].

1.3.3 Scale-free networks

Scale-free networks are constructed using BA preferential attachment method [39] in which each node prefers to connect with the existing higher degree nodes. Starting with a network with m_0 nodes, we start adding a new node at each time step having m connections such that $m \leq m_0$. The new nodes can be connected to any existing node and to incorporate preferential attachment, the probability of it getting connected to the i^{th} nodes is proportional to k_i where k_i is the degree of the i^{th} node. Thus, after t time steps, the network will have $t + m_0$ nodes and mt edges. The network evolves into a scale-free network with degree distribution following power law, that is, $P(k) \sim k^{-\gamma}$ where $\gamma = 3$.

1.4 Technique and Methods

1.4.1 Inverse participation ratio

By localization of the eigenvector, it is meant that few entries of the eigenvector have a very high value compared with the other entries. On the other hand, in the case of delocalized eigenvector, all the entries have almost equal value. We quantify localization of the $\boldsymbol{x}_j$ eigenvectors by measuring the inverse participation ratio (IPR) denoted as $Y_{\boldsymbol{x}_j}$. The IPR of an eigenvector $\boldsymbol{x}_j$ is defined as [19]

$$Y_{\boldsymbol{x}_j} = \sum_{i=1}^{N} (x_i)_j^4 \tag{1.1}$$

where $(x_i)_j$ is the i^{th} component of the normalized eigenvectors $\boldsymbol{x}_j$ with $j \in \{1, 2, 3 \ldots, N\}$. The most delocalized eigenvector $\boldsymbol{x}_j$ will have all its components equal, i.e., $(x_i)_j = \frac{1}{\sqrt{N}}$, with IPR value being $1/N$. Whereas, for the most localized eigenvector, only one component of the eigenvector will be non-zero, and the normalization condition of the eigenvectors ensures that the non-zero component should be equal to unity. Thus the value of IPR for the most localized eigenvector is equal to 1. It is also worth noting that there may exist fluctuations in the IPR values for a given state $\boldsymbol{x}_j$ for different network realizations. Thus, one has to take the ensemble average of IPR to know the localized or delocalized nature of given eigenvector. However, it is not possible that λ_j and corresponding $\boldsymbol{x}_j$ remain the same for different random realizations of the network, as in that case, one would have simply added all the IPR's for $\boldsymbol{x}_j$ of corresponding λ_j for the different realizations and divided it by the number of realization which would have been an ideal case. However, in absence of that, we consider a small width $d\lambda$ around λ_j and average all the IPR values corresponding to those λ_j which fall inside this small width [40]. Note that, even after the calculation of IPR, one can not guarantee if the given eigenvector is localized or not and one has to do a scaling analysis of IPR. For this, one has to calculate $Y_{\boldsymbol{x}_j}(\lambda)$ for different network sizes and obtain the scaling parameter as

$$Y_{\boldsymbol{x}_j}(\lambda) \sim N^{-\alpha} \tag{1.2}$$

If $Y_{\boldsymbol{x}_j}(\lambda)$ does not depend upon system size, i.e. $\alpha = 0$, then the corresponding eigenvectors are localized. On the other hand, if the $Y_{\boldsymbol{x}_j}(\lambda)$ scale inversely with system size ($\alpha = 1$), then the corresponding eigenvectors are delocalized. If $0 < \alpha < 1$, then the eigenvectors are neither localized nor delocalized.

1.4.2 Multifractality in eigenvector localization

Further, in the seminal paper of Wegner [41] it was found that at the criticality, the generalized IPRs (GIPR) defined as $\chi_q = \sum_{i=1}^{N} {x_i}^{2q}$ shows an anomalous scaling with the system size N, i.e., $\langle \chi_q \rangle \propto N^{-\tau(q)}$, where $-\tau(q) = (q-1) \times D_q$. For the localized eigenvectors, $\langle \chi_q \rangle \propto N^0$, and for the completely delocalized eigenvectors $\langle \chi_q \rangle \propto N^{-d(q-1)}$ where d is the dimension of the system. However, if the eigenvector corresponds to the critical state, D_q becomes non-linear function of q and therefore the scaling is described by many exponents D_q indicating that a critical eigenvector depicts multifractal behavior. We use the standard box-counting method as described in [42] for the multifractal analysis. Let us consider an eigenvector $\boldsymbol{x}_j$ whose components are represented as $(x_1)_j, (x_2)_j \dots (x_N)_j$. We then divide the N sites into N_L number of boxes with each box having the size l. The box probability $\mu^k(l)$ of the k^{th} box of the size l is defined as

$$\mu^k(l) = \sum_{i=(k-1)l+1}^{kl} (x_i)_j^2. \tag{1.3}$$

The q^{th} moment of the box probability is thus

$$\chi_q = \sum_k \mu_k^q(l) \sim l^{-\tau(q)}, \tag{1.4}$$

In the above equation, if the scaling exponent $\tau(q)$ is a linear function of the parameter q, it corresponds to the mono-fractal behavior, and for the nonlinear relation, it indicates the multifractal property of the eigenvector.

Note that, apart from the box-counting method there exists an alternative method widely used in the localization theory through multifractal analysis. In this method, instead of varying the length of the box (l), the system size (N) is varied by keeping the value of l = 1 fixed. One usually first calculates χ_q and observes its scaling with the linear size of the system L i.e. $\chi_q \sim L^{-\tau(q)}$. This is also equivalent to $\chi_q \sim N^{-\delta(q)}$ where $N = L^d$ and $\delta(q) = \tau(q)/d$. The linear size of a network is defined as its diameter which is the longest of the shortest path between all the pairs of nodes. Thus, approaching the problem through this method will require varying the network size to a very large value which becomes computationally very exhaustive.

1.4.3 Eigenvalue ratio statistics

The eigenvalue ratio statistics is known to be very useful to identify localized and delocalized eigenvectors. The eigenvalue ratio statistics corresponding to the localized eigenvectors is known to depict the Poisson statistics, while for delocalized eigenvectors, it is known to manifest the GOE statistics [43]. Following Ref. [44], the ratio of consecutive eigenvalue spacing is defined here as

$$r_i = \frac{min(s_{i+1}, s_i)}{max(s_{i+1}, s_i)} \tag{1.5}$$

where s_i = $\lambda_{i+1} - \lambda_i$ is the spacing between eigenvalues λ_{i+1} and λ_i with $i \in (1, 2, 3 \dots N-1)$. Also, one can verify that $0 < r_i < 1$. Ref. [44] provides only numerical estimation of $P(r)$ for the GOE distribution, and discussions on the other two symmetry classes (GUE and GSE) were lacking. This gap was filled in Ref. [45] where an exact distribution function of r was derived which was not restricted only to GOE but includes GUE and GSE classes as well. The distribution function ($P(r)$) approximating GOE statistics is given as

$$P(r) \sim \frac{54/8 \times (r + r^2)}{(1 + r + r^2)^{5/2}} \tag{1.6}$$

and the theoretical average value of r for GOE and Poisson statistics has been estimated to be equal to 0.53 and 0.38, respectively, with the distribution function for Poisson statistics is given by

$$P(r) \sim \frac{2}{(1 + r)^2} \tag{1.7}$$

1.5 Thesis Overview

We have divided our study on localization into three parts. In the first part (chapter 2), we have studied the localization of eigenvectors induced due to the topological disorder. By topological disorder, we mean heterogeneity in the degrees of nodes. Starting with initial $1D$ lattice where each node have same number of neighbors, we rewire the links with some probability p_r where $0 < p_r \leq 1$. Thus, this setup will allow us to investigate localization instigated due to increasing disorder in the topology. In this part of the thesis, we hire multi-fractal technique already very popularly used in condensed matter physics to study localization. Here, we characterized the eigenvalue spectrum into different regimes based on their localization characteristics. The central part of the eigenvalue spectrum depicts strong multi-fractal features with a wide range of D_q while the tail part shows $D_q \to 1$. We found that for initial rewiring probability, increasing p_r enhances the strength of multi-fractality while after some threshold strength of multi-fractality shows a decreasing trend with the increase in p_r. Further, we emphasized that distorting the initial regular topology (1D lattice) topology by rewiring few connections does not lead to localization of the eigenvectors, instead, it drives them toward the critical states i.e. neither localized nor delocalized.

In the second part of the thesis (chapter 3), along with distorting the initial 1D lattice, we also introduce diagonal disorder in the adjacency matrix. Thus, rewiring parameter p_r quantifying randomness allows us to investigate the effect of the interplay of diagonal disorder and randomness on localization. The motivation behind this work is that most of the work including the original anderson tight-binding model considered only the nearest neighbor's interactions while there exist many real-world systems where the constituent elements are connected randomly and also include long range connections. Thus, it would be fascinating to probe the effect of randomness along with diagonal disorder on localization. In this part of the thesis, we adopt Random matrix theory (RMT) which first originated in nuclear physics and later found its application in different areas of Physics. We found that upon increasing diagonal disorder, eigenvectors go from the delocalized to localized state captured by the gradual transition of eigenvalue ratio statistics from GOE to Poisson statistics. Moreover, the more random a network is, the more resilient it is toward diagonal disorder on inducing localization. Further in this chapter, we relate the localization transition to the transient dynamics of the maximal entropy random walker.

In the third part of the thesis (chapter 4), we study localization in hypergraphs.

The motivation to include the hypergraph in the study is due to the fact that networks are restricted to pair-wise interactions but many real-world systems entail simultaneous interactions between more than two nodes popularly known as higher-order interactions. These systems can be better understood in the framework of hypergraphs which consists of hyperedges accounting for the multi-body interactions. By defining a single parameter γ on a single node, we find that for $\gamma \leq 1$, there is no impact of pair-wise links on eigenvector localization. For $\gamma > 1$, even though the total number of higher-order links is very less as compared with the pair-wise links, higher-order links play a crucial role in instigating localization of the eigenvectors for the larger eigenvalues. On the other hand, for the smaller eigenvalues, pair-wise links play a significant role than the higher-order links in steering localization.

Finally, chapter 5 summarizes the thesis and also discusses the intriguing conclusion of future interests as an extension of the investigation explored in the thesis.

Chapter 2

Localization induced due to disorder in topology

2.1 Introduction

Since the pioneering work of Anderson on localization of electronic wave function in disordered media, eigenvector localization has become a fascinating and an active area of research [1]. In his original paper, Anderson argued that disorder introduced in the diagonal elements of a Hamiltonian matrix will lead to localization of the electronic wave function. Later this theory successfully explained the phenomenon of metal-insulator transition. The theory of Anderson localization found its application in almost all the areas of physics including condensed matter physics [46], chaos [47], photonics [48], etc. Additionally, the phenomenon of localization-delocalization transition has been investigated for different systems such as random banded matrix [49], power-law random banded matrix (PRBM) [7], vibration in glasses [50], percolation systems [51], etc. Most of these studies concentrated in analyzing an impact of the diagonal and off-diagonal disorder on the localization properties. Further, there exist systems in which disorder is originated from randomness in their geometry, leading to extensive research on localization in topologically disorder systems [52, 53].

Many complex systems can be described as graphs or networks consisting of *nodes* and *links*. The *nodes* correspond to the elements of a system and links represent the interactions between these elements. Various network models have been proposed to capture and mimic properties of real-world complex systems, among which Erdös-Renyi random network [54], scale-free network [39], and small-world network [35] models have been the most popular ones. The small-world networks are characterized by high clustering coefficient and small characteristic path length arising due to the topological disorder or random distributions of the connections in an originally regular network. The real-world systems exhibiting topological disorder are ramified fractals, percolation networks, polymers [55–57], etc. Other examples of real-world complex systems depicting the small-world characteristics include brain network [37] and ecological network [38]. Here, we construct small-world networks using the Watts and Strogatz algorithm [35] as follows. Starting from a regular network where each node is connected with its k nearest neighbors, the connections are rewired randomly with a probability p_r. For the intermediate rewiring probability, the network undergoes the small-world transition characterized by high clustering and low path-length.

Further, several dynamical processes on networks can be better understood by spectra of the corresponding adjacency and Laplacian matrices. For example, the small-world network as a quantum model has been studied in terms of localization-delocalization transition of the spectra of underlying adjacency matrices [58]. Using the level statistics, it was shown that the small-world networks having diagonal disorder and rewired links with different values of coupling constant manifest localization-delocalization transition at a critical rewiring probability. Furthermore, quantum diffusion of a particle localized at an initial site on small-world networks was demonstrated to have its diffusion time being associated with the participation ratio and higher for the case of regular networks than that of the networks with the shorter path-length [15]. Further, quantum transport modeled by continuous-time quantum walk (CTQW) in small-world networks has also been investigated [16]; however, here the small-world model was a bit different than the one proposed by Watts and Strogatz in [35]; additional bonds were added to a ring lattice to make it a small-world network. It was argued that adding a large number of bonds leads to suppression of the transition probability of CTQW which is just opposite to its classical counterpart, i.e., continuous-time random walk where adding shortcuts leads to an enhancement of the transition probability.

Furthermore, an understanding to the localization behavior of the principal eigenvector (PEV) provides insight into the propagation of perturbation in the underlying mutualistic ecological networks and [20], disease spreading [19]. Ref. [59] has shown that for the scale-free networks, the PEV localization relates to the power-law exponent. Note that, though PEV provides insight into various dynamical processes in the corresponding networks, other eigenvectors have also been discussed to affect the dynamics on the networks drastically [60]. For example, network activities, discussed in [61], can be better hypothesized by having an understanding of the localization behavior of the central part of the eigenvalue spectrum which is discussed later in this chapter.

This chapter investigates localization properties of eigenvectors of the adjacency matrix considering the entire eigenvalue spectrum of the small-world networks due to the presence of disorder in the network's topology arising due to random rewiring of the links to the originally regular network structure. We emphasize that unlike the original Anderson tight-binding model having diagonal disorder and nearest-neighbor interactions, we do not introduce diagonal disorder and rather consider long-range connections. We probe the localization properties of the entire eigenvalue spectrum since the existence of even a fraction of delocalized eigenvectors has been shown to impart crucial changes in the behavior of the corresponding system [60]. Using multi-fractal technique, we find that the central part of the eigenvalue spectrum is characterized by strong multifractality whereas the tail part of the spectrum have $D_q \to 1$. Further, before the onset of the small-world transition, an increase in the random connections leads to an enhancement in the eigenvectors localization, whereas just after the onset, the eigenvectors show a gradual decrease in the localization. The idea of the multifractal system was first introduced by Mandelbrot [62] which later found its application in various different areas of real-world complex systems such as stock market data [63], foreign exchange data [64], time-series data of sunspots [65], traffic [66], air pollution [67], heartbeat dynamics, [68], etc.

2.2 Theoretical framework

A network denoted by $G = \{\text{V}, \text{E}\}$ consists of set of *nodes* and interaction *links*. The set of *nodes* are represented by $\text{V} = \{v_1, v_2, v_3, \ldots, v_N\}$ and *links* by $\text{E} = \{e_1, e_2, e_3, \ldots, e_M\}$ where N and M are size of V and E respectively. Mathematically, a network can be represented by its adjacency matrix A whose elements are defined as $A_{ij} = 1$ if node i and j are connected and 0 otherwise. Further, here we consider simple network without any self-loop or multiple connections. The eigenvalues of the adjacency matrix A are denoted by $\{\lambda_1, \lambda_2, \lambda_3, \ldots, \lambda_N\}$ where $\lambda_1 \geq \lambda_2 \geq \ldots \geq \lambda_N$ and the corresponding orthonormal eigenvectors as $\{\boldsymbol{x}_1, \boldsymbol{x}_2, \boldsymbol{x}_3, \ldots, \boldsymbol{x}_N\}$. Starting with a regular network in which all the nodes have an equal degree, we rewire each edge of the network with a probability p_r. This procedure of the rewiring allows to transform a regular network with $p_r = 0$, to a random network with $p_r = 1$. In the intermediate p_r values, network manifests the small-world behavior which is quantified by a very high clustering coefficient and a very small average shortest path length [35]. We would also like to divulge important topological properties of the network capturing various topological transitions upon links rewiring. First, the initial regular network ($p_r = 0$) has periodic boundary condition and each node is connected to its $(k/2)$ nearest neighbours on each side of it. Let the shortest distance between any given pair of the nodes i and j be denoted by $r_{i,j}$ and thus the average shortest path length of the network would be $r = \sum_{i \neq j} r_{i,j}/N(N-1)$. For $p_r = 0$, r scales like $r \sim N/2k$ which leads to its Hausdorff dimension being equal to 1. The Hausdorff dimension d can be determined by the scaling of r with the network size N, defined as $r \sim N^{1/d}$. When the initial regular network is perturbed, for $p_r <$

0.01, the networks have finite dimensions i.e r grows as $r \sim N^{\gamma}$ where $0 < \gamma < 1$. For p_r = 0.001, fitting $r \sim N^{\gamma}$ yields $\gamma \approx 0.27$ and $d \approx 3.7$. Upon an increase in the rewiring probability which leads to occurrence of the small-world transition for $p_r \geq 0.01$, r scales like $r \sim \ln N$ which makes the network having infinite dimension [69].

We investigate the localization property of the eigenvectors as the network undergoes from the regular structure to a random one. Localization of an eigenvector means that a few entries of the eigenvector have much higher values compared to the others. We quantify localization of the $\boldsymbol{x}_j$ eigenvectors by measuring the inverse participation ratio (IPR) denoted as $Y_{\boldsymbol{x}_j}$. The IPR of an eigenvector $\boldsymbol{x}_j$ is defined as [19]

$$Y_{\boldsymbol{x}_j} = \sum_{i=1}^{N} (x_i)_j^4, \tag{2.1}$$

where $(x_i)_j$ is the i^{th} component of the normalized eigenvectors $\boldsymbol{x}_j$ with $j \in \{1, 2, 3 \ldots, N\}$. The most delocalized eigenvector $\boldsymbol{x}_j$ will have all its components equal, i.e., $(x_i)_j = \frac{1}{\sqrt{N}}$, with IPR value being $1/N$. Whereas, for the most localized eigenvector, only one component of the eigenvector will be non-zero, and the normalization condition of the eigenvectors ensures that the non-zero component should be equal to unity. Thus the value of IPR for the most localized eigenvector is equal to 1. It is also worth noting that there may exist fluctuations in the IPR values for a given state $\boldsymbol{x}_j$ for different realizations of the network for a given rewiring probability. However, it is not possible that λ_j remain the same for all the random realizations of network, as in that case we would have simply added all the IPR's for λ_j for the different realizations and divided it by the number of realizations which would have been an ideal case. However, in absence of that, for the robustness of the results, we consider a small width $d\lambda$ around λ and average all the IPR values corresponding to those λ values which fall inside this small width [40]. We further elaborate the averaging process for discrete eigenvalue spectrum. Let λ^R = $\{\lambda_1$,λ_2, $\ldots$,$\lambda_{N\times R}\}$ such that $\lambda_1 \leq \lambda_2 \leq \ldots \leq \lambda_{N\times R}$ is a set of eigenvalues of a network for all R random realizations where $N \times R$ is the size of λ^R. The corresponding eigenvector set of the λ^R are denoted by $\boldsymbol{x}^R = \{\boldsymbol{x}_1, \boldsymbol{x}_2, \boldsymbol{x}_3, \ldots, \boldsymbol{x}_{N\times R}\}$. We then divide λ^R for a given value

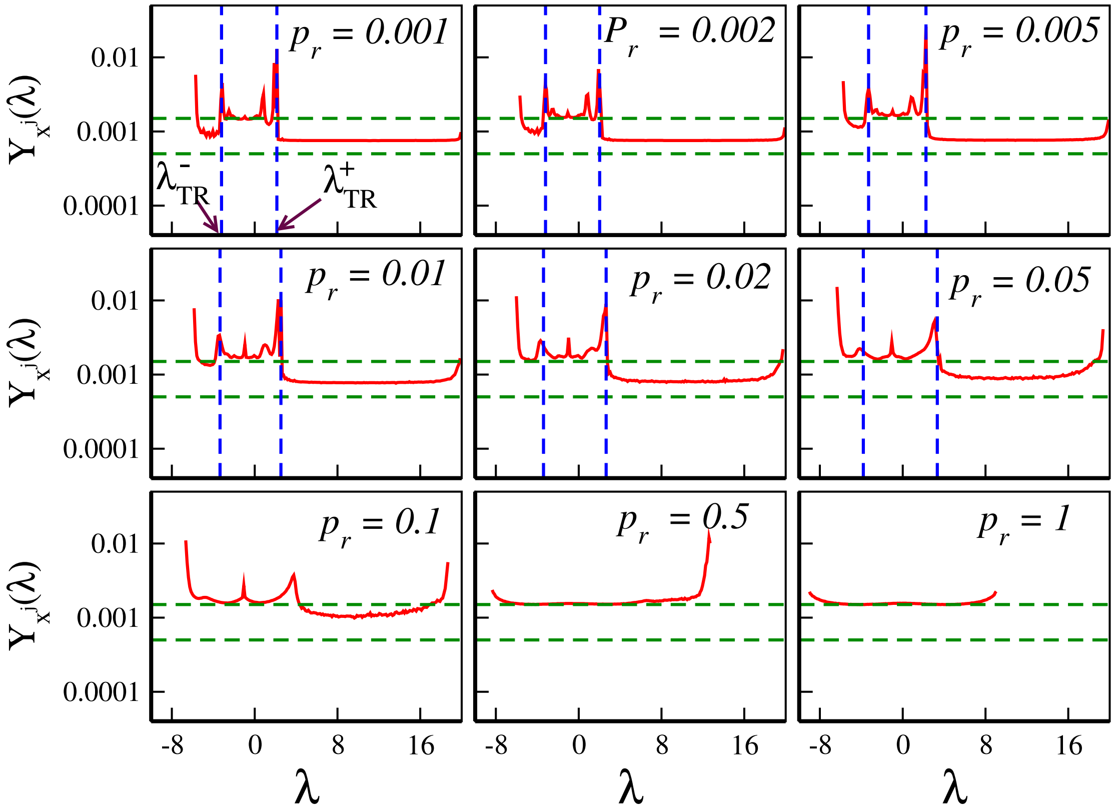

Figure 2.1: IPR of the eigenvectors plotted as a function of the corresponding eigenvalues for various values of the rewiring probability. The dashed green lines plotted at 0.0005 and 0.0015 correspond to the minimum possible value of the IPR $(1/N)$ and the random matrix predicted value for the maximum delocalized state $(3/N)$. Here, $N = 2000$ and $\langle k \rangle = 20$ are kept fixed for all the networks.

of $d\lambda$ into further m subsets where m = $(\lambda_{N\times R} - \lambda_1)/d\lambda$. For each $\lambda^j \subset \lambda^R$ and the corresponding eigenvectors $\boldsymbol{x}^j \subset \boldsymbol{x}^R$, $\forall j = 1, 2,\dots, m$; λ^j = $\{\lambda_1, \lambda_2,\dots, \lambda_{l^j}\}$ and corresponding eigenvector $\boldsymbol{x}^j$ = $\{\boldsymbol{x}_1, \boldsymbol{x}_2, \boldsymbol{x}_3, \dots, \boldsymbol{x}_{l^j}\}$ where l^j is the size of j^{th} subset such that $\sum_{j=1}^{m} l^j$ = $N \times R$ with a constraint that $\lambda_{l^j} - \lambda_{1^j} \leq d\lambda$ for each subset, the corresponding set of IPRs for $\boldsymbol{x}^j$ will be $\{Y_{\boldsymbol{x}_1}, Y_{\boldsymbol{x}_2},\dots, Y_{\boldsymbol{x}_{l^j}}\}$. Hence, the average IPR $(Y_{\boldsymbol{x}_j}(\lambda))$ for each subset $\boldsymbol{x}^j$ can be calculated as $\frac{\sum_{i=1}^{l^j} Y_{\boldsymbol{x}_i}}{l^j}$ where λ is central value for each subset i.e. λ + $\frac{d\lambda}{2}$ = λ_{l^j} and λ - $\frac{d\lambda}{2}$ = λ_{1^j}. Here, we have taken, $N = 2000$, $m = 200$ and $R = 50$ for each rewiring probability. All the physical quantities follow the same averaging procedure in this chapter.

Further, in the seminal paper of Wegner [41] it was found that at the criticality, the generalized IPRs (GIPR) defined as $\chi_q = \sum_{i=1}^{N} {x_i}^{2q}$ shows an anomalous scaling with the system size N, i.e., $\langle \chi_q \rangle \propto N^{-\tau(q)}$, where $-\tau(q) = (q-1) \times D_q$. For the localized eigenvectors, $\langle \chi_q \rangle \propto N^0$, and for the completely delocalized eigenvectors $\langle \chi_q \rangle \propto N^{-d(q-1)}$ where d is the dimension of the system. However, if the eigenvector corresponds to the critical state, D_q becomes non-linear function of q and therefore the scaling is described by many exponents D_q indicating that a critical eigenvector depicts multifractal behavior. We use the standard box-counting method as described in [42] for the multifractal analysis. Let us consider an eigenvector $\boldsymbol{x}_j$ whose components are represented as $(x_1)_j, (x_2)_j \ldots (x_N)_j$. We then divide the N sites into N_L number of boxes with each box having the size l. The box probability $\mu^k(l)$ of the k^{th} box of the size l is defined as

$$\mu^k(l) = \sum_{i=(k-1)l+1}^{kl} (x_i)_j^2. \tag{2.2}$$

The q^{th} moment of the box probability is thus

$$\chi_q = \sum_k \mu_k^q(l) \sim l^{-\tau(q)}, \tag{2.3}$$

In the above equation, if the scaling exponent $\tau(q)$ is a linear function of the parameter q, it corresponds to the mono-fractal behavior, and for the nonlinear relation, it indicates the multifractal property of the eigenvector.

Note that, apart from the box-counting method there exists an alternative method widely used in the localization theory through multifractal analysis. In this method, instead of varying the length of the box (l), the system size (N) is varied by keeping the value of l = 1 fixed. One usually first calculates χ_q and observes its scaling with the linear size of the system L i.e. $\chi_q \sim L^{-\tau(q)}$. This is also equivalent to $\chi_q \sim N^{-\delta(q)}$ where $N = L^d$ and $\delta(q) = \tau(q)/d$. The linear size of a network is defined as its diameter which is the longest of the shortest path between all the pairs of nodes. Thus, approaching the problem through this method will require varying the network size to a very large value which becomes computationally very exhaustive. We prefer the box-counting method in our analysis instead of the above described method. Nevertheless, both methods will yield the same results.

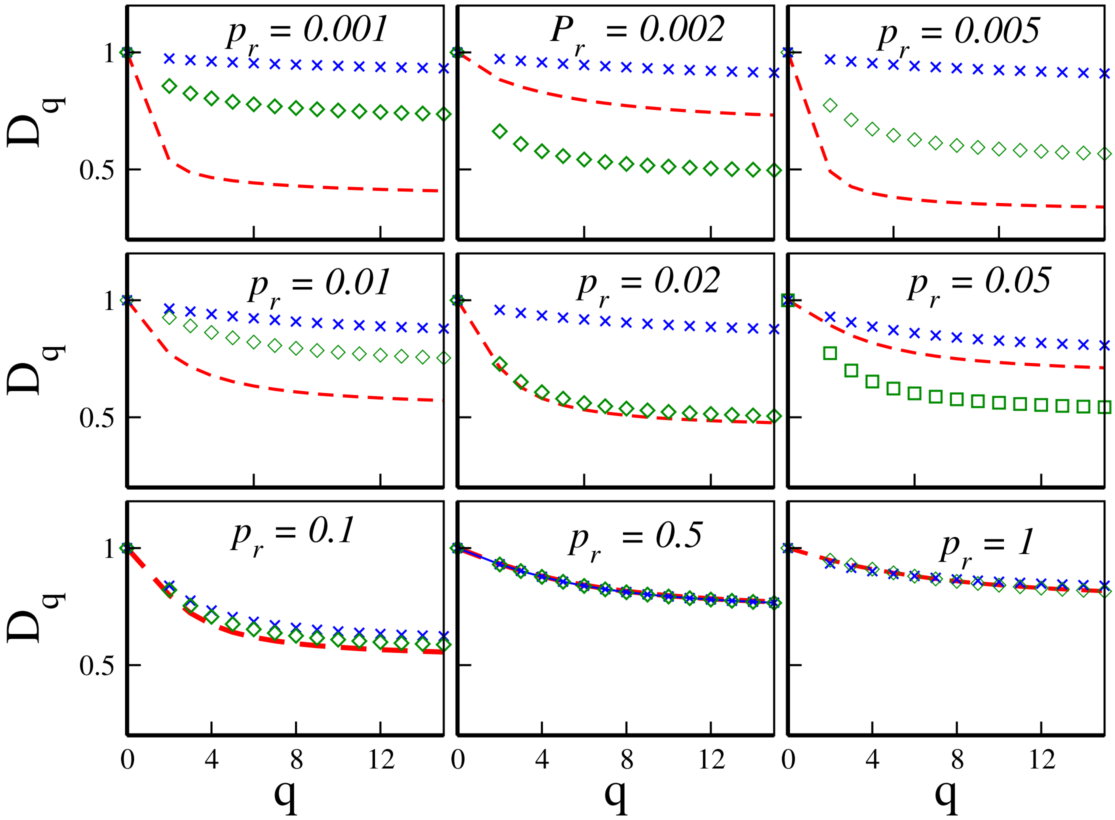

Figure 2.2: The generalized fractal dimension D_q plotted as a function of the exponent q for the eigenvector $\boldsymbol{x}^j$ corresponding to $\lambda^+_{TR}, \lambda^+_{TR-1}, \lambda^+_{TR+1}$ for various rewiring probabilities p_r. The – – – , $\times$, $\diamond$ are for $\lambda^+_{TR}, \lambda^+_{TR+1}, \lambda^+_{TR-1}$, respectively.

2.3 Results

We analyze the localization properties of the eigenvectors of the adjacency matrix of networks with the variation of p_r. Rewiring of the connections affects two major structural properties of the network: clustering coefficient (CC) and average shortest path-length (r). For small values of the rewiring probability ($p_r < 0.01$), CC remains at a very high value whereas r shows a drastic drop and attains a very low value. For $p_r \geq 0.01$, there is no further change in r as it has already attained a very low value but CC starts decreasing. Note that a higher clustering is known to drive localization whereas a smaller path-length is believed to support delocalization [70] [71]. Thus, to understand the contrasting impact of these two structural properties on the eigenvector localization, we first characterize the eigenvalue spectrum into different regimes based on the localization properties of the corresponding eigen-

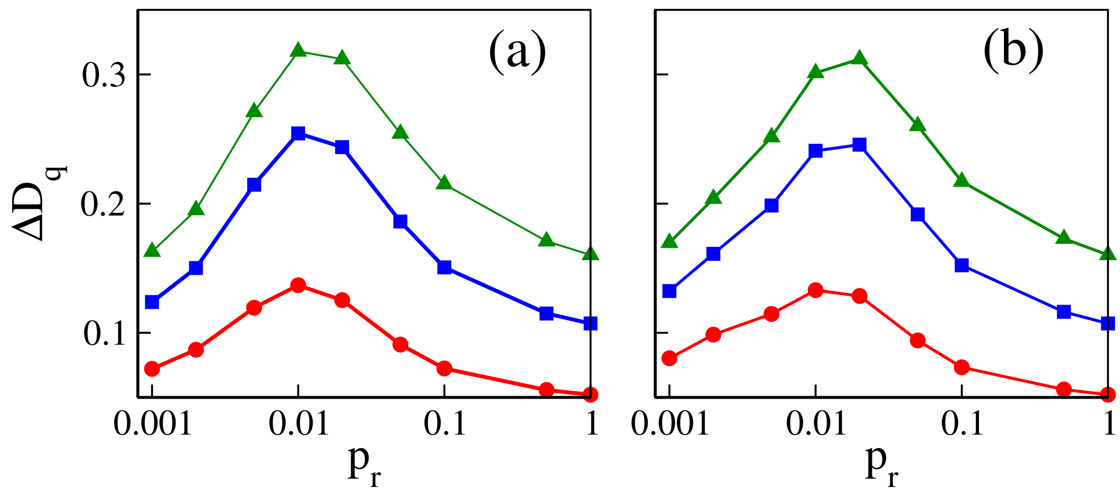

Figure 2.3: Plot of ΔD_q as a function of rewiring probability p_r for $q = 2$ (●) , 5 (■) and 10 (▲) respectively. (a) $\lambda \approx 1.271$ (b) $\lambda \approx 1.371$. These are the eigenvalues from the central regime.

vectors. The central part ($\lambda_{TR}^- \leq \lambda \leq \lambda_{TR}^+$) of the spectrum consists of critical eigenvectors having IPR of the order of 10^{-3}. This is the most localized part of the eigenvalue spectrum. Further, $Y_{x_j}(\lambda)$ has U-shape for the smaller eigenvalues ($\lambda < \lambda_{TR}^-$) while it remains almost constant for the higher eigenvalues ($\lambda > \lambda_{TR}^+$) forming the tail part of the spectra. The eigenvalues λ_{TR}^- and λ_{TR}^+ separate the central part from the smaller and the larger eigenvalues, respectively. We refer to the central regime as a critical state regime, since here all the eigenvectors are at the critical state identified using the multifractal analysis. Both sides of the central part are referred to as the mixed state as in this regime both the delocalized eigenvector (with IPR $\sim 10^{-3}$) and critical states eigenvector (with IPR $\sim 10^{-4}$) co-exist. Using the multifractal analysis, we first determine λ_{TR}^+ for various values of the rewiring probability. This will help us to know the nature of the change in the width of the central part (critical states regime) with the change in the rewiring probability. We then analyze the change in the degree of localization of eigenvectors with the change in the rewiring probability.

Calculation of $\boldsymbol{\lambda_{TR}^+}$: Figure 2.1 plots $Y_{x_j}(\lambda)$ as a function of λ for various values of the rewiring probabilities. All the different regimes, critical and the mixed can easily be identified from the Figure 2.1 . First, we discuss the impact of rewiring on the value of λ^+_{TR}, which helps us to further understand the change in the width of the central part (critical states regime) with the variation in p_r. To achieve this, we analyze the multifractal behavior of a few eigenvectors separating the critical regime with the mixed regime corresponding to the higher eigenvalue, i.e., $\boldsymbol{x}^j$ corresponding to λ^+_{TR}, λ^+_{TR+1}, and λ^+_{TR-1}. Here, λ^+_{TR+1} and λ^+_{TR-1} refer the eigenvalues just after and before λ^+_{TR}, respectively such that $\lambda^+_{TR-1} < \lambda^+_{TR} < \lambda^+_{TR+1}$ relation holds. The eigenvectors $\boldsymbol{x}^j$ corresponding to λ^+_{TR+1} are delocalized, hence we expect them having $D_q \rightarrow 1$; whereas λ^+_{TR-1} lies on the critical regime and therefore should have a multifractal property. Figure 2.2 plots D_q as a function of q for the eigenvector $\boldsymbol{x}^j$ corresponding to $\lambda^+_{TR}, \lambda^+_{TR+1}$ and λ^+_{TR-1} for different values of p_r. For $0.001 \leq p_r \leq 0.05$, $\boldsymbol{x}^j$ corresponding to $\lambda^+_{TR}, \lambda^+_{TR-1}$ show the multifractal characteristics accompanied by a wide range of the generalized multifractals dimension values, while for $\boldsymbol{x}^j$ corresponding to λ^+_{TR+1} have $D_q \rightarrow 1 \, \forall \, q > 0$. Note that, for a completely delocalized eigenvectors, $D_q = 1$, as in the case of principal eigenvector (PEV) of regular network ($p_r = 0$). Otherwise, for slight variations in the values of eigenvector's components (delocalized eigenvectors), $D_q \rightarrow 1$. We find that λ^+_{TR} for various values of the rewiring probability lies in the range $2.03 \leq \lambda^+_{TR} \leq 3.34$, i.e., there exists no significant change in the value of λ^+_{TR} with the change in the rewiring probability for a fixed value of network parameters such as size N and the average degree k and hence the width of the central part remains almost fixed. We furthermore notice that λ^+_{TR} for various values of the rewiring probability always remains equal to the boundary of the bulk part of the eigenvalue density ($\rho(\lambda)$) and the tail part of the eigenvalue density. Since the radius of the bulk part of the eigenvalues largely depends on the network's parameters [72], it is not surprising that the value of λ^+_{TR} remains almost the same. The tail part of the eigenvalue spectrum has a very low value of probability density. Mathematically, this means that, $\rho(\lambda^+_{TR} + \epsilon)$ $\rightarrow 0$ and $\rho(\lambda^+_{TR} - \epsilon) \rightarrow \delta$ where $\delta > \epsilon$ and $\epsilon \ll 1$. This can be easily understood with the following argument. The eigenvalue spacing $\lambda_{i+1} - \lambda_i \ll \xi$ for $\lambda < \lambda^+_{TR}$ whereas for $\lambda > \lambda^+_{TR}$, $\lambda_{i+1} - \lambda_i > \zeta$ where $\zeta > \xi$ and $\xi \ll 1$. It has been argued that the eigenvalue spectra corresponding to the localized states is continuous while that

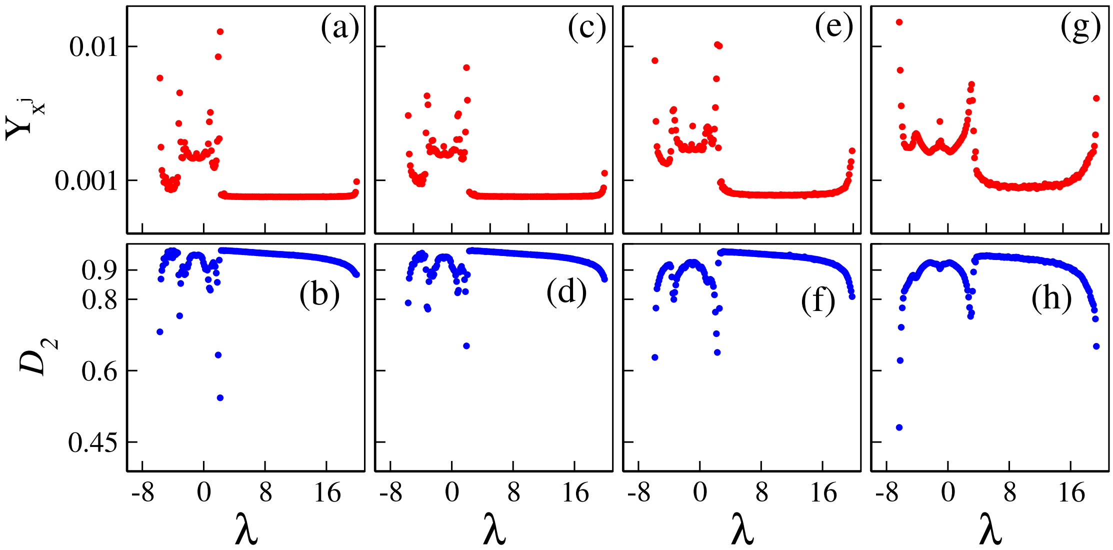

Figure 2.4: The correlation dimension D_2 and IPRs of the eigenvectors are plotted as a function of the corresponding eigenvalues for the following four different rewiring probabilities: (a)-(b) $p_r = 0.001$; (c)-(d) $p_r = 0.0021$; (e)-(f) $p_r = 0.01$; and (g)-(h) $p_r = 0.05$.

of the eigenvalue spectra of the delocalized states is discrete [73]. Thus, λ^{+}_{TR} is the eigenvalue separating the central regime of high IPR values from the regime of low IPR values. Additionally, it also separates the bulk part from the tail of the density of the eigenvalues. Therefore, these calculations of eigenvalues separating the regime of higher IPR values with lower IPR values are in agreement with the previously known conjecture on localization. More interestingly, the methodology followed here provides the exact value of the eigenvalue separating the critical regime and mixed regime. After $p_r \geq 0.05$, as randomness increases further, it is difficult to divide the spectrum into different regimes based on the localization properties of eigenvectors and all the three regimes start coinciding with each other (Figure 2.1). Additionally, it can be seen that D_q for $\boldsymbol{x}^j$ corresponding to λ^{+}_{TR}, λ^{+}_{TR+1} and λ^{+}_{TR-1} starts coinciding with each other (Figure 2.2).

Change in the localization properties with p_r: We next discuss the impact of rewiring on the degree of localization of the eigenvectors. Specifically, we focus on the eigenvectors belonging to the central regime as this part of the spectrum undergoes the localization-delocalization transition with the increase in the rewiring probability. The other eigenvectors lying outside the central regime do not witness a significant change in their localization properties. For p_r = 0.001, the eigenvectors which are nearer to the band edge, i.e. $\boldsymbol{x}^j$ corresponding to λ^+_{TR}, λ^+_{TR-1} are characterized by strong multifractality having a wide range of the generalized multifractal dimensions. On the other hand, the eigenvectors inside the band are characterized by weak multifractality satisfying D_q = $1 - \beta q \; \forall \; q > 0$ and $\beta \ll 1$. The weak multifractality means that the eigenvectors corresponding to the critical state are close towards the extended states which are analogous to Anderson transition in $d = 2 + \epsilon$ with $\epsilon \ll 1$ dimension. Furthermore, a strong multifractality means that the corresponding eigenvectors are more inclined towards the localization which is similar to the conventional Anderson transition in $d \gg 1$ dimensions [74]. As the rewiring probability is increased further, for $0.001 < p_r \leq 0.05$, we do not find any significant change in the multifractal characteristics of the eigenvectors lying at the band edge. However, the eigenvectors lying inside the band are now described by the strong multifractal characteristics. To demonstrate the change in the strength of multifractality of the eigenvectors with the variation in p_r, we calculate the decay in D_q with respect to q. For this, we define $\Delta D_q = D_0 - D_q$. Note that, D_0 = d (in our case: $d = 1$) irrespective of the nature of the eigenvector. Hence, ΔD_q provides a correct measure to compare the decay in D_q with respect to q in turn providing insight into the strength of multifractality. Thus, we use ΔD_q as a measure of the degree of localization. Figure 2.3 plots ΔD_q as a function of p_r for two different eigenvalues from the central part. Figure 2.3 demonstrates that as the rewiring probability increases, ΔD_q manifests an increase until the onset of small-world transition ($p_r \approx 0.01$). Thereafter, it shows a decrease for a further increase in the p_r values till $p_r = 1$. The increase in ΔD_q for the initial p_r values indicates that there exists an increase in the multifractal characteristics indicating an enhancement in the degree of localization with the increase in the rewiring probability. Thus, based on the effect of rewiring of the connections on the localization properties of the eigenvectors, p_r can be divided into two domains. First, $0.001 < p_r \leq 0.01$ where an increase in the rewiring probability leads to an increase in the degree of

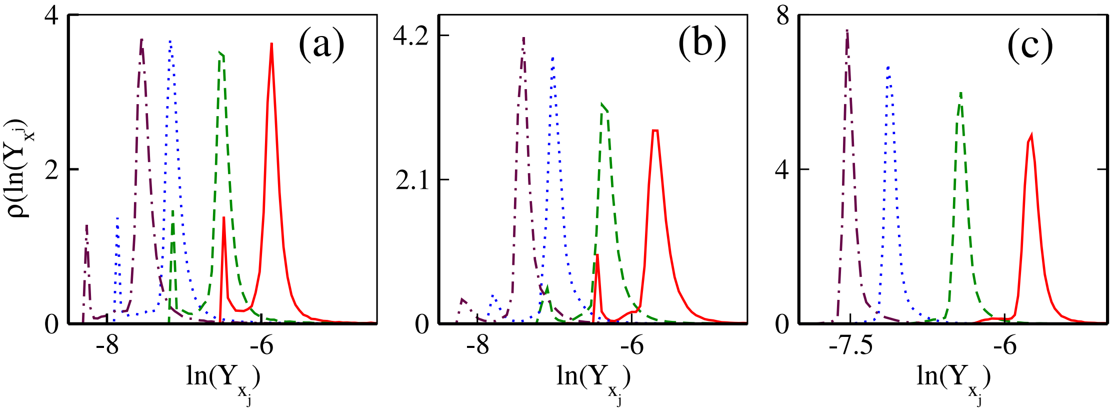

Figure 2.5: Distribution function of $P(ln(Y_{x_j}))$ for rewiring probability (a) 0.001 (b) 0.01 (c) 0.2. –, – – –, · · ·, – · – · – are used for $N = 1000, 2000, 4000, 6000$ respectively.

localization of eigenvectors; while for $0.01 \leq p_r \leq 1$, eigenvectors undergo a continuous decrease in the localization. Moreover, the transition takes place exactly at the onset of the small-world transition. This can be further explained by the following. For $0 < p_r \leq 0.01$, the average clustering coefficient of the network remains constant at $CC = 3/4$, while the average shortest path drops down drastically. It is a common belief that a shorter r supports diffusion whereas a higher clustering is known to drive toward the localization transition [70]. Therefore, there exists an interplay of these two structural quantities in deciding the localization properties of the eigenvectors. For $p_r \leq 0.01$, a high number of triangles accounted for localization, whereas for $p_r \geq 0.01$, there exists a significant decrease in the CC with r being small, and thereby leading to decrease in the degree of localization of eigenvectors. We would like to stress that distorting the initial regular network by rewiring a few connections (for p_r being very small) does not cause localization of the eigenvectors, rather they reach the critical states detected by the calculation correlation dimension (D_2).

The correlation dimension (D_2) of the eigenvectors provides insight into the scaling of the IPRs. For the localized eigenvectors, $D_2 \to 0$, while $D_2 \to 1$ for the completely delocalized eigenvector. On the other hand, if $0 < D_2 < 1$, the eigenvector is said to be at the critical state. Therefore, we next calculate the correlation dimension of the eigenvectors for various values of p_r. Figure 2.4 presents results of D_2 and IPR for the eigenvectors as a function of the corresponding eigenvalues for four different p_r values. The plot clearly depicts that there exists a sharp change in D_2 at a point which separates the central and the delocalized regime. For $\lambda > \lambda^+_{TR}$, $D_2 > 0.94$ for all the values of the rewiring probability indicating delocalized eigenvector. However, at the critical point, which separates the critical and the mixed regimes, the values of D_2 is different for the different p_r values. For $p_r = 0.001, 0.002, 0.01$ and 0.05, the values of D_2 are equal to $0.53, 0.66, 0.66$ and 0.72, respectively. The range $0.4 < D_2 < 0.90$ for the eigenvectors in the critical regime clearly suggests that though they reach at the critical state arising due to the links rewiring, they do not get completely localized ($D_2 \rightarrow 0$). Further, the value of D_2 at λ^+_{TR} is the minimum for the entire spectrum. Thus, the eigenvectors at the boundary of the central part are the most localized in the spectrum for the values of the initial rewiring probabilities.

IPR Statistics: So far, we have discussed the impact of rewiring on the localization properties of the eigenvectors when IPR and other physical measures of eigenvectors are being averaged over in the small eigenvalue window. However, an analysis of the IPR statistics can provide us with further information about the system. For instance, in the case of the power-law random banded matrix (PRBM), it was found that at the critical point of the localization-delocalization transition, the width and the shape of the distribution of the logarithm of IPR do not change with the system size, or we can say that it is scale invariant [75]. We calculate the distribution function of IPR for various rewiring probabilities for different system sizes. Figure 2.5 shows that, for p_r = 0.001, $\rho(\ln(Y_{x_j}))$ remains invariant with the change in the network size as neither its shape nor its width changes with N. For $p_r \geq 0.001$ the distribution function $\rho(\ln(Y_{x_j}))$ witness a continuous decrease in the width with an increase in N (Figure 2.5). Thus, we can infer that, p_r = 0.001 is the critical rewiring probability for the localization-delocalization transition.

Impact of variation in average degree (k) on D_q: In this section, we discuss the impact of average degree k on D_q. Note that the largest eigenvalue of network

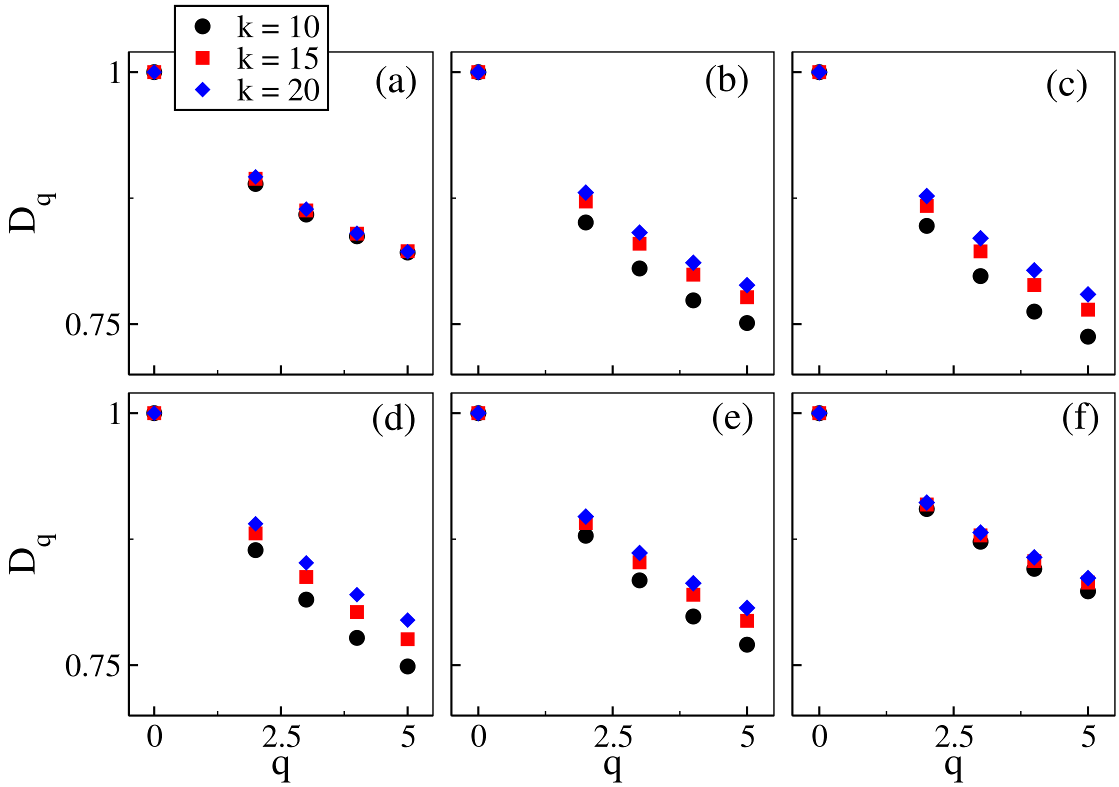

Figure 2.6: Plot of D_q as a function of q and k for various rewiring probabilities. (a) p_r = 0.001 (b) p_r = 0.005 (c) p_r = 0.01 (d) p_r = 0.05 (e) p_r = 0.1 (f) p_r = 1. In all the cases , $\lambda \approx 0$ is considered and D_q is average over all the eigenvectors belonging to d$\lambda = 0.25$ as described in Sec. $Methods$.

is bounded with the largest degree k^{max} [72]. Moreover, for a random network λ_1 $\approx [1 + o(1)]k$, where $o(1)$ means a function that converges to 0 [76]. Thus, varying k may affect the eigenvalue spectrum drastically even for the fixed network size. Here, we have considered three sets of k = 10, 15, 20 with N = 2000 being fixed. First we calculate the value of λ^+_{TR} for k = 10 and 15. For such a small change in the average degree though leads to notable changes in λ_1, there exist no such significant impact of k on λ^+_{TR}.

We next probe the impact of k on D_q for various values of the rewiring probabilities. We witness no significant changes in the nature of D_q for the tail part of the eigenvalue spectrum ($\lambda > \lambda^+_{TR}$) with the change in the average degree. However, for the central regime, a decrease in the average degree leads to an increase in the strength of the multifractality of the eigenvectors as depicted in Figure2.6. As we

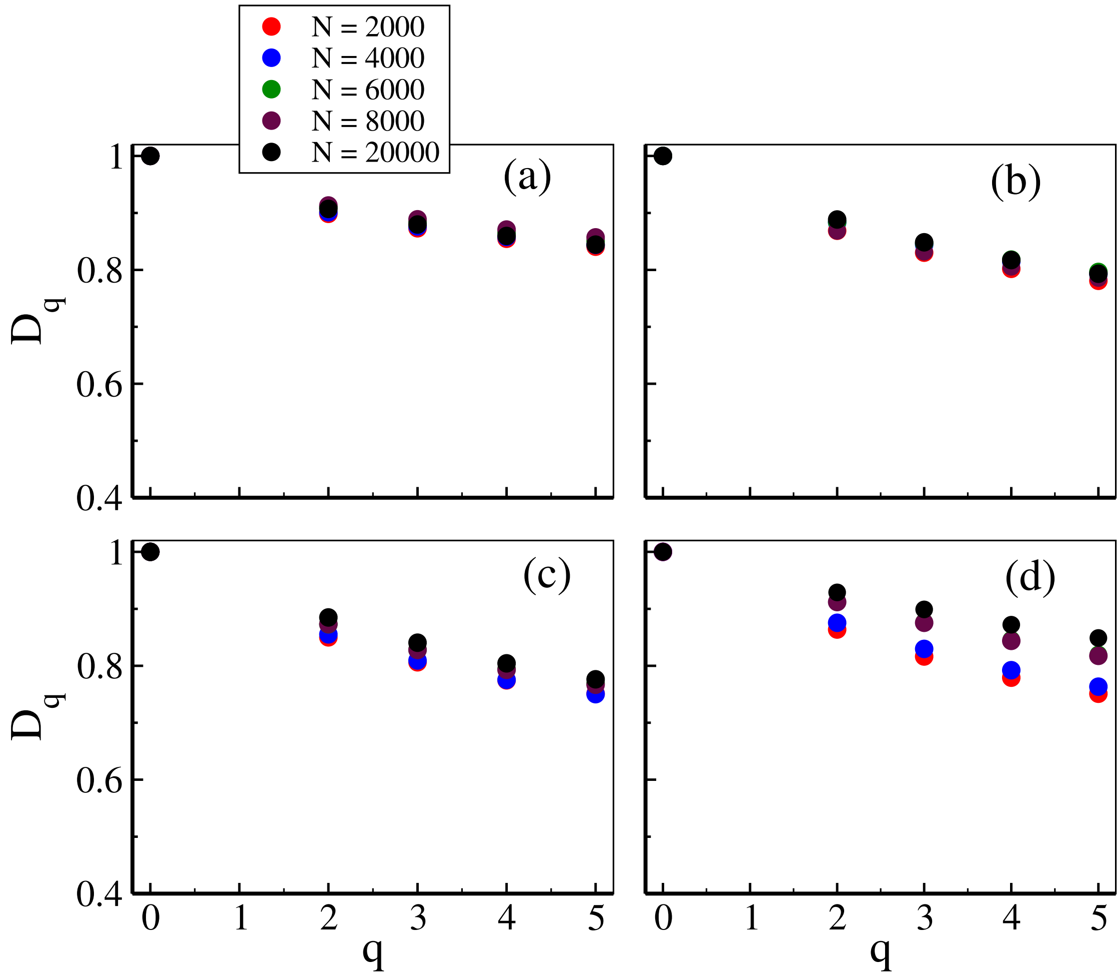

Figure 2.7: Plot of D_q as a function of q and N for various rewiring probabilities. (a) p_r = 0.001, $\lambda \approx 1.47$ (b) p_r = 0.005, $\lambda \approx 1.403$ (c) p_r = 0.01, $\lambda \approx 1.527$ (d) p_r = 0.05, $\lambda \approx 1.69$. Here, λ belongs to the central regime and D_q is average over all the eigenvectors belonging to dλ as described in Sec. $Methods$.

have already discussed that the strength of the multifractality of eigenvectors indicates the degree of localization. Thus, decreasing the average degree suggests an enhancement in the degree of eigenvector localization.

Effect of Finite Size: It is well known that critical phenomena are accurately defined only in the thermodynamics limit i.e., $N \to \infty$. Further, the multifractality of the eigenvectors might be due to the finite size of the system, which may not exist at the infinite size limit. Hence, one needs to be careful regarding the critical point. Nevertheless, D_q certainly reveals the tendency towards a more localized or a more delocalized behavior of a given eigenvector. Therefore, we have calculated D_q for various system sizes to check the impact of the finite-size effect in our analysis. Figure 2.7, is a plot of D_q for the eigenvalues lying in the central regime for various different values of the rewiring probability as the network size varied from 2000 to 20000. It is evident from the Figure 2.7 (a,b) there is no significant change in D_q as the network size is changed from 2000 to 20000. This is also supported by Figure 2.5 (a), where the distribution $\rho(\ln(Y_{x_j}))$ remains to scale invariant and thus gives rise to the unique fractal dimension D_q. However, there exists a slight change between D_q at $N = 2000$ and D_q at $N = 20000$ in the case of p_r = 0.01 [Figure 2.7 (c)] though D_q gets saturated after $N = 8000$. However, we do find a significant change in D_q with a change in the network size in the case of p_r = 0.05 though it still keeps showing the multifractal characteristics. Thus, we see that change in the value of D_q by varying N increases with an increase in the rewiring probability which appears very intriguing. One of the possible reasons for the larger fluctuations in Figure 2.7 (d) could be the higher rewiring probability as for a given rewiring probability, the number of the rewired links (N_r) on average equals to ($N \times p_r \times k$)/2. Thus, for Figure 2.7 (d), N_r equals to 10^3 and 10^4 for $N = 2000$ and 20000, respectively. This difference is very high as compared with that of the smaller rewiring probabilities leading to higher changes in the network topology with higher N. Note that fluctuation of D_2 for a critical eigenvector of the power-law random banded matrix (PRBM) with system size was also reported and investigated in [77].

2.4 Discussion and Conclusion

We have investigated the localization behavior of the eigenvectors of the small-world networks. First, we characterize the eigenvalue spectrum into different regimes. The central regime corresponds to the critical state eigenvectors and the mixed regime where we found delocalized eigenvectors along with some critical states eigenvectors. Using the multifractal analysis, we find that there exists no significant change in the eigenvalue (λ^+_{TR}) separating the central regime and the mixed regime. Additionally, we notice no significant change in λ^+_{TR} with an increase in N, i.e. for

$N \to \infty$, $\lambda^{+}_{TR}(N) \sim \mathcal{O}(1)$. Further, we demonstrated that the rewiring procedure can be divided into two domains. For small rewiring, $p_r \leq 0.01$, with an increase in the random connections, there exists a continuous enhancement in the localization of the eigenvectors corresponding to the central regime, while for the higher rewiring probability $p_r \geq 0.01$, eigenvectors gradually lose their degree of localization. Interestingly, this change in the behavior of the eigenvectors takes place at the onset of the small-world transition possibly arising due to the fact that for $p_r \leq 0.01$, there exists a decrease in the characteristics path length (r) co-existing with a high clustering coefficient (CC = 3/4). It is well known that a higher clustering drives localization of the eigenvectors. On the other hand, for $p_r \geq 0.01$, there exists a significant decrease in CC with r being small, eigenvectors undergo continuous decrease in the degree of localization with an increase in randomness in connections for $p_r \geq 0.01$. We would also like to emphasize here that distorting the initial regular network topology by rewiring a few connections does not lead to localization of the eigenvectors, instead, it drives them toward the critical states with $0.4 < D_2 < 0.90$. Further, it requires very few rewiring of connections, i.e., a small amount of randomness from the regular structure to achieve the critical states which we have captured here using the IPR statistics. The probability density function of the logarithm of IPR remains the scale-invariant for the critical rewiring probability corresponding to the transition. Our work can be useful to understand various dynamical processes occurring on the small-world networks. For instance, in [61], epilepsy in small-world neural networks was investigated and it was argued that network activities depend on the proportion of long-distance connections. For this particular example, for a small, intermediate, and high proportion of long-distance connections, the network activity was shown to behave as normal, seizure and bursts, respectively. Normal activity was characterized by a low population of firing rates neurons. The Seizure activity was characterized by significantly higher population firing rates while burst activity in the network was characterized by higher firing rates which rise and fall rapidly. A spontaneous active potential in one neuron was shown to lead to the activity in neurons having a common post-

postsynaptic target. Thus, once a wave got initiated, it could give rise to new waves of activity in other regions through long-distance connections. In this chapter, we have shown that for a small proportion of long distance connections ($p_r < 0.01$), eigenvectors are more localized as compared to those for higher p_r values. Thus, it suggests that the probability that if a wave has been initiated will generate another wave through long-distance connections is less since it dies out at the local region perhaps due to constructive interference making this region behave normal. On the other hand, for the intermediate proportion of long distance connections ($0.01 \leq p_r$ < 0.1), the eigenvectors are less localized as compared to those at the small rewiring probability thus there is a finite probability that if a wave is initiated can initiate new waves through the long-distance connections which may lead to seizure. Finally, at higher rewiring probability eigenvectors are again least localized which can lead to burst activity in the network.

Chapter 3

Interplay of diagonal disorder and randomness on localization

3.1 Introduction

In chapter 2, we studied the localization induced due to disorder in topology but we didn't introduce diagonal disorder in the adjacency matrix. In this chapter, along with distorting the initial regular topology, we introduce diagonal disorder in the adjacency matrix. Thus, rewiring parameter p_r quantifying randomness allows us to investigate the effect of the interplay of diagonal disorder and randomness caused by the occurrence of ones in off-diagonal elements representing pair-wise connections on localization. We hire eigenvalue ratio statistics of random matrix theory (RMT) to investigate the localization-delocalization transition upon increasing the strength of diagonal disorder. RMT first came conceived during the 1950s when E. Wigner envisioned that the complex Hermitian operator of heavy nuclei could be replaced by random matrices whose elements are chosen randomly from some distribution [78]. He and others proposed that the statistical properties of the eigenvalue spectrum of random matrices should mimic the original system under consideration without any detailed knowledge of the structure and show universality with the appropriate symmetry class of the system. There exist exactly three symmetry classes; Gaussian orthogonal ensemble (GOE) for real, Gaussian unitary ensemble (GUE) for complex, and Gaussian symplectic ensemble (GSE) for quaternionic random numbers. The GOE matrices remain invariant under orthogonal transformation, i.e., $A \to Q^{-1}AQ$ for any orthogonal matrix Q. Correspondingly, the other two symmetry classes remain invariant under unitary and symplectic transformations, respectively. Random matrix theory (RMT) found its application in different areas of research; statistical physics [79], quantum chaos [80], and condensed matter physics [81]. For example, in tight binding models, it is used to characterize localized and delocalized states [81]. In quantum systems, RMT is often used to identify if the system is integrable, chaotic, or a mixture of both of them [80].

In the RMT framework, one usually compares the spectral fluctuation of the system with those predicted by RMT [82]. The nearest neighbor level spacings, defined as the difference between the consecutive eigenvalues of the given operator, is the most accepted spectral measure. However, to compare the spectral fluctuations, one needs to unfold the original eigenvalues to separate the smooth global part and fluctuating local part (system dependent), and then spacings are calculated on the unfolded eigenvalues [83]. Usually, unfolding procedures are not unique and non-trivial, which can lead to misleading statistical results [84, 85]. For instance, in the case of the Bose-Hubbard model at considerable interaction strength, the density of states is not a smooth function of energy, and it becomes non-trivial to separate them into the smooth global part and fluctuating local part [86]. Oganesyan and Huse solved this impediment of unfolding by introducing a new measure called the ratio of consecutive eigenvalue spacings (r), independent of the local density of states and hence requiring no unfolding [44]. Additionally, it is easy to compute it with a lower computational cost.

Moreover, RMT has been extensively used in network science to capture phase transition and study various phenomena. For example, using spectral statistics, localization transition was studied for ER random network, Cayley tree, and Barabasi-

Albert scale-free networks [29]. The value of critical disorder as a function of average degree for Anderson transition was calculated for these model networks using the distribution of eigenvalue spacings. Further, to obtain a clear Anderson transition, a low value of the average degree as a threshold was proposed, above which no clear Anderson transition could occur for any of these networks. However, the absence of a transition could also be attributed to the small size of the considered networks. In Ref. [28], using the level statistics, it was shown that Anderson-like transition can be obtained in complex networks without a diagonal disorder and just by tuning the clustering coefficient. In Ref. [87], RMT was applied on random geometric graphs (RGG), and it was found that as a deterministic connection parameter increases, eigenvalue spacing shows a gradual transition from the Poisson to the GOE statistics. Also, spectral analyses have been carried out for random networks with an expected degree and β-skeleton graphs [88, 89]. Further, Ref. [90] has shown the universality of nearest neighbors spacing distribution $(P(s))$ with network size by calculating the Brody parameter for random networks. However, it did not investigate the impact of variation in the strength of diagonal disorder on spectral properties of complex networks.

Here, we study the localization-delocalization transition with the increasing strength of the diagonal disorder in the adjacency matrix In Anderson's model [1], the diagonal disorder in the Hamiltonian matrices depicts the onsite potential of different sites. Diagonal disorders in complex networks, i.e self-loops in the graph representation, may represent various intrinsic properties of the nodes, and depending upon the system under consideration, they may carry different physical meanings. For example, in the case of excitatory dynamics of photosynthesis molecules, the diagonal disorder corresponds to the excitation energies of pigment molecules in different protein environments or imperfect fabrication of the structures [91–93]. In an economic model with nodes representing firms and links representing interactions between firms in terms of their production, the diagonal disorder corresponds to the productivity of each firm [21]. Another example is optical systems where diagonal disorder is akin to variations in the refractive indices of the optical fibers, and connections represent the random position of the fibers [94–96].

Further, note that the term 'distribution of the ratios of consecutive eigenvalue spacing' and 'eigenvalue ratio statistics' will mean the same in this chapter and be used interchangeably. The eigenvalue ratio follows GOE statistics for all the model networks, namely small-world, ER random, and dis(assortative) ER networks. We show that upon increasing the strength of the diagonal disorder in the adjacency matrix of a network, the eigenvalue ratio statistics gradually depicts a transition from the GOE to the Poisson statistics. However, for small-world networks, the critical disorder needed to obtain the Poisson statistics increases with an increase in the value of the rewiring probability. Additionally, we probe the impact of degree-degree correlation or (dis)assortative degree mixing of networks on eigenvalue ratio statistics. We further relate the critical disorder required to obtain the Poisson statistics with the transient dynamics of a random walker.

The chapter is organized as follows. Sec. 4.2 consists of definitions of eigenvalue spacing ratio, construction of model networks, and measure of localization. Secs. 4.4 and 4.5 contain results about the effect of the interplay of disorder and randomness on the eigenvalue ratio statistics for various model networks. Sec. 4.6 relates the critical disorder which is required to obtain the GOE to Poisson transition with the dynamics of the maximally entropy random walker. Finally, Sec. 3.4 concludes the chapter.

3.2 Methods and Techniques

A network denoted by $G = \{$V,E$\}$ consists of set of *nodes* and *links*. The set of *nodes* is represented by $V = \{v_1, v_2, v_3, \ldots, v_N\}$ and *links* with $E = \{e_1, e_2, e_3, \ldots, e_M\}$ where N and M are sizes of V and E respectively. Mathematically, a network can be represented by its adjacency matrix A whose elements are defined as $A_{ij} = 1$ if node i and j are connected and 0 otherwise. The eigenvalues of the adjacency matrix A are denoted by $\{\lambda_1, \lambda_2, \lambda_3, \ldots, \lambda_N\}$ where $\lambda_1 \geq \lambda_2 \geq \ldots \geq \lambda_N$.

We perturbed the adjacency matrix (A) by adding a diagonal matrix. The new adjacency matrix becomes $A' = A + D$, where D is a diagonal matrix added to the original adjacency matrix. The diagonal elements of D i.e. D_{ii} are random numbers drawn uniformly from a box distribution between $(-w, w)$ with a width $2w$. We probe the effect of the impact of an increase in the diagonal strength $(2w)$ on the eigenvalue ratio statistics. The eigenvalue ratio statistics is known to be very useful to identify localized and delocalized eigenvectors. Localization of eigenvectors means that few eigenvector entries take very high values compared with the other entries. On the other hand, in the case of delocalized eigenvector, all the entries take almost an equal value. Further, the eigenvalue ratio statistics corresponding to the localized eigenvectors is known to depict the Poisson statistics, while for delocalized eigenvectors, it is known to manifest the GOE statistics [43].

Ratio of eigenvalue spacing: Following Ref. [44], the ratio of consecutive eigenvalue spacing is defined here as

$$r_i = \frac{min(s_{i+1}, s_i)}{max(s_{i+1}, s_i)} \tag{3.1}$$

where $s_i = \lambda_{i+1} - \lambda_i$ is the spacing between eigenvalues λ_{i+1} and λ_i with $i \in (1, 2, 3 \ldots N-1)$. Also, one can verify that $0 < r_i < 1$. Ref. [44] provides only numerical estimation of $P(r)$ for the GOE distribution, and discussions on the other two symmetry classes (GUE and GSE) were lacking. This gap was filled in Ref. [45] where an exact distribution function of r was derived which was not restricted only to GOE but includes GUE and GSE classes as well. The distribution function ($P(r)$) approximating GOE statistics is given as

$$P(r) \sim \frac{54/8 \times (r + r^2)}{(1 + r + r^2)^{5/2}} \tag{3.2}$$

and the theoretical average value of r for GOE and Poisson statistics has been estimated to be equal to 0.53 and 0.38, respectively, with the distribution function for Poisson statistics is given by

$$P(r) \sim \frac{2}{(1 + r)^2} \tag{3.3}$$

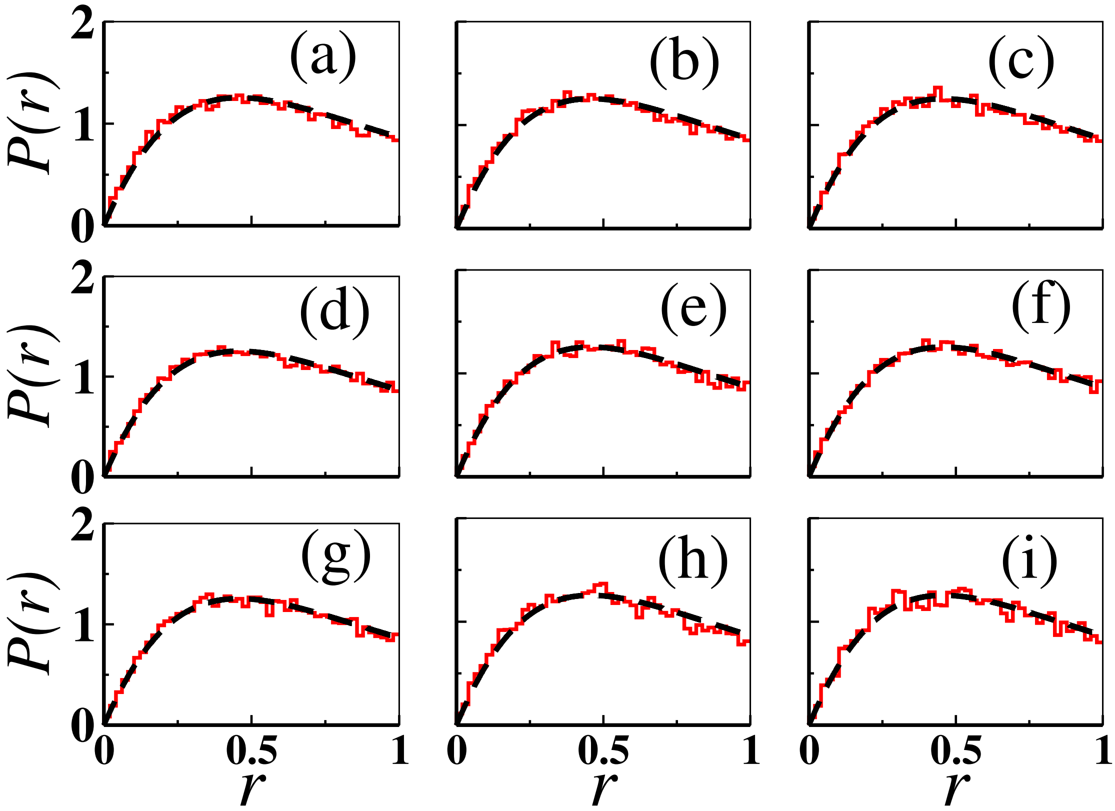

Figure 3.1: (Color online) Distribution of ratio of consecutive eigenvalue spacing for various rewiring probabilities. Black line (dashed) indicates distribution function for GOE statistics and red stairs indicate the data. Here, we have considered $N = 2000$ and $\langle k \rangle = 20$ with 20 network realizations. (a) p_r = 0.001 (b) p_r = 0.002 (c) p_r = 0.005 (d) p_r = 0.01 (e) p_r = 0.02 (f) p_r = 0.05 (g) p_r = 0.1 (h) p_r = 0.5 (i) p_r = 1.

3.3 Results

3.3.1 Eigenvalue ratio statistics of Small-World Networks

We first analyze the eigenvalue ratio statistics for the small-world networks generated using the Watts and Strogatz algorithm. Starting with a 1D lattice, links are rewired with a probability p_r such that $0 \leq p_r \leq 1$. For some intermediate rewiring probabilities, the network undergoes the small-world transition characterized by a high clustering and a shorter average path-length. We numerically diagonalize the adjacency matrix to obtain its eigenvalues. We focus on the eigenvalues on the central part of the spectrum more precisely, inside the width $d\lambda \approx 1.5$ on both sides of $\lambda \approx 0$, a usual practice while analyzing the eigenvalues statistics to localization transition. We wish to emphasize here that a slight increase or decrease in the width does not affect the results which is discussed later. It is evident from Fig. 3.1 that $P(r)$ fits very well with the exact form of the GOE statistics (Eq. (3.2)) for all the values of the rewiring probability. We then calculate the average value of r numerically using Simpson's rule, which comes out to be around 0.52 for all p_r values and thus validate the GOE statistics. We would also like to mention here that a similar observation was found through the distribution of eigenvalue spacings in Ref. [97]. The authors had shown a change in the Brody parameter (β) value with the rewiring probability, finally leading to the GOE transition at the onset of the small-world transition. However, in [97], authors had considered the entire eigenvalue spectrum to depict the GOE transition, whereas the present study focuses only on the central part of the eigenvalue spectrum which shows the GOE statistics for all p_r values.

Disorder vs. randomness: Let us now discuss results when the diagonal disorder is introduced in the adjacency matrix. An increase in w leads to a gradual transition from the GOE to the Poisson statistics, as depicted in Fig. 3.2. However, the critical disorder w_c required to achieve this transition increases with the increase in the value of p_r. The change in $\langle r \rangle$ with a change in w for various values of p_r and N is plotted in Fig. 3.3. $\langle r \rangle$ changes its value from $\langle r \rangle \approx 0.52$ for $w = 0$ to $\langle r \rangle \approx 0.38$ for $w = w_c$. However, the value of w_c increases with an increase in p_r. In fact, for higher rewiring probabilities, $p_r(\geq 0.1)$, it requires a much higher value of w_c. To obtain exact w_c, finite-size scaling analysis (FSS) would be required since the critical phenomenon is defined only in the thermodynamic limit ($N \to \infty$). The crossing point of the order parameter should remain the same with a change in the system size [81, 98]. However, as argued in [99], for $d \to \infty$ ($l \sim ln(N)$), finite-size scaling analysis is nontrivial for many systems, for example, random regular or tree-like graphs, and one does not witness any crossing point. The order parameter $\langle r \rangle$ for such cases keeps drifting towards the Poisson statistics with increasing N. Since for small-world networks, $d \to \infty$, we are not performing any FSS analysis

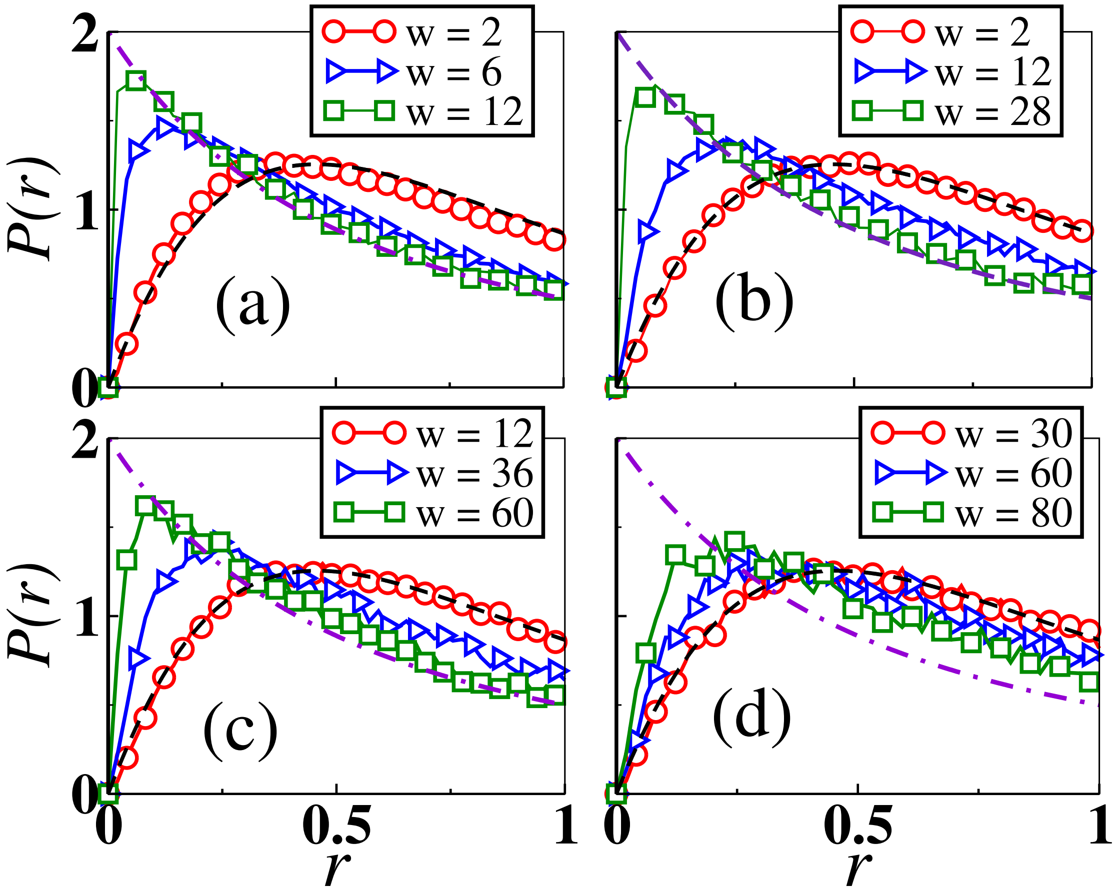

Figure 3.2: (Color online) Distribution of ratio of consecutive eigenvalue spacing of adjacency matrices having diagonal disorder drawn from uniform distribution of width $2w$ for different values of p_r. Black (dashed) and violet (dashed-dotted) lines, respectively indicate GOE and Poisson distribution function. Here, $N = 2000$ and $\langle k \rangle = 20$ with 20 network realizations and 40 disorder realizations. (a) p_r = 0.001 (b) p_r = 0.01 (c) p_r = 0.1 (d) p_r = 1

as it would require networks with very large sizes as done in [100]. Nevertheless, we present the results for $N \leq 32000$, demonstrating a similar trend as in Fig. 3.3.

Further, rewiring affects the adjacency matrix of the initial 1D lattice ($p_r = 0$) in two ways. First, there is a distortion in the diagonal band, and second is the random addition of $ones$ in the off-diagonal entries. Thus, we perform the following experiments to get an insight into which one of these two plays a role in changing the eigenvalue ratio statistics. First, we keep the diagonal band undisturbed and randomly add $ones$ in the off-diagonal entries with a probability p. In this case, the eigenvalue ratio statistics keeps depicting the GOE statistics irrespective of the

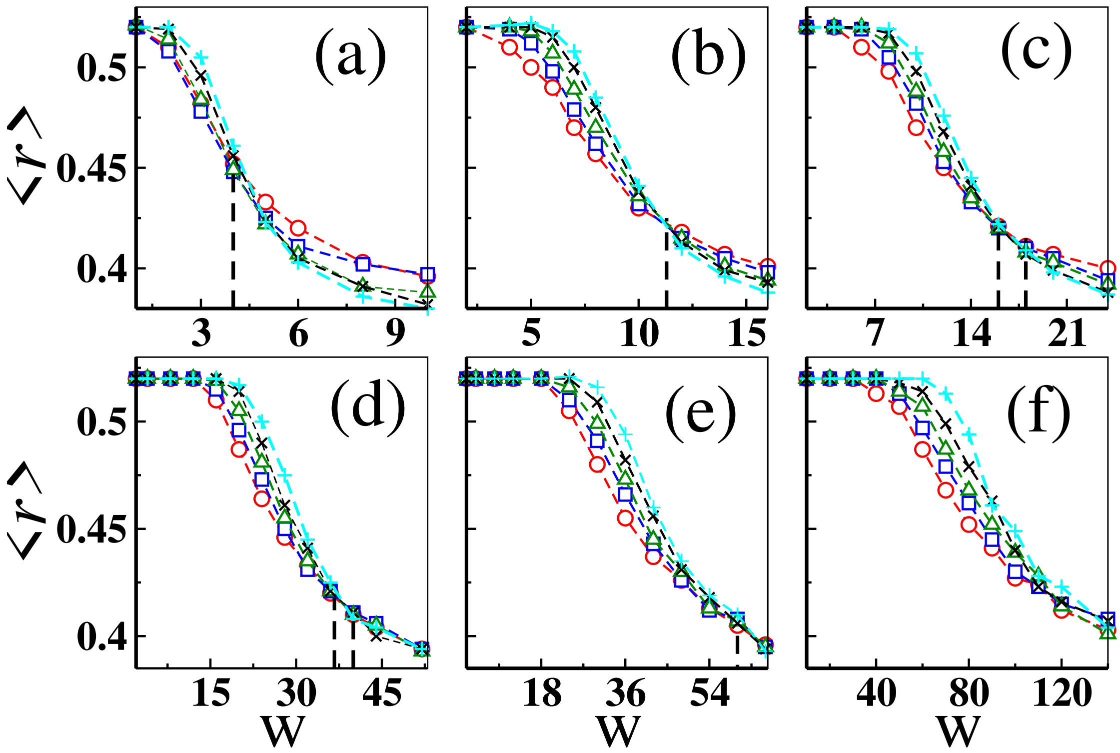

Figure 3.3: (Color online) Plot of $\langle r \rangle$ as a function of diagonal disorder (w) for various rewiring probabilities. $\circ$, $\square$, $\triangle$, $*$ and $+$ symbols are used for $N = 2000, 4000, 8000$, 16000 and 32000 respectively with $\langle k \rangle = 20$. (a) $p_r = 0.001$ (b) $p_r = 0.005$ (c) $p_r = 0.01$ (d) $p_r = 0.05$ (e) $p_r = 0.1$ (f) $p_r = 1$. Vertical lines represent crossing point of $\langle r \rangle$ for different N

probability p and the strength of the diagonal disorder (Fig. 3.4). Here, results are shown only for one value of the diagonal disorder, but the same results for higher diagonal disorder strength have been obtained (see SM).

In the second experiment, we omit the *ones* from the diagonal band uniformly with the probability p and investigate its impact on the eigenvalue ratio statistics. Distorting the diagonal band with a small probability ($p = 0.001$) leads to a change from the GOE statistics for a small disorder strength. In fact, for p = 0.1, even a very small value of w leads to the Poisson statistics (Fig. 3.5). The above observation could be useful to explain the reason behind the increase in the critical value of disorder (w_c) with the increase in p_r. Small p_r values yield small distortions in the diagonal band of the adjacency matrix accompanied by a few filling up of *ones* in the off-diagonal entries. This setup leads to the Poisson statistics for a small w_c as

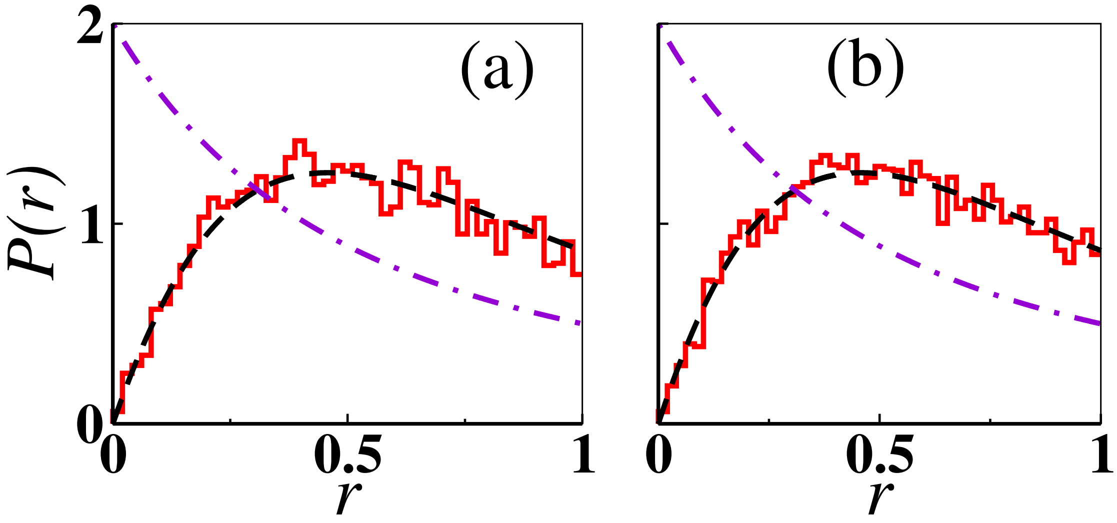

Figure 3.4: (Color online) Distribution of ratio of consecutive eigenvalue spacing with $w = 20$ from uniform distribution of width $2w$ for various probabilities of adding $1s$ in off diagonal entries of the adjacency matrix of 1D lattice. Black (dashed) and violet (dashed-dotted) lines, respectively indicate distribution function from Eq. (3.2) and (3.3) respectively. Here, $N = 1000$ and $\langle k \rangle = 20$ with 20 network realizations and 40 disorder realizations. (a) $p = 0.1$ (b) $p = 0.2$

omitting $ones$ even with a small probability leads to the Poisson statistics. When rewiring probability is increased, though there is a distortion of the diagonal band, sufficient $ones$ have also been randomly distributed in the off-diagonal entries driving to the GOE statistics and thus higher w_c is required.

Impact of change in $d\lambda$: Since we consider the eigenvalues in the central part of the eigenvalue spectrum, specifically those lying in the $d\lambda$ width around the $zero$ eigenvalue, let us discuss the rationale behind taking such an approach and an impact of $d\lambda$ on the results. First, the middle part of the spectrum is appreciably occupied, and the spacings become similar with different network sizes and thus help to reduce the finite-size effect to some extent [101]. On the other hand, at the edges of a spectrum, the eigenvalues are not smooth for smaller N, but for $N \to \infty$, the eigenvalues spectrum becomes continuous, and thus the finite-size effect is more prominent. Second, to choose appropriate $d\lambda$, one has to pick an interval which is statistically sound and at the same time does not mix localized or delocalized eigen-

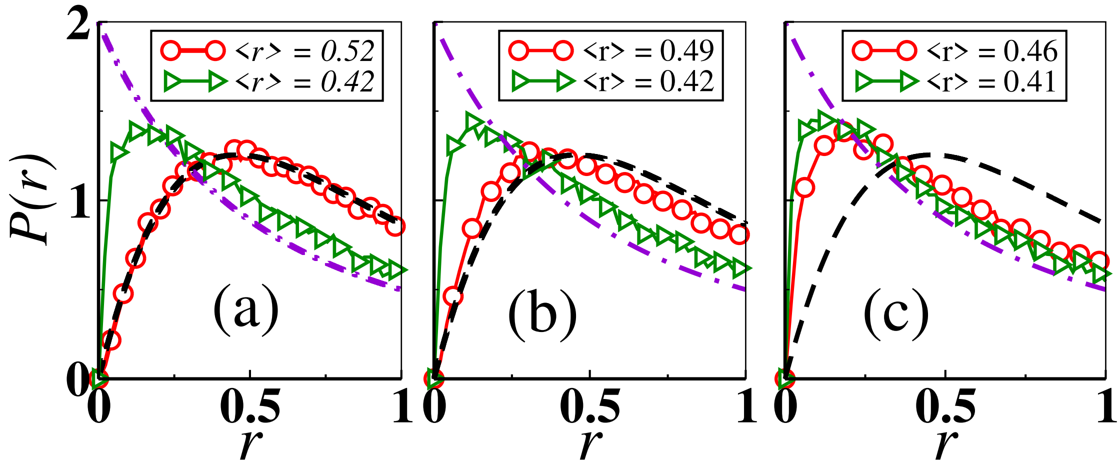

Figure 3.5: (Color online) Distribution of ratio of consecutive eigenvalue spacing with diagonal disorder from uniform distribution of width $2w$ for various probabilities of deleting $1s$ from diagonal band of the adjacency matrix of 1D lattice. ○ and ▷ are used for $w = 1$ and $w = 4$ respectively. Black (dashed) and violet (dashed-dotted) lines, respectively indicate distribution function from Eq. (3.2) and (3.3) respectively. Here, $N = 1000$ and $\langle k \rangle = 20$ with 20 network realizations and 40 disorder realizations. (a) $p = 0.001$ (b) $p = 0.01$ (c) $p = 0.1$

vectors for different values of w [102]. Fig. 3.6 reflects that for $0.25 \leq d\lambda \leq 3$, a slight increase or decrease in the width does not have any noticeable impact on the value of $\langle r \rangle$ (for a given w) for all p_r values. However, for $d\lambda \approx 0.10$, changes in $\langle r \rangle$ with respect to other $d\lambda$ values can be witnessed for higher rewiring probabilities ($p_r \geq 0.1$) (Fig. 3.6[c][d]). It is also important to note that as w increases, there is a shortfall in the number of eigenvalues that are close to $zero$. In fact, we find that for the network parameters considered here, for $w > 70$, even 10^4 random realizations yield a total number of eigenvalues in the order of 10^3 for $d\lambda \approx 0.10$. Thus, it is convenient to take $0.25 \leq d\lambda \leq 3$, in which $\langle r \rangle$ remains statistically sound for the same number of realizations for different $d\lambda$ values. Additionally, we checked using other measures like inverse participation ratio (not shown) that localized-delocalized eigenvectors do not mix in this range. We further add that a decrease in the value of $\langle k \rangle$ for a given N may yield a quantitatively different impact for $d\lambda$, and there could be a larger number of eigenvalues in a given width $d\lambda$.

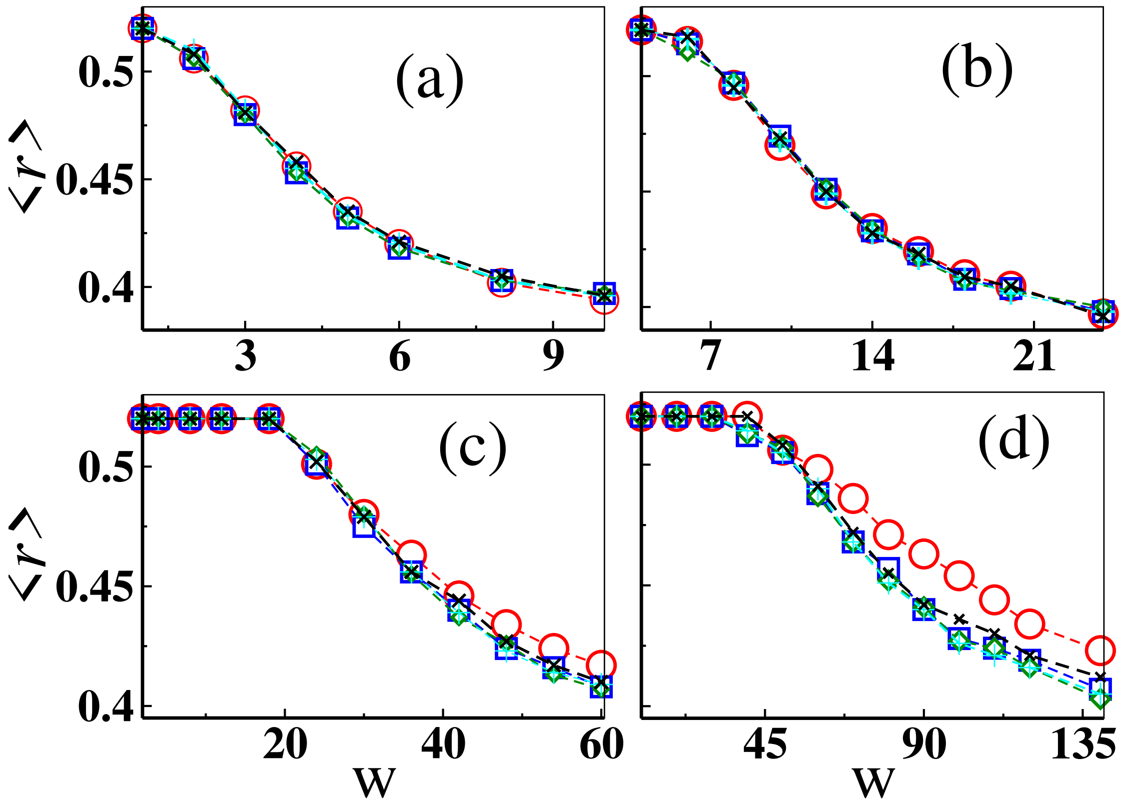

Figure 3.6: (Color online) Plot of $\langle r \rangle$ as a function of diagonal disorder (w) and also with $d\lambda$ for various rewiring probabilities. $\circ$, $*$, $\square$, $\diamond$ and $+$ are used for $d\lambda \approx 0.10, 0.25, 0.50, 1.50$ and 3 respectively. Here, $N = 2000$ and $\langle k \rangle = 20$. (a) $p_r = 0.001$ (b) $p_r = 0.01$ (c) $p_r = 0.1$ (d) $p_r = 1$

Impact of average degree: We further probe the impact of average degree on the statistics of ratios of consecutive eigenvalue spacings. Note that the largest eigenvalue of the network is bound with the largest degree k^{max} [103]. Moreover, for a random network $\lambda_1 \approx \langle k \rangle$. Thus, varying $\langle k \rangle$ may affect the eigenvalue spectrum drastically even for fixed network size. In our analyses, we have considered, $\langle k \rangle = 6, 10$, and 20 with $N = 2000$ being fixed. It is also worth noting that a decrease in the average degree may affect the probability (p_c) at which small-world transition occurs. However, we notice that reducing $\langle k \rangle$ from 20 to 10 does not affect p_c and it remains equal to 0.01. Fig. 3.7 illustrates the change in $\langle r \rangle$ when $\langle k \rangle$ is varied. It is apparent from the figure that when $\langle k \rangle$ is decreased, the critical disorder (w_c) required to procure the transition also decreases for all the values of the rewiring probabilities.

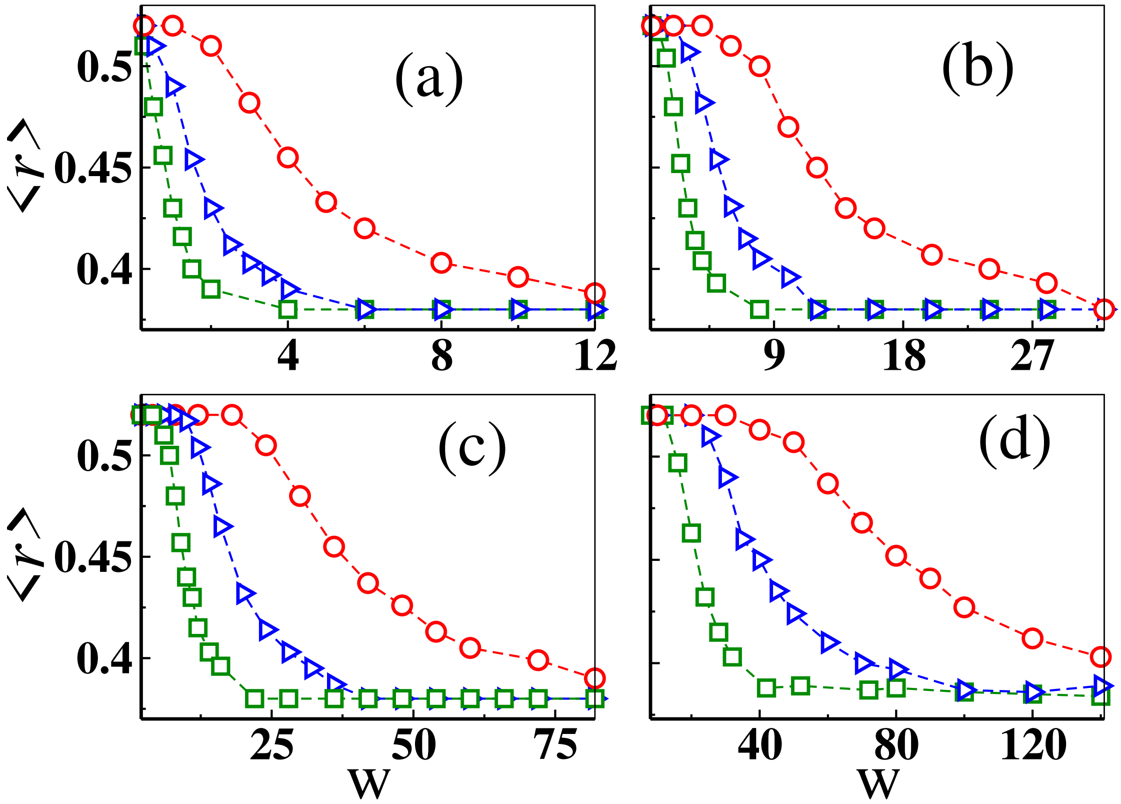

Figure 3.7: (Color online) Plot of $\langle r \rangle$ as a function of diagonal disorder (w) and also with average degree $\langle k \rangle$ for various rewiring probabilities. ○, ▷ and □ are used for $\langle k \rangle = 20, 10$ and 6 respectively. Here, $N = 2000$. (a) $p_r = 0.001$ (b) $p_r = 0.01$ (c) $p_r = 0.1$ (d) $p_r = 1$

3.3.2 Eigenvalue ratio statistics of ER random networks

We now extend the investigation to ER random networks.ER random networks are constructed using ER model [34] as follows. Starting with N nodes and average degree $\langle k \rangle$, each pair of the nodes is connected with a probability $p = \langle k \rangle / N$. The degree distribution of ER random networks follows a binomial distribution. It is also worth noting that small-world random networks with $p_r = 1$ and ER random networks are slightly different in the sense that while the former has fixed links with different realizations, it may change in the latter. Additionally, the small-world random network ($p_r = 1$) retains the initial regular structure ($p_r = 0$) as its memory and degree distribution follow a normal distribution with a peak at $\langle k \rangle$ and small variance. On the contrary, in ER random network, though the degree distribution peak stays around $\langle k \rangle$, the variance is larger than the small-world random networks.

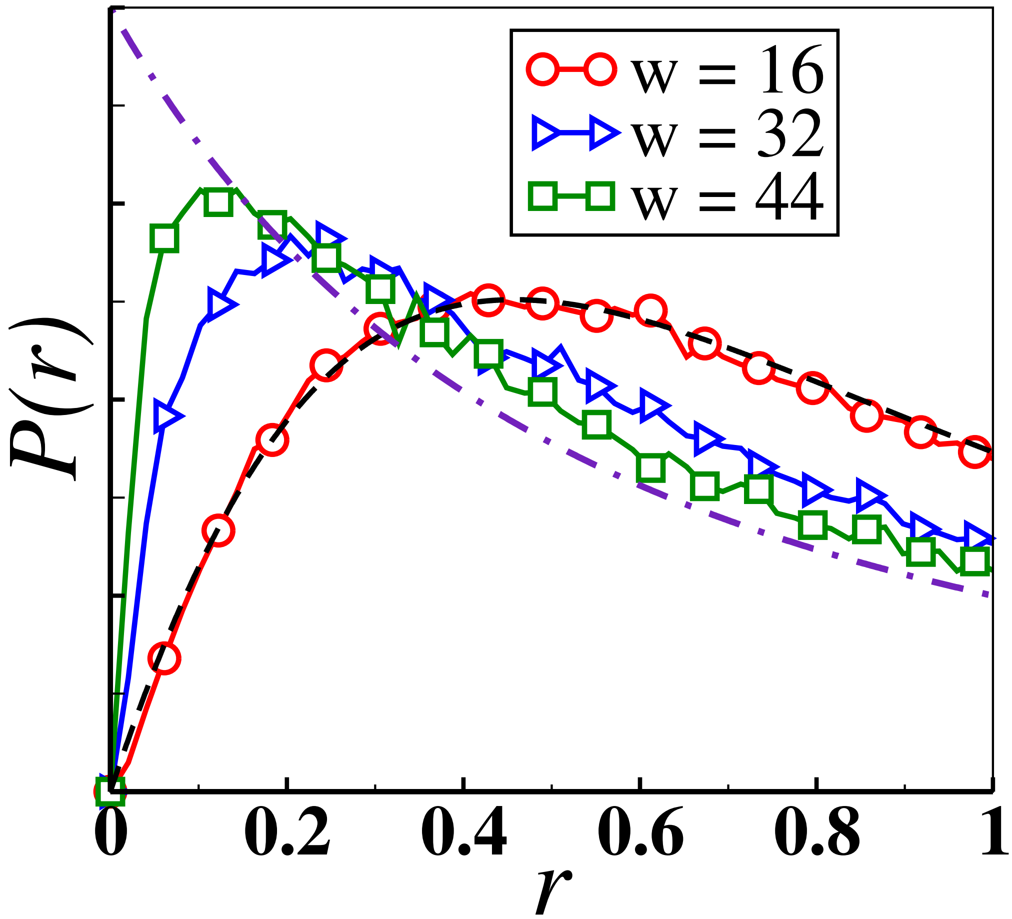

Figure 3.8: (Color online) Distribution of ratio of consecutive eigenvalue spacing for ER random network. Black (dashed) and violet (dashed-dotted) lines, respectively indicate GOE and Poisson distribution from Eq. (3.2) and (3.3) respectively. $N = 2000$ and $\langle k \rangle = 8$ with 20 network and 40 disorder realizations.

It is evident from Fig. 3.8 that, similar to small-world networks, the eigenvalue ratio statistics of ER random networks depict GOE to the Poisson transition with an increase in the diagonal disorder.

Assortative-disassortative networks: The degree-degree correlation is one of the key characteristics of real-world networks [32]. In many real-world networks, like social networks, a node with a high degree tends to connect with similar high degree nodes, commonly known as assortative networks [104]. This characteristic of networks is known as assortativity or assortative mixing. On the other hand, in biological and technological networks, high degree nodes prefer to connect with

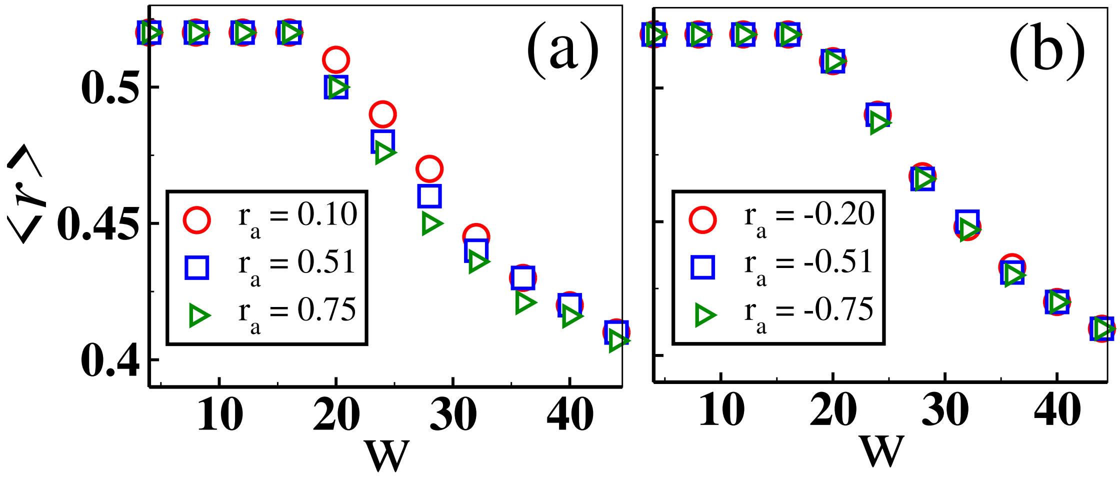

Figure 3.9: (Color online) $\langle r \rangle$ is plotted as a function of w. (a) Assortative ER networks (b) Disassortative ER networks. Here, we have considered $N = 2000$ and $\langle k \rangle = 8$ with 20 network and 40 disorder realizations.

the nodes having a low degree, referred to as disassortative networks, and the property is known as disassortativity or disassortative mixing [105]. To incorporate assortative or disassortative mixing in the original ER random network, we use the reshuffling algorithm [106]. The degree of (dis)assortativity is quantified by the Pearson (degree-degree) correlation coefficient, denoted as r_a where $-1 \leq r_a \leq 1$. For most assortative network r_a will be closer to 1 while for most disassortative network, r_a will be close to -1. Note that the probability distribution of eigenvalues (spectral density) changes drastically with the change in r_a [107]. Thus, it would be interesting to probe eigenvalue ratio statistics for the (dis)assortative ER network.

We considered $N = 2000$ and $\langle k \rangle = 8$ in our analyses. The average degree is kept at this small value to ensure GOE to Poisson transition for a finite value of w otherwise, for larger $\langle k \rangle$, w will be far-reaching. First, we study the distribution of the ratio of consecutive eigenvalue spacing without the diagonal disorder in the adjacency matrix. We find that it follows GOE statistics irrespective of the value of r_a. We next introduce diagonal disorder in the adjacency matrix and study eigenvalue ratio statistics. We find that if the degree of assortativity ($0 \leq r_a \leq 1$) is increased, though there is no significant change in w_c, $\langle r \rangle$ shows slightly lesser values as compared with the corresponding less assortative networks (Fig. 3.9 [a]). On the other hand, with an increasing degree of disassortativity ($-1 \leq r_a < 0$), we do not find its effects on eigenvalue ratio statistics (Fig. 3.9 [b]). It is important to note here that increasing the degree of assortativity leads to a decrease in the randomness, as discussed in [107]. Moreover, changing the degree of disassortativity does not affect the randomness in networks, which is also reflected in our analysis as for any w, $\langle r \rangle$ remains the same with a change in r_a. We want to stress here that randomness induced in small-world networks upon links rewiring is more notable as compared with that brought upon by the (dis)assortative mixing in the ER network [107, 108]. Hence, variation in w_c as a function of p_r is more significant.

3.3.3 Maximal entropy random walk (MERW)

Localization of eigenvectors of the adjacency and Laplacian matrices is known to influence various dynamical processes on the corresponding networks. For example, localization of the principal eigenvector of an adjacency matrix is known to play a pivotal role in disease spreading [19], perturbation propagation in ecological networks [20], etc. However, the exact underlying mechanism remains elusive, particularly such understandings for the non-principal eigenvalues and eigenvectors are missing. Though most of the spectral investigations have revolved around the principal eigenvectors and the corresponding eigenvalue, sporadic investigations indicate that non-principal eigenvectors and associated eigenvalues of the adjacency matrices of networks contribute to the transient relaxation dynamics [24, 25].

This section studies dynamics of maximal entropy random walker (MERW) in various model networks. It then relates its dynamics with the localization (Poisson statistics) and delocalization (GOE statistics) properties of the underlying model networks. MERW was first introduced in [109] where it was argued that MERW localizes in a few nodes, which is not with the case of generic random walk (GRW). To begin with, we first discuss a general framework for the maximal entropy random walk. Let us consider a random walker hopping from node to node on a connected, undirected, unweighted graph $G = \{V,E\}$. At each time step, a walker sitting at any node, say i, jump to its neighboring node j with a probability P_{ij} indicating the probability of jumping of the random walker from the node i to the node j independent of the previous history. Note that, $P_{ij} = 0$, if $A_{ij} = 0$, since a walker can jump to its neighbouring nodes only. The elements of the transition matrix P can be determined as,

$$P_{ij} = \frac{A_{ij}}{\lambda_1}\frac{\psi_j}{\psi_i} \tag{3.4}$$

where λ_1 is the largest eigenvalue of the corresponding adjacency matrix and ψ_j and ψ_i, respectively, are the j^{th} and i^{th} components of the normalized principal eigenvector. The Perron-Frobenius theorem states that all the elements of the principal eigenvector have the same sign, so that $P_{ij} \geq 0$. Also, one can easily see that for each node i, $\sum_j P_{ij} = 1$. One quantity of interest is probability of finding the walker at any node i at a time t denoted as $p_i(t)$. One can easily compute $p_i(t+1) = \sum_j p_j(t)P_{ji}$. After a time t, $p_i(t)$ will reach to a steady state, $p_i^* = \sum_j p_j^* P_{ji}$. One of the most important properties of MERW is that for a given length t and a pair of the end points, say, walker started from node i_o and ends at i_t, all trajectories are equiprobable which is not the case of generic random walkers. For a generic random walk (GRW), $P_{ij} = \frac{A_{ij}}{k_i}$ where k_i is the degree of the i^{th} node. Note that in GRW, trajectories for given length t and given endpoints i_o, i_t, are not equiprobable. Let $\vec{p}(t) = \{p_1(t), p_2(t), p_3(t), \ldots, p_N(t)\}$ be the probability distribution of a random walker on a given network. For a given initial probability distribution of the walker on the graph, ($\vec{p}(0)$) and transition matrix P, one can easily compute the probability distribution of the walker at any time t as,

$$\vec{p}(t) = \vec{p}(0)P^t \tag{3.5}$$

Next, we consider the Shannon entropy S of the walker at each time step t, as

$$S(t) = -\sum_i p_i(t)ln(p_i(t)) \tag{3.6}$$

Note that, $S \to 0$, if the walker is sitting at one node only, say, i_o; $p_{i_o} = 1$ and $p_i = 0$ for all the other nodes. On the other hand, if the probability of finding the walker is equal at each node, $p_i = 1/N$, $S \to ln(N)$. Thus, $0 \leq S \leq ln(N)$. Also, in large time t, $S(t)$ will reach to the steady state, and $S(t+1) = S(t) \approx c$, where c is some constant. In the steady state, probability of finding the walker at different nodes does not change with time. We denote τ be the time taken by the walker to reach

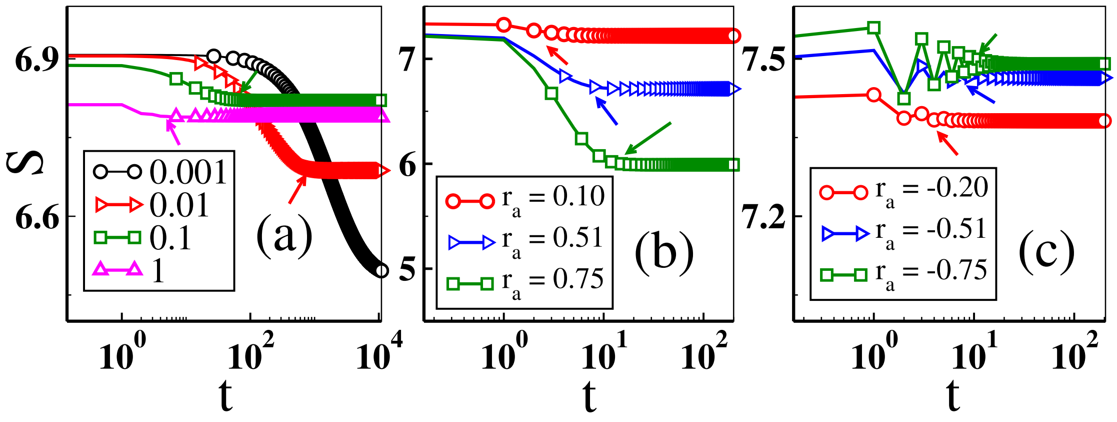

Figure 3.10: (Color online) S as a function of t for various model networks when initial condition is homogeneous distribution, (a) Small-world networks, (b) assortative ER networks, and (c) disassortative ER networks. Here, (a) $N = 1000$ and $\langle k \rangle = 10$ and (b)-(c) $N = 2000$ and $\langle k \rangle = 8$. Arrow indicate position where S hits the steady state.

the steady state starting from a given initial condition. We evolve the random walker following MERW transition matrix on the following model networks; small-world, ER random, and (dis)assortative ER networks. We choose two initial conditions to avoid any predilection in our analysis. (1) In the first case, we choose homogeneous probability distribution for the walker, i.e., the probability of finding the walker at each node is equal to $1/N$ at $t = 0$. We then evolve the walker for a sufficiently long time until it reaches the steady state and calculate S for each time step. (2) We randomly choose a node, say i_0, which acts as the starting point for the random walker with a probability 1.

We first discuss the results for small-world networks. As discussed in the previous section that the critical disorder (w_c) required to procure the Poisson statistics shows an increase with an increase in the value of p_r. Figs. 3.10(a), and 3.11(a) represent the entropy of the random walker against time t for different values of p_r of small-world networks. The time τ after which the random walker reaches the steady state, i.e., $S \to c$ for $t > \tau$ decreases with the increase in p_r for both cases of the initial conditions. Thus, $\tau \propto 1/w_c$. This is a crucial observation that may provide important insight into the localization of the random walker. When the walker starts from a randomly chosen node, say i_o, for smaller t, the probability of

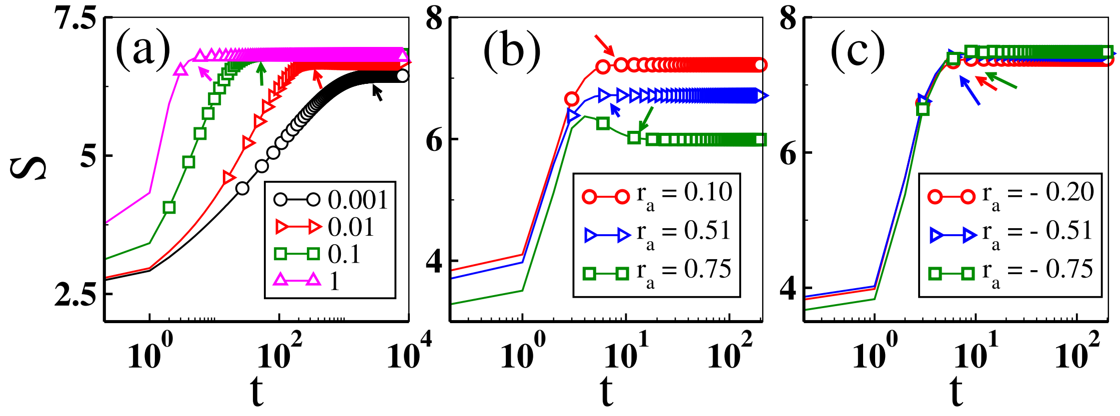

Figure 3.11: (Color online) S as a function of t for various model networks when a random walker starts from a randomly chosen node with probability 1; (a) small-world networks, (b) assortative ER networks, and (c) disassortative ER networks. Other parameters are same as Fig. 10.

finding the walker is finite only for the nodes which are neighbors of i_0. However, for larger t, there is a finite probability of finding the walker on any node. Further, for $t \geq \tau$, $p_i > 0 \; \forall i \in \{1, 2, 3 \ldots, N\}$ and does not change with time. Next, for smaller values of the rewiring probability, τ is very high, and thus even after a larger t, the probability of finding the walker on most of the nodes remains $p_i \to 0$. On the contrary, for higher values of the rewiring probability, τ is very small. Hence, the probability of finding the walker on all the nodes of the network becomes finite even for a shorter t. Therefore, the probability of finding the walker being finite for all the nodes (for small t), we would need a higher disorder strength to localize it on a limited set of the nodes, as is the case for the high p_r values. On the other hand, if the probability of finding the walker remains nonzero only for the few nodes even after a long time, a low diagonal disorder strength would be enough to localize the walker as it still remains in the purview of a few nodes, which is the case of small p_r values.

We further extend this analyses to the (dis)assortative ER networks. As apparent from Figs. 3.10 (b) and 3.11 (b), the value of τ increases with assortativity which is consistent with the earlier observation of $\tau \propto 1/w_c$. Further, for disassortative networks, as discussed earlier, there exists no visible effect of disassortativity ($-1 \leq r_a < 0$) on the eigenvalue ratio statistics (Fig. 3.9[b]). From Figs. 3.10 [c], 3.11 [c], it is visible that the change in the value of τ remains insignificant as $\langle r \rangle$ is unchanged with the change in value of r_a for disassortative networks.

3.4 Conclusion

To conclude, we studied the eigenvalue ratio statistics of various model networks. For the small-world networks, we find that as the strength of diagonal disorder increases, the eigenvalue ratio distribution depicts a gradual transition from the GOE to the Poisson statistics. However, the critical disorder (w_c) required to obtain the transition increases with the increase in the value of the rewiring probability. Thus, higher w_c is required to obtain GOE to Poisson transition when randomness in the network increases. Next, we analyzed the impact of change in the network's average degree on the eigenvalue ratio statistics. As expected, a decrease in the average degree leads to a decrease in the value of the critical disorder required to induce Poisson statistics. Next, we extend our analysis to the ER random networks. In this case, also, we found the gradual transition of GOE to Poisson statistics upon the introduction of diagonal disorder. Finally, to check the effect of degree-degree correlation, we perform (dis)assortative mixing in the original ER random network. Interestingly, we find that an increase in the degree of assortativity leads to a slight decrease in the value of $\langle r \rangle$ for a given w. On the other hand, when the degree of disassortativity increases, there is no noticeable impact on the eigenvalue ratio statistics. Further, we relate the value of the critical disorder (w_c) with the time taken by the maximal entropy random walker to reach to the steady state. The lower the w_c (for fixed N and $\langle k \rangle$), the higher time is taken by the walker to reach the steady state. Further, we argued that when the walker has reached the steady state, the probability of finding it on all the nodes becomes finite. For small τ, the walker would be able to access all the nodes in a sufficiently shorter time, and thus it requires a high value of the diagonal disorder strength to make the network localized. On the other hand, for sufficiently longer τ, probability of finding the walker remains finite on a few nodes, and consequently, a low w_c would be enough to make it localized. Additionally, we have shown the localization of maximal entropy random walker on fewer nodes with increasing strength of diagonal disorder in the adjacency matrix and the same trend is found which is obtained from the eigenvalue ratio statistics.

Few previous studies have investigated the implications of extremal eigenvectors localization of adjacency matrices of networks for various dynamical behavior of the corresponding system. For example, in [19], it was shown that if the infection rate is slightly higher than the threshold and the principal eigenvector is localized, the disease will be localized on a finite set of vertices. Also, recently in [21], the importance of localization of eigenvector corresponding to λ_{min} was discussed. The authors argued that the stability of the system will depend on the localization nature of the eigenvector corresponding to λ_{min}. Furthermore, importance of the spread of the bulk part of the eigenvalues spectrum with an increase in the diagonal disorder for steering localization behavior of eigenvector corresponding to λ_{min} was also argued by the authors. Additionally, in [26, 27], communities in real-world networks were characterized/identified using RMT and properties of highly localized eigenvectors. However, the exact applications of non-principal eigenvalues and corresponding eigenvectors is still missing in the network science literature except that they are known to be contributing in transient dynamics. In this work, we analyze the localization-delocalization transition using the eigenvalue ratio statistics and its implications for the maximally entropy random walkers. The eigenvalue ratio statistics is already a popular technique in condensed matter research for capturing the localization-delocalization transition in various systems and in regular graphs. We anticipate that the eigenvalue ratio statistics has the same scope in network science and can be used to capture or quantify different phase transitions, as well as to get insight into various dynamical processes like disease spreading, random walker, evolutionary dynamics, etc. We further expect that our work can be applied to the systems having diagonal disorders, such as [21, 110, 111] which can be characterized by the underlying network structure.

Chapter 4

Origin of localization in hypergraphs

4.1 Introduction

In the last two chapters, we studied the localization properties of eigenvectors of small-world networks with and without diagonal disorder in the adjacency matrix having only binary interactions. However, with the increasing accumulation of data, it has been realized that often real-world interactions occur among more than two nodes at a time, while the network theory is best described for the binary relationship between nodes [112]. Thus, the inefficacy of networks to model many-body interactions compelled researchers to look beyond the realm of pair-wise interactions and develop appropriate higher-order models. The two most popular approaches for modeling higher-order interactions are hyper-graphs [113, 114] and simplicial complexes[115–117] .

Hypergraphs, capturing higher-order interactions, provide a more generalized model for real-world complex systems. A hypergraph consists of nodes and hyperedges; a hyperedge connects d nodes at a time where typically $d \geq 2$. The size of the hyperedges of a hypergraph may differ, but if all the hyperedges consist of the same number of nodes d, it is referred to as $d-$uniform hypergraph. Thus, a $2-$uniform hypergraph would correspond to conventional graphs. Hypergraphs have been successfully used to model various real-world interactions such as biological [118, 119], social [120, 121], evolutionary dynamics [122, 123], etc. A simplicial complex is a special type of hypergraph which is closed under the subset operation. A simplicial complex not only consists of nodes and links but also incorporates structures of higher-order dimensions, like triangles, tetrahedrons, etc. Accordingly, a $k-$simplex describes simultaneous interactions between $k+1$ nodes forming a set $I = \{v_1, v_2, v_3, \ldots v_{k+1}\}$. Thus, $1-$simplex corresponds to pair-wise interactions with $I = \{v_1, v_2\}$, $2-$simplex would mean triangles with $I = \{v_1, v_2, v_3\}$ and so on. A fundamental difference between modeling many-body interactions with the hypergraphs and simplicial complexes is that a $k-$simplex subsumes all the possible $k-1$ dimensions simplices which is not true with the former.

The spectra of Laplacian matrices are known to affect various dynamical processes on networks. For example, spectra of the Laplacian matrices are related to the diffusion and other spreading phenomena on networks [124]. The ratio of the largest to the first non-zero eigenvalue of a Laplacian matrix helps in determining the stability of generalized synchronization in the coupled dynamical system [125, 126]. Further, Refs. [127–129], highlight the existence of relationships among topological, spectral, and dynamical properties of networks. In addition to the eigenvalues, eigenvectors of the Laplacian matrices have also been shown to be useful in providing insight into various structural and dynamical properties of the corresponding systems. In particular, localization of the Laplacian eigenvectors is useful in characterizing or identifying community structures [26, 27], stability of system against external shocks [21], network-turing patterns, [130, 131] etc.

Here, we consider hypergraphs as a higher-order model to probe the localization properties of eigenvectors. We study hypergraphs instead of simplicial complexes as the latter involves complicated combinatorics, and thus the applications are limited to the lower-order dimensions simplexes such as triangles and tetrahedrons [132]. On the other hand, in the case of hypergraphs, the information of

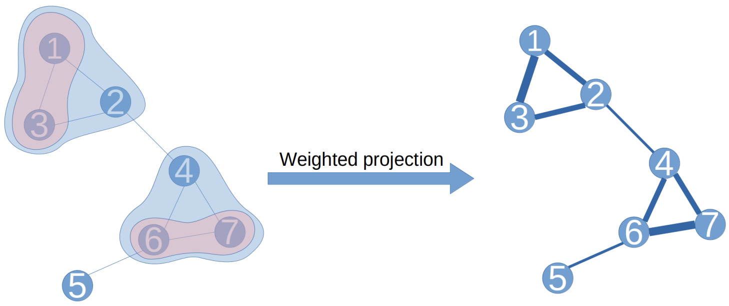

Figure 4.1: (Color online) Schematic diagram representing hypergraphs and corresponding weighted pair-wise projection. Different sizes of the hyperedges are shaped (colored) differently, blue solid circles correspond to for size 3 and pink open circles are for size 2. In the weighted projection, links are weighted according to the size of the hyperedge and the number of the hyperedges containing both the nodes involved.

higher-order structures is installed in a matrix form with the dimension equal to the number of nodes. Further, hypergraphs allow handling heterogeneous sizes of the hyperedges more efficiently than the simplicial complexes. Recent work on hypergraphs includes random walks [132, 135], social contagion [133, 134], synchronization [136–138], evolutionary dynamics [122, 123], etc. Most of these works, revolving around hypergraphs, focus on projecting hypergraphs into their weighted pair-wise networks (Fig. 4.1), and thereupon comparing structural and dynamical properties between the hypergraphs and the projected pair-wise networks. In this work, we take a slightly different approach, and instead of projecting a hypergraph into a corresponding pair-wise network, for each node, we consider contributions from the higher-order and pair-wise interactions and compare these contributions in steering localization of the eigenvectors of hypergraph Laplacians.

The chapter is organized as follows. Sec. 4.2 consists of definitions of the Laplacian matrices of hypergraphs. Sec. 4.3 introduces the hypergraph model. Sec. 4.4 discusses the methodology and techniques involved. Sec. 4.5 contain results about the impacts of the interplay of pair-wise and higher-order links on eigenvector localization. Finally, Sec. 4.6 concludes the study.

4.2 Laplacian Matrix

A hypergraph denoted by $H = \{V, E^H\}$ consists of set of *nodes* and *hyperedges*. The set of *nodes* are represented by $V = \{v_1, v_2, v_3, \ldots, v_N\}$ and *hyperedges* by $E^H = \{E_1, E_2, E_3, \ldots, E_M\}$ where N and M are size of V and E^H respectively. Note that, each hyperedge E_α, $\forall \alpha = 1, 2, \ldots, M$, will contain a collection of nodes i.e. $E_\alpha \subset V$. Thus, when $|E_\alpha| = 2$ for all α, the hypergraph reduces to standard graph. Mathematically, a hypergraph can be represented by its incidence matrix $(e_{i\alpha})_{N\times M}$ whose elements are defined as

$$e_{i\alpha} = \begin{cases} 1 & v_i \in E_\alpha \\ 0 & \text{otherwise}\,. \end{cases} \tag{4.1}$$

One can easily construct, the $N \times N$ adjacency matrix for a hypergraph using Eqn. 4.1, as $A = ee^T$. The entries of the adjacency matrix A_{ij} represents the number of hyperedges containing both nodes i and j. It is important to note here that the adjacency matrix is often obtained by setting 0 to the main diagonal. We would like to further define $M \times M$ hyperedges matrix $C = e^T e$, whose entries $C_{\alpha\beta}$ represent the number of nodes common between hyperedges E_α and E_β.

There does not exist a unique way to define the Laplacian matrix, L, of a hypergraph [112]. One of the conventional way is as follows; $L_{ij} = k_i\delta_{ij} - A_{ij}$ where $k_i = \sum_{j=1}^{N} A_{ij}$ denotes the number of hyperedges containing the node i. However, it is not consistent with the full higher-order structures encrypted in the hypergraph. More specifically, it does not account for the sizes of the hyperedges incident on a node. Ref. [132] solved this limitation by defining a new Laplacian matrix for a random walk which is also consistent with the higher-order structures. The transition probability of the random walker defined in [132] takes care of the size of the hyperedges involved. More precisely, the Laplacian of the random walk defined in [132] is as follows

$$L_{ij}^{RW} = \delta_{ij} - \frac{k_{ij}^H}{\sum_{i\neq l} k_{i\ell}^H}, \tag{4.2}$$

and the entries of K^H matrix are given by

$$k_{ij}^H = \sum_\alpha (C_{\alpha\alpha} - 1) e_{i\alpha} e_{j\alpha} = (e\hat{C}e^T)_{ij} - A_{ij} \quad \forall i \neq j \tag{4.3}$$

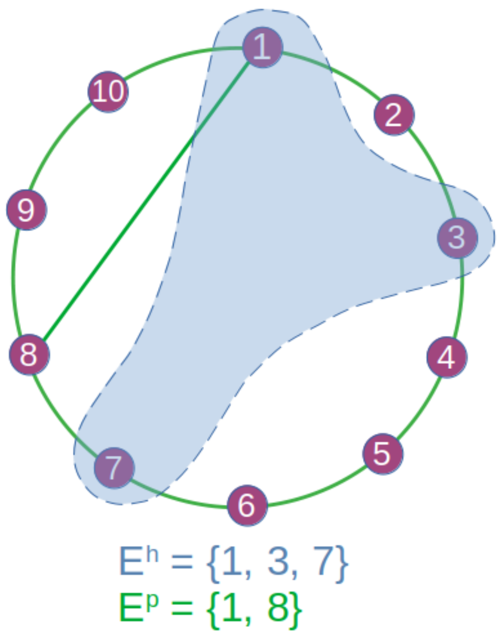

Figure 4.2: (Color online) Schematic diagram of hypergraph model used in the chapter. One pair-wise link, $E^p = \{1, 8\}$ and One hyperedge, $E^h = \{1, 3, 7\}$ are added into the ring lattice with size $N = 10$. The pair-wise links are colored in green and hyperedge with sky-blue enclosing the involved nodes.

where $\hat{C}$ is a matrix whose diagonal entries coincide with that of C and other entries are $zero$. Using Eqs. 4.2 and 4.3 [135], we construct the combinatorial Laplacian matrix for the hypergraph, given by

$$L^H = K^H - D \tag{4.4}$$

Here, D is the diagonal matrix whose entries are $D_{ii} = k_i^H = \sum_{i \neq \ell} k_{i\ell}^H$, and $zero$ otherwise. Note that, in accordance with the earlier convention, $k_{ii} = 0$. The Laplacian matrix is given by Eqn. 4.4 takes into account both the number and size of the hyperedges incident on the nodes and thus incorporates the higher-order structures completely. By considering L^H as a Laplacian of the hypergraph, here we study the effect of higher-order structures on steering the eigenvector localization.

4.3 Model

There are various ways in which a random hypergraph can be constructed [112]. We generate the hypergraph in this work as follows. First, a ring lattice is constructed in which each node is connected to its nearest neighbors on both sides. We then randomly choose d nodes uniformly from all the existing nodes. If already there is no hyperedge comprising of the chosen d nodes, we add a hyperedge consisting of these d nodes. we present here the results for $d = 3$, for each iteration. Next, we add pair-wise links by choosing $d = 2$ nodes uniformly and randomly from the existing nodes. The pair-wise links are added to the model so that an interplay of the higher-order and pair-wise links on the eigenvector localization can be investigated. The schematic diagram of the model is illustrated in Fig. 4.2. Note that, a similar model was also used in [139], but no pair-wise links were added to the original ring lattice. We would like to further mention here that one can choose an alternate algorithm to generate the given model as introduced in [140]. In the alternate approach, for each node, one can choose two other nodes with a probability p, and add hyperedges containing the nodes under consideration. Similarly, one can add pair-wise links by associating one node for a given node. Thus, the total number of hyperedges, and pair-wise links, each, will be equal to pN. However, in one loop only N pair-wise links can be added for $p = 1$. To add more pair-wise links one has to again repeat the entire algorithm. Hence, we use the former algorithm in which the number of pair-wise links and hyperedges are known from the beginning.

4.4 Methods

As discussed earlier, a hypergraph can be represented by its Laplacian matrix L^H. Let the eigenvalues of the Laplacian matrix denoted by $\{\lambda_1, \lambda_2, \lambda_3, \ldots, \lambda_N\}$ where $\lambda_1 \geq \lambda_2 \geq \ldots \geq \lambda_N$ and the corresponding orthonormal eigenvectors as $\{\boldsymbol{x}_1, \boldsymbol{x}_2, \boldsymbol{x}_3, \ldots, \boldsymbol{x}_N\}$. The Laplacian matrix is positive semi-definite, i.e., $\sum_{i,j} L^H_{i,j} x_i x_j \geq 0$ for any vector $\boldsymbol{x} = (x_1, x_2, x_3, \ldots, x_N)$. Therefore, all the eigenvalues of the Laplacian matrix are positive with one and only one being zero for the connected network. The entries of eigenvector corresponding to this $zero$ eigenvalue will be uniformly distributed $(1, 1, \ldots, 1)/\sqrt{N}$. The generalized degree of a node i in the hypergraph is given by k_i^H which can be further decomposed into $k_i^H = k_i^h + k_i^p$ where k_i^h and k_i^p are the contributions from the higher-order and the pair-wise links, respectively. Similarly, the average degree, $\langle k \rangle = \frac{\sum_i k_i^H}{N}$, can be decomposed as $\langle k \rangle = \langle k \rangle^h + \langle k \rangle^p$ where $\langle k \rangle^h = \frac{\sum_i k_i^h}{N}$ and $\langle k \rangle^p = \frac{\sum_i k_i^p}{N}$. We would like to further define $\langle k \rangle$ in terms of total number of the higher-order and pair-wise links as $\langle k \rangle = \frac{2 \times M^p}{N} + \frac{12 \times M^h}{N}$, where M^p and M^h are total number of the pair-wise edges ($d = 2$) and the hyperedges ($d = 3$) in the hypergraph. Also, it is important to note that if a node, say i, gets 1 additional pair-wise links and 1 higher-order links, its degree will be increased by 1 and 4 from the pair-wise and higher-order links, respectively. For example, if we consider the hypergraph depicted in Fig. 4.2, the first row of K^H matrix ($i = 1$) is the following, $K_{1j}^H = [0, 1, 2, 0, 0, 0, 2, 1, 0, 1]$. Notice that, $K_{13}^H = 2, K_{17}^H = 2$ from the hyperedge. Therefore, $k_i^H = 7$ with $k_i^h = 4$ and $k_i^p = 3$. Hence, $k_i^h = 4 \times M_i^h$, where M_i^h is the total number of higher-order links incident on the node i. To provide an equal opportunity to the pair-wise and higher-order links for steering localization on a given node, we introduce the total number of pair-wise links 4 times greater than the higher-order links, i.e., $M^p = 4 \times M^h$ for $k_i^h = k_i^p$. Next, we define a parameter $\gamma = \frac{M^p}{4 \times M^h}$ to measure relative contribution for both the types of the links. Thus, if $\gamma > 1$ then $k_i^p < k_i^h$; if $\gamma < 1$ then $k_i^p > k_i^h$ holds.

We study the localization property of the eigenvectors of the hypergraph and analyze the changes in the localization behavior as the pair-wise and the higher-order links are introduced on the initial ring lattice. Localization of an eigenvector refers to a state where a few entries of the eigenvector have much higher values compared to the others. Degree of localization of the $\boldsymbol{x}_j^{th}$ eigenvectors can be quantified by measuring the inverse participation ratio (IPR) denoted as $Y_{\boldsymbol{x}_j}$. The IPR of an eigenvector $\boldsymbol{x}_j$ is defined as [19]

$$Y_{\boldsymbol{x}_j} = \sum_{i=1}^{N} (x_i)_j^4, \tag{4.5}$$

where $(x_i)_j$ is the i^{th} component of the normalized eigenvectors $\boldsymbol{x}_j$ with $j \in \{1, 2, 3 \ldots, N\}$. One can easily verify that, for the most delocalized eigenvector all its components

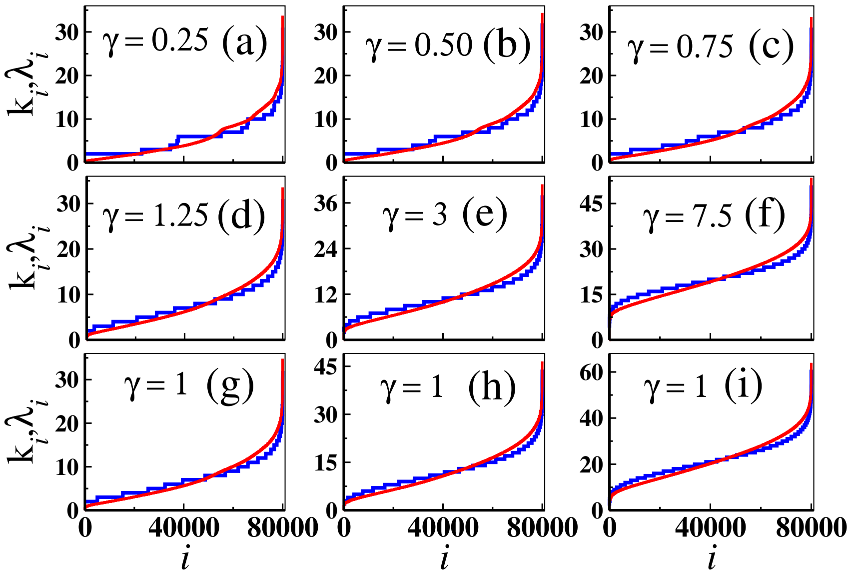

Figure 4.3: (Color online) Laplacian eigenvalues λ_i (red dotted line) and node degree k_i (blue solid line) of hypergraph against index i arranged in a increasing order for the γ values. The size of the hypergraph $N = 2000$ and $M^h = 500$ remain fixed for all γ values with 40 random realizations.

should be equal, i.e., $(x_i)_j = \frac{1}{\sqrt{N}}$, with IPR value being $1/N$. Whereas, for the most localized eigenvector, only one component of the eigenvector will be non-zero, and consequently IPR will be equal to 1. It is also important to note here that there may exist fluctuations in the IPR values for a given state $\boldsymbol{x}_j$ for different realizations. However, it is not possible that λ_j remains the same for all the random realizations, and one has to be very careful in carrying the averaging. So, for the robustness of the results, we consider a small width $d\lambda$ around λ and average all the IPR values corresponding to those λ values which fall inside this small width [40].

We further elaborate on the averaging procedure for the discrete eigenvalue spectrum achieved through the numerical calculations as follow. Let $\lambda^R = \{\lambda_1,\lambda_2, \ldots,\lambda_{N\times R}\}$ such that $\lambda_1 \leq \lambda_2 \leq \ldots \leq \lambda_{N\times R}$ is a set of eigenvalues of the hypergraph for all R random realizations where $N \times R$ is the size of λ^R. The corresponding eigenvector of λ^R are denoted by $\boldsymbol{x}^R = \{\boldsymbol{x}_1, \boldsymbol{x}_2, \boldsymbol{x}_3, \ldots, \boldsymbol{x}_{N\times R}\}$. We then divide λ^R for a given value of $d\lambda$ into further m subsets where $m = (\lambda_{N\times R} - \lambda_1)/d\lambda$. For each $\lambda^j \subset \lambda^R$ and the corresponding eigenvectors $\boldsymbol{x}^j \subset \boldsymbol{x}^R$, $\forall j = 1, 2, \ldots, m$; $\lambda^j = \{\lambda_1, \lambda_2, \ldots, \lambda_{l^j}\}$ and corresponding eigenvector $\boldsymbol{x}^j = \{\boldsymbol{x}_1, \boldsymbol{x}_2, \boldsymbol{x}_3, \ldots, \boldsymbol{x}_{l^j}\}$

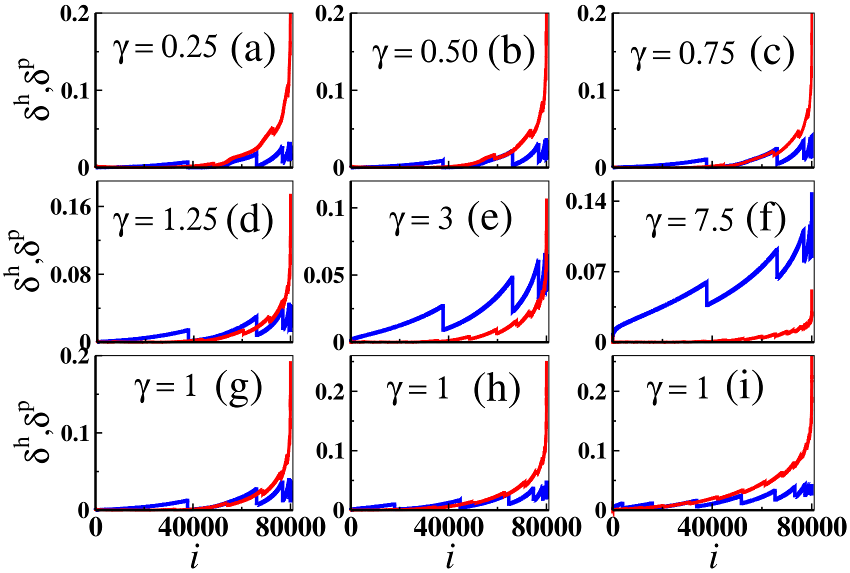

Figure 4.4: (Color online) The relative deviations of eigenvalues from the higher-order degrees, δ_i^h and pair-wise degrees, δ_i^p against index i. The hypergraph parameters, $N = 2000$ and $M^h = 500$, remain fixed for all γ values with 40 random realizations.

where l^j is the size of j^{th} subset such that $\sum_{j=1}^{m} l^j = N \times R$ with a constraint that $\lambda_{l^j} - \lambda_{1^j} \leq d\lambda$. For each subset, the corresponding set of IPRs for $\boldsymbol{x}^j$ will be $\{Y_{\boldsymbol{x}_1}, Y_{\boldsymbol{x}_2}, \ldots, Y_{\boldsymbol{x}_{l^j}}\}$. Hence, the average IPR ($Y_{\boldsymbol{x}_j}(\lambda)$) for each subset $\boldsymbol{x}^j$ can be calculated as $\frac{\sum_{i=1}^{l^j} Y_{\boldsymbol{x}_i}}{l^j}$ where λ is the central value for each subset, i.e., λ + $\frac{d\lambda}{2}$ = λ_{l^j} and λ - $\frac{d\lambda}{2}$ = λ_{1^j}. Here, Here, we define few more physical quantities, $k^h(\lambda)$, $k^p(\lambda)$, $\hat{k}^h(\lambda)$, $\hat{k}^p(\lambda)$ used in the chapter. For any eigenvector $\boldsymbol{x}_j$, these quantities can be calculated as the following.

$k^h_{\boldsymbol{x}_j}$: higher-order degree of the node i_o with the maximum component in $|(x_i)_j|$, i.e., $(x_{io})_j = \max\{|(x_1)_j|, |(x_2)_j|, \ldots |(x_N)_j|\}$

$k^p_{\boldsymbol{x}_j}$: pair-wise degree of the node i_o with the maximum component in $|(x_i)_j|$ i.e. $(x_{io})_j = \max\{|(x_1)_j|, |(x_2)_j|, \ldots |(x_N)_j|\}$

$\hat{k}^h_{\boldsymbol{x}_j}$: higher-order degree expectation value of eigenvector, defined as $\sum_{i=1}^{N}(x_i)_j^2 k_i^h$.

$\hat{k}^p_{\boldsymbol{x}_j}$: pair-wise degree expectation value of eigenvector, defined as $\sum_{i=1}^{N}(x_i)_j^2 k_i^p$.

All these physical quantities follow the same averaging procedures over λ and $\lambda + d\lambda$ as described for IPR and we obtain $k^h(\lambda)$, $k^p(\lambda)$, $\hat{k}^h(\lambda)$, $\hat{k}^p(\lambda)$.

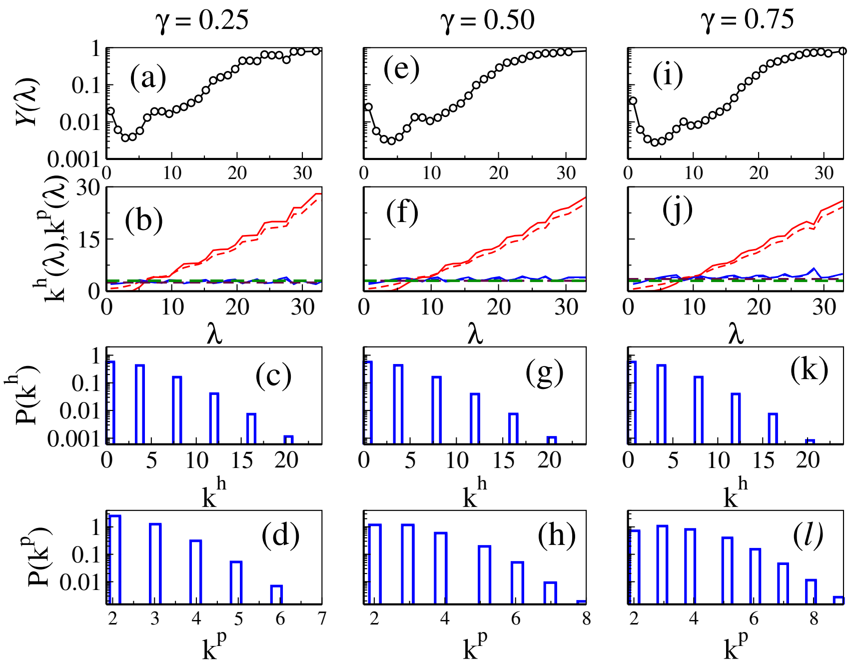

Figure 4.5: (Color online) Average IPR ($Y_{\boldsymbol{x}_j}(\lambda)$) (black), $k^h(\lambda)$ (red), $k^p(\lambda)$ (blue), $\hat{k}^h(\lambda)$(red-dashed), $\hat{k}^p(\lambda)$ (blue dashed) against λ for various $\gamma < 1$. The corresponding higher-order and pair-wise degree distribution are also plotted in last two rows. The green dashed and brown dashed lines are at $\langle k^h \rangle$ and $\langle k^p \rangle$ on y axis. The size of the hypergraph, $N = 2000$ and $M^h = 500$ remain fixed for all γ values with 40 random realizations.

4.5 Results

We first discuss the degree-eigenvalue correlation of the Laplacian of hypergraphs. It was shown for pair-wise interactions [141] that the eigenvalues of the Laplacian matrices have similar distributions as that of the nodes degree. The relative average deviation between the eigenvalues and degrees of a network can be defined as $\frac{||\lambda(L)-k||_2}{||k||_2} \leq \sqrt{\frac{||k||_1}{||k||_2^2}}$, where $\lambda = (\lambda_1, \lambda_2, \dots \lambda_N)^T$ and $k = (k_1, k_2 \dots k_N)^T$ are the eigenvalue set of the Laplacian matrix and node degree set arranged in the increasing order, respectively. The $||y||_p$ represents the p-norms of any vector $y = (y_1, y_2, \dots y_n)$ and is defined as $(\sum_i |y_i|^p)^{\frac{1}{p}}$. Thus, we see that $\sqrt{\frac{||k||_1}{||k||_2^2}} \ll 1$ which implies that eigenvalue distribution and degree distribution will have similar nature. Also, it is well known that $\langle k \rangle = \langle \lambda \rangle$. Fig. 4.3 plots the eigenvalues (λ_i) and degree (k_i^H) of the hypergraph arranged in increasing order with $N = 2000$ and 40 random realizations for various γ values. A clear degree-eigenvalue correlation can

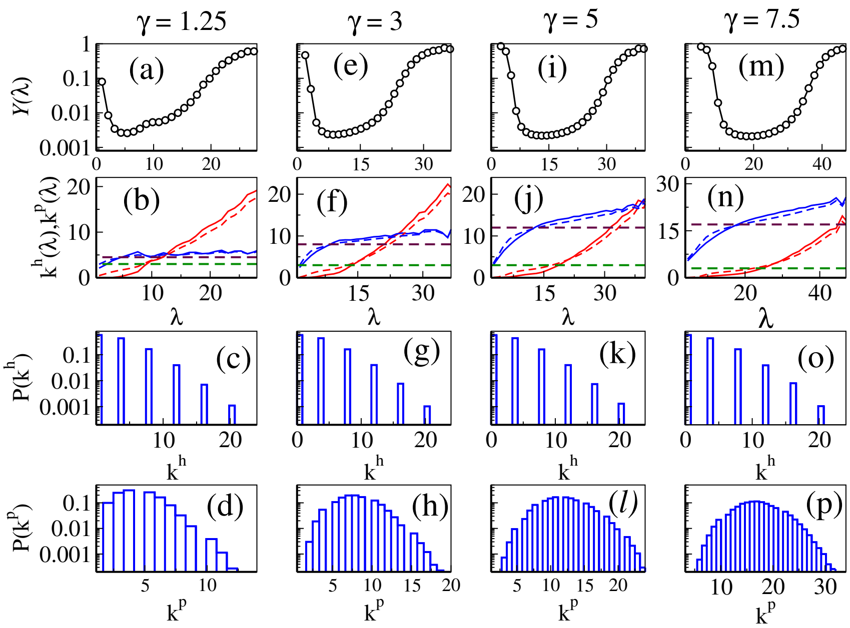

Figure 4.6: (Color online) Average IPR ($Y_{\boldsymbol{x}_j}(\lambda)$) (black), $k^h(\lambda)$ (red), $k^p(\lambda)$ (blue), $\hat{k}^h(\lambda)$(red-dashed), $\hat{k}^p(\lambda)$ (blue-dashed) against λ for various $\gamma > 1$. The corresponding higher-order degree distribution and pair-wise degree distribution are also plotted in last two rows. The green-dashed and brown-dashed lines are at $\langle k^h \rangle$ and $\langle k^p \rangle$ on y axis. The size of the hypergraph, $N = 2000$ and $M^h = 500$ remain fixed for all γ values with 40 random realizations.

be seen similar to the pair-wise networks from the Fig. 4.3.

Next, it is difficult to decompose the eigenvalue λ_i exactly into $\lambda_i^h + \lambda_i^p = f(k_i^h) + f(k_i^h)$, as done for the node degree. Nevertheless, we can put few heuristic arguments as follows. First, we define $\delta_i^h = \frac{(|\lambda_i - k_i^h|)}{\lambda_i}$ and $\delta_i^p = \frac{(|\lambda_i - k_i^p|)}{\lambda_i}$ to analyze the relative deviations of the eigenvalues from the higher-order and pair-wise degrees. Fig. 4.4 plots δ_i^h, δ_i^p against i for various γ values. For $\gamma \leq 1$, for the initial eigenvalues ($\lambda \leq 6$) and index ($i \leq 40000$), $\delta_i^h > \delta_i^p$. Thus, the eigenvalues are more correlated with the pair-wise degree than that of the higher-order degree. Thus, $\lambda_i^h < \lambda_i^p$ and also $k_i^h = 0$ for $i < 40000$ (not shown). For the intermediate eigenvalues, $\delta_i^h \approx \delta_i^p$ and thus $\lambda_i^h \approx \lambda_i^p$. For the extremal eigenvalues and large index, we see that $\delta_i^h \ll \delta_i^p$ and therefore $\lambda_i^p \ll \lambda_i^h$. We further mention here that for the said parameter, i.e., $\gamma < 1$, $M^h = 500$, $k_{max}^p = 10$ and $k_{max}^h = 24$, and therefore for the extremal eigenvalues, the higher-order degrees play a governing role. For $1 < \gamma \leq 3$, $\delta_i^h < \delta_i^p$ for the extremal eigenvalues, since $k_{max}^p < k_{max}^h$, for

$1 < \gamma \leq 3$. However, for $\gamma > 3$, $\delta_i^h > \delta_i^p$ and thus $\lambda_i^h < \lambda_i^p$ for entire eigenvalue spectrum. Next, we discuss the interplay of higher-order and pair-wise links on instigating localization.

For $\gamma < 1$: Figs. 4.5 [a][e][i] plot the results for $Y_{\boldsymbol{x}_j}(\lambda)$ against λ for various values of $\gamma < 1$. The larger eigenvalues in the eigenvalue spectrum ($\lambda > 22$) are localized with $Y_{\boldsymbol{x}_j}(\lambda) \rightarrow 1$. For $\lambda \leq 22$, eigenvalues are relatively less localized as compared with the larger eigenvalues. It is interesting to note here that, there exists no change in the nature of the plot with an increase in γ, depicting the inefficacy of the pair-wise links on instigating localization. Next, it is visible from Figs. 4.5 [b][f][j] that $k^p(\lambda)$ remains constant to a value around $\langle k^p \rangle$ for all the γ values. Further, in [40], it was argued that the localization of a eigenvector is centred on the node with degree either very low or high, i.e., taking values which are from the average degree. One can also note that for a completely delocalized eigenvector, degree expectation value $\hat{k} = \sum_{i=1}^{N}(x_i)_j^2 k_i = \frac{(k_1+k_2+k_3 \ldots k_N)}{N} = \langle k \rangle$. However, upon scrutinizing $k^h(\lambda)$ closely, we find that the its behavior is significantly different from $k^p(\lambda)$. $k^h(\lambda)$ exhibits an increasing trend with the increase in the eigenvalue, and takes the maximum possible value in the localized region. Thus, the eigenvectors are localized on the set of the nodes with k^h being significantly higher than the $\langle k^h \rangle$. Further, in the same plot, $k^h(\lambda)$ and $k^p(\lambda)$ are shown to be in good approximation with the $\hat{k}^h(\lambda)$ and $\hat{k}^p(\lambda)$ values, respectively. We also plot the higher-order degree distribution $P(k^h)$ and pair-wise degree distribution $P(k^p)$ in Fig. 4.5 [c][d][g][h][k][ℓ]. Few interesting observations are; The number of nodes with $k^h > 16$, $k^h > 12$, and $k^h > 8$ are only 0.04%, 0.64% and 4%, respectively and still the eigenvectors are localized on these nodes in the localized region. All these observations clearly suggest prime role of higher-order degree on instigating localization, and rather no visible impact of pair-wise links on the same.

For $\gamma > 1$: Here, we discuss the localization properties of the eigenvectors for $\gamma > 1$. Figs. 4.6 [a][e][i][m] present the results for $Y_{\boldsymbol{x}_j}(\lambda)$ as a function of λ for various values of $\gamma > 1$. The extremal part of the eigenvalue spectrum (larger

Table 4.1: Number of nodes common between the sets $N_o(k^h)$ and $N_o(k^p)$. For $N = 2000$ and 40 random realizations.

	$\gamma = 3$	$\gamma = 5$	$\gamma = 7.5$
$N_o(k^h > 8)$	3227	3212	3193
$N_o(k^h > 12)$	585	582	611
$N_o(k^h > 16)$	78	93	82
$N_o(k^h > 20)$	10	7	13
$N_o(k^p > 8)$	31509	69698	70494
$N_o(k^p > 12)$	3418	582	79400
$N_o(k^p > 16)$	125	6698	428561
$N_o(k^p > 20)$	2	508	14487
$N_o(k^h > 8) \cap N_o(k^p > 8)$	1286	2806	3168
$N_o(k^h > 12) \cap N_o(k^p > 12)$	31	237	532
$N_o(k^h > 16) \cap N_o(k^p > 16)$	0	7	46
$N_o(k^h > 20) \cap N_o(k^p > 20)$	0	0	1

and smaller eigenvalues) are highly localized with $Y_{\boldsymbol{x}_j}(\lambda) \to 1$. On the contrary, the central part of the eigenvalue spectrum are delocalized with $10^{-3} \leq Y_{\boldsymbol{x}_j}(\lambda) < 10^{-2}$. Also, as γ increases the eigenvectors corresponding to the smaller eigenvalues get more localized captured by the IPR value. The nature of the plots is similar to those of the small-world networks (pair-wise) shown in [40]. Further, we report that the eigenvectors are localized on the nodes with degree (k_i^H) being abnormally high or low from the average degree ($\langle k \rangle$), which is in consistent with the observations made in [40, 142].

Next, we discuss the role of pair-wise (k_i^p) and higher-order links (k_i^h) separately on steering the localization. Figs. 4.6 [b][f][j][n] illustrate the results for $k^h(\lambda)$, $k^p(\lambda)$, $\hat{k}^h(\lambda)$, $\hat{k}^p(\lambda)$ for various γ values. For $\gamma = 0.25$, $k^p(\lambda)$ remains constant around $\langle k^p \rangle$, but deviates slightly at the extremal part of the eigenvalue spectrum. On the contrary, $k^h(\lambda)$ manifests an increasing trend with the increase in the eigenvalues and takes large possible values in the localized region of the spectrum. As γ increases, the pair-wise links also start playing role in driving the localization. First, the degree of localization of the eigenvectors corresponding to the smaller eigenvalues enhances. This can be explained as follows. As γ increases, the number of pair-wise links also increases which in turn leads to an increase in $\langle k^p \rangle$. Thus, $k^p(\lambda) \ll \langle k^p \rangle$ for the case of smaller eigenvalues, which consequently intensifies

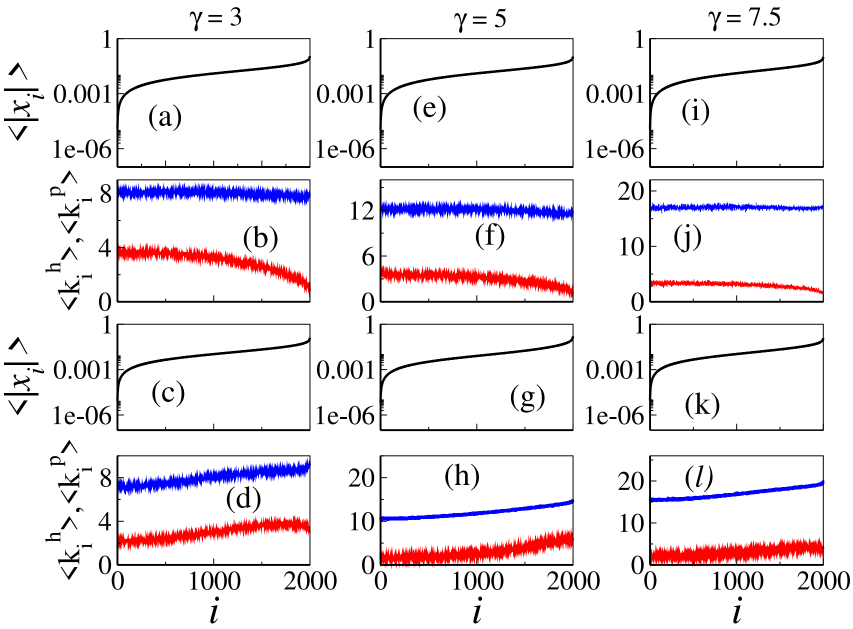

Figure 4.7: (Color online) $\langle|x_i|\rangle$ (black), $\langle k_i^h\rangle$ (red) and $\langle k_i^p\rangle$ (blue) against index i for λ belonging to the delocalized region. (a)-(b) $\lambda \approx 8.5$, (c)-(d) $\lambda \approx 14$, (e)-(f) $\lambda \approx 12.5$, (g)-(h) $\lambda \approx 23.5$, (i)-(j) $\lambda \approx 18$, (k)-(ℓ)$\lambda \approx 26$. The size of the hypergraph, $N = 2000$ and $M^h = 500$ remain fixed for all γ values with 40 random realizations.

the degree of localization. It is important to note that, $\langle k^h\rangle = 3$ remains fixed for all the γ values with the $M^h = 500$. Therefore, $k^h(\lambda)$ for smaller eigenvalues can not be much lesser than $\langle k^h\rangle$, therefore suggesting no visible role of higher-order links in localization for smaller eigenvalues. It is worth mentioning here that a similar result was obtained for degree-eigenvalue correlation.

Next, we discuss the localization properties of the eigenvectors corresponding to those large eigenvalues which are highly localized. From the Fig. 4.6[b][f][j][n], it is visible that for $\gamma \geq 3$, $k^p(\lambda)$ start deviating from $\langle k^p\rangle$, and hence, the pair-wise links also start participating in instigating localization along with the higher-order links. Few interesting things to be noted here are; The number of nodes with large k^h values are always very less as compared to the number of nodes with large k^p values for $\gamma \geq 3$ (Fig. 4.6 [c][g][k][o]). Scrutinizing more closely, we witness that the number of nodes with $k^h > 8, k^h > 12, k^h > 16$ and $k^h > 20$ are roughly around $4\%, 0.73\%, 0.11\%, 0.06\%$, respectively for all γ values. On the other hand. For $\gamma = 3$, the number of nodes with $k^p > 8$ and $k^p > 12$ are 39% and 4.27%,

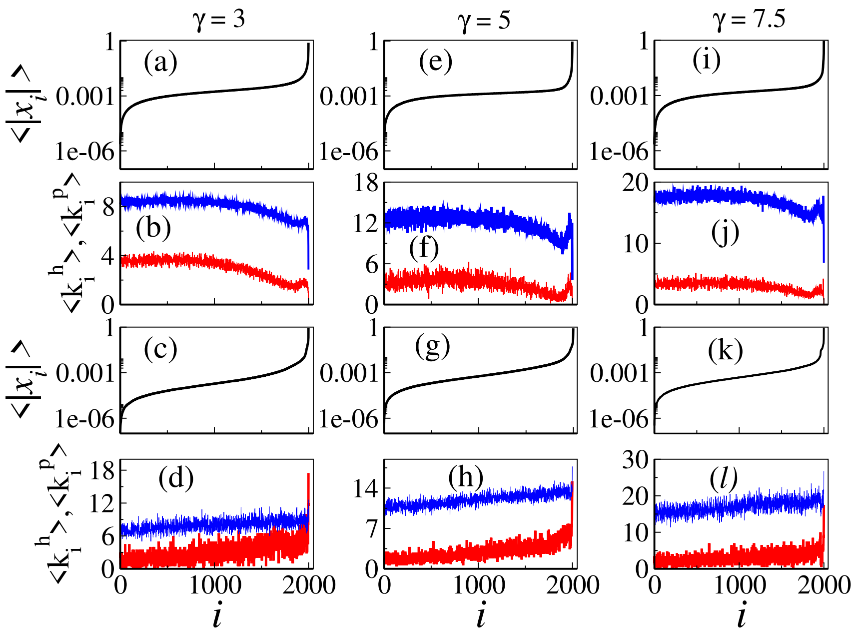

Figure 4.8: (Color online) $\langle|x_i|\rangle$ (black), $\langle k_i^h\rangle$ (red) and $\langle k_i^p\rangle$ (blue) against index i for λ belonging to the localized region. (a)-(b) $\lambda \approx 2$, (c)-(d) $\lambda \approx 33$, (e)-(f) $\lambda \approx 3$, (g)-(h) $\lambda \approx 36$, (i)-(j) $\lambda \approx 5$, (k)-(ℓ)$\lambda \approx 46$. The size of the hypergraph, $N = 2000$ and $M^h = 500$ remain fixed for all γ values with 40 random realizations.

respectively. For $\gamma = 5$, the number of nodes with $k^p > 12$ and $k^p > 16$ are 41% and 8%, respectively. For $\gamma = 7.5$, the number of nodes with $k^p > 16$ and $k^p > 20$ are 53% and 18%, respectively. Therefore, despite the number of nodes with large k^h being very small, the higher-order links still keep playing very crucial roles in steering localization for the larger eigenvalues. To get further insight into the role of higher-order links, we define the following quantities. Let $N_o(k^h > c)$ and $N_o(k^p > c)$ denote the set of nodes with $k^h > c$ and $k^p > c$, respectively. We are interested to find out the number of nodes which are common between these two sets, i.e., $N_o(k^h > c) \cap N_o(k^p > c)$ (Table 4.1). It is evident from the table that total number of nodes in $N_o(k^h > c) \cap N_o(k^p > c)$ is less than 50% of the set $N_o(k^h > c)$ for all γ values and $c > 8$. Therefore, the impact of the higher-order links, over the pair-wise links, in steering localization for larger eigenvalues is apparent more profoundly, which can be attributed to the increase in $\langle k^p\rangle$ value with the increase in γ, while $\langle k^h\rangle = 3$ taking a constant value. Thus, $k^h(\lambda) \gg \langle k^h\rangle$ for the case of large eigenvalues for all the γ values. On the contrary, though the largest pair-wise degree k^p_{max} experience an increase with the increase in γ, at the same-time $\langle k^p \rangle$ also increases, and hence $k^h(\lambda) - \langle k^h \rangle > k^p(\lambda) - \langle k^p \rangle$. We obtain the same results are obtained for $\gamma \leq 15$ (not shown).

So far, we have discussed the localization properties of the eigenvectors by using $k^h(\lambda)$ and $k^p(\lambda)$, and demonstrated that eigenvectors are localized on the node having the degree abnormally high or low either with respect to $\langle k^h \rangle$ or $\langle k^p \rangle$. Also, $k^h(\lambda)$ and $k^p(\lambda)$ come in the good approximation with $\hat{k}^h(\lambda)$ and $\hat{k}^p(\lambda)$. However, it is also important to scrutinize other eigenvector components to obtain the holistic idea of the localization. For this, we calculate the absolute value of the eigenvector components $|x_i|$, the higher-order degree of the corresponding node k_i^h, the pair-wise degree k_i^p, and average them over λ and $\lambda \pm d\lambda$ denoted by $\langle |x_i| \rangle$, $\langle k_i^h \rangle$ and $\langle k_i^p \rangle$. We consider different regions of the eigenvalue spectrum to calculate $\langle |x_i| \rangle$, $\langle k_i^h \rangle$ and $\langle k_i^p \rangle$. For the delocalized region, we consider the λ values where $k^h(\lambda)$ intersects with $\hat{k}^h(\lambda)$, and $k^p(\lambda)$ intersects with $\hat{k}^h(\lambda)$. For the localized region, we take λ from the extremal eigenvalues, i.e., smaller and larger eigenvalues. Fig. 4.7 presents the results for $\langle |x_i| \rangle$ arranged in an increasing order, and corresponding $\langle k_i^h \rangle$ and $\langle k_i^p \rangle$ for two λ values belonging to the delocalized region for various γ values. It is clearly visible that max($\langle |x_i| \rangle$) $\ll 1$ and most of the $\langle |x_i| \rangle$ are in the order of 10^{-2} and 10^{-3}, respectively. It becomes more interesting to look at the behavior of $\langle k_i^h \rangle$ and $\langle k_i^p \rangle$. Both $\langle k_i^h \rangle$ and $\langle k_i^p \rangle$ remain constant to values which are around $\langle k^h \rangle$ and $\langle k^p \rangle$, respectively and thus validating the earlier results. Further, in Fig. 4.8 plots $\langle |x_i| \rangle$, $\langle k_i^h \rangle$ and $\langle k_i^p \rangle$ for λ belonging to the localized region. It is apparent from that max($\langle |x_i| \rangle$) $\to 1$, and only a few entries are in the order of 10^{-1} depicting the localized nature of the eigenvectors. Further, for smaller eigenvalues, $\langle k_i^h \rangle$ remain fixed to the values which lie in the close vicinity to $\langle k^h \rangle \approx 3 \pm 2$ for all i, however, $\langle k_i^p \rangle$ deviates from $\langle k^p \rangle$ and dips down to a value which is lower than $\langle k^p \rangle$ for the node contributing maximum in $\langle |x_i| \rangle$. For the larger eigenvalues, $\langle k_i^h \rangle$ remains constant at around $\langle k^h \rangle$ for the nodes contributing minimal in $\langle |x_i| \rangle$, and takes value much larger than $\langle k^h \rangle$ for the nodes contributing maximal in $\langle |x_i| \rangle$. On the other hand, $\langle k_i^p \rangle$ always keeps oscillating around $\langle k^p \rangle$ for all i, and shows a little deviation for $\langle k^p \rangle$ for large i. The above observations clearly validate the earlier obtained result that localization at smaller eigenvalues is instigated by the pair-wise links, with higher-order links playing a dominant role in inducing localization for larger eigenvalues.

4.6 Conclusion

To conclude, we have investigated the interplay of higher-order and pair-wise links in instigating the localization of the eigenvectors of the hypergraphs. We find that eigenvectors are localized on the set of nodes having degrees very high or low from the average degree, a result which is in consistent with the earlier known result for the networks having only pair-wise interactions. Further, by defining a single parameter γ on a single node, we find that there exists no impact of pair-wise links on localization for $\gamma \leq 1$. For $\gamma > 1$, we find that with increasing γ, the degree of the localization of the eigenvectors corresponding to the smaller eigenvalues increases. Also, the role of higher-order links is not significant as compared to the pair-wise links in inducing localization for smaller eigenvalues. This is due to the fact that $\langle k^p \rangle$ increases with the increase in γ, but $\langle k^h \rangle = 3$ remains to a fixed value. Thus, the higher-order degree of a node contributing maximum in the eigenvector, $k^h(\lambda)$ for smaller eigenvalues is not very small against $\langle k^h \rangle$ for all γ values. On the contrary, the difference between the pair-wise degree of a node contributing the maximum in the eigenvector, $k^p(\lambda)$ and $\langle k^p \rangle$ start increasing with the increase in γ. Ergo, the pair-wise links play a significant role in the eigenvector localization for smaller eigenvalues. Whereas, for larger eigenvalues, the higher-order links play a crucial role in instigating localization despite the fact that the number of nodes with high higher-order degree (k^h) remains very small for all the γ values. This can also be explained in a similar fashion which we adopted for the smaller eigenvalues. As $k^h = 3$ remains fixed to a constant value for all γ values, the difference between $k^h(\lambda)$ and $\langle k^h \rangle$ for larger eigenvalues always remain very high, while for the pair-wise links though the largest pair-wise degree k^p_{max} exhibits an increase with γ, there exists a simultaneous increase in $\langle k^p \rangle$. Therefore, $k^h(\lambda) - \langle k^h \rangle > k^p(\lambda) - \langle k^p \rangle$

for larger eigenvalues which in turn indicates importance of the higher-order links on localization for larger eigenvalues.

Chapter 5

Conclusion and Future Scope

In this dissertation, we have explored the localization properties of eigenvector of complex networks. Though most of the work revolving around localization focus on the extremal eigenvectors. In this thesis, we focus on the localization properties of the non-principal eigenvectors. Non-principal eigenvalue and eigenvectors are known to affect transient dynamics in networks. Further, we considered the small-world networks in our study as the rewiring parameter quantifying randomness allows us to investigate the effect of interplay of diagonal disorder along with topological disorder on localization. In the following, we chapter wise summarize our work.

5.1 Summary

In Chapter 2, We studied the localization behavior of the eigenvectors of the small-world networks arising due to topological disorder. First, we characterize the eigenvalue spectrum into different regimes such as critical state regime, mixed state regime, and delocalized regime. The central regime corresponds to the critical state eigenvectors and the mixed regime where we found delocalized eigenvectors along with some critical states eigenvectors. Using the multifractal analysis, we find that there exists no significant change in the eigenvalue (λ^{+}_{TR}) separating the central regime and the mixed regime. Additionally, we notice no significant change in λ^{+}_{TR} with an increase in N, i.e. for $N \to \infty$, $\lambda^{+}_{TR}(N) \sim \mathcal{O}(1)$. Further, we demonstrated that the rewiring procedure can be divided into two domains. For small rewiring, $p_r \leq 0.01$, with an increase in the topological disorder, there exists a continuous enhancement in the localization of the eigenvectors corresponding to the central regime, while for the higher rewiring probability, $p_r \geq 0.01$, eigenvectors gradually lose their degree of localization. Interestingly, this change in the behavior of the eigenvectors takes place at the onset of the small-world transition, possibly arising due to the fact that for $p_r \leq 0.01$, there exists a decrease in the characteristics path length (r) co-existing with a high clustering coefficient (CC = 3/4). It is well known that a higher clustering drives localization of the eigenvectors. On the other hand, for $p_r \geq 0.01$, there exists a significant decrease in CC with r being small, eigenvectors undergo continuous decrease in the degree of localization with an increase in randomness in connections (or topological disorder) for $p_r \geq 0.01$. Further, we argued that distorting the initial regular network topology by rewiring a few connections does not lead to localization of the eigenvectors. Instead, it drives them toward the critical states with $0.4 < D_2 < 0.90$.

Then, in chapter 3, along with topological disorder, we added diagonal disorder in the adjacency matrix from a uniform distribution of width $2w$. In this chapter, we hire eigenvalue ratio statistics of Random matrix theory (RMT) to study localization-delocalization transition of eigenvectors. We found that as the strength of diagonal disorder increases, eigenvectors go from the delocalized to the localized state captured by the gradual transition of eigenvalue ratio statistics from GOE to Poisson statistics. However, the critical disorder (w_c) required to obtain the transition increases with the increase in the value of the rewiring probability. The above observations infer that the more random a network is, the more resilient it is to diagonal disorder on inducing localization. We also extend our analysis to dis(assortative) ER networks. Interestingly, we find that there is no significant impact of degree-degree correlation on w_c. Further, we relate the value of the critical disorder (w_c) with the time taken by the maximal entropy random walker to reach the steady state. The lower the w_c (for fixed N and $\langle k \rangle$), the higher time is taken by the walker to reach the steady state.

Moving forward to chapter 4, we discussed the origin of localization in hypergraph. Here, we have investigated the interplay of higher-order and pair-wise links in instigating the localization of the eigenvectors of the hypergraphs. We find that eigenvectors are localized on the set of nodes having degrees very high or low from the average degree, a result which is consistent with the earlier known result for the networks having only pair-wise interactions. Further, by defining a single parameter γ on a single node, we find that there exists no impact of pair-wise links on localization for $\gamma \leq 1$. For $\gamma > 1$, we find that with increasing γ, the degree of the localization of the eigenvectors corresponding to the smaller eigenvalues increases. Also, the role of higher-order links is not significant as compared to the pair-wise links in inducing localization for smaller eigenvalues. On the other hand, for larger eigenvalues, the higher-order links play a crucial role in instigating localization despite the fact that the number of nodes with high higher-order degree (k^h) remains very small for all the γ values.

5.2 Future direction

- Many real-world systems can be better understood in the framework of multiplex networks which consist of different layers, and each layer consists of nodes and links. For example, in social systems, each layer can account for different kinds of social ties such as those relatives, friends, social network apps, etc. Additionally, each layer of multiplex networks is connected with each other via multiplexing strength. It can also be realized in our daily life experience, where our behavior in one layer affects the interaction in another layer. Thus, a straight forward extension of our work can be to multiplex networks. It would also be interesting to investigate the impact of multiplex strength on the localization properties of the eigenvectors.

- In this thesis, we have only considered homogeneous networks, and there exists a vast number of real-world networks having heterogeneous degree distributions, for example, scale-free. Thus, one interesting future direction is to extend the present framework for scale-free networks. Also, one can incorporate degree-degree correlation in the scale-free network and study their impact on localization properties of the eigenvectors.

- Further, many real-world systems are also best described as directed networks. Thus, the adjacency matrix of such systems becomes non-hermitian. Thus, the matrix will have both left and right eigenvectors associated with them. Additionally, a few eigenvalues may become complex also. Therefore, a thorough investigation of localization in such networks can be a nice contribution to the localization literature.

- Though small-world networks are very common in a real-world system, there also exist many real-world systems in which interaction can happen only at some specific range, thus, imposing restrictions on the range at which rewiring is possible as defined in [143]. An investigation of the localization behavior of eigenvectors of such networks could be an interesting problem. Note that the network model proposed in [143] controls the dimension of the network (via a range parameter), which plays a vital role in the eigenvector localization.

Bibliography

[1] P. W. Anderson (1958), Absence of diffusion in certain random lattices, *Phys. Rev.*, **109**, 1492 (DOI: 10.1103/PhysRev.109.1492)

[2] PD Antoniou and EN Economou (1977), Absence of Anderson's transition in random lattices with off-diagonal disorder, *Phys. Rev. B*, **16**, 3768 (DOI:10.1103/PhysRevB.16.3768)

[3] K. Tsujino, M. Yamamoto, A. Tokunaga and F. Yonezawa (1979), Numerical results for electron localization with site-diagonal and off-diagonal disorder, *Solid State Commun.*, **30**, 531 (DOI:10.1016/0038-1098(79)91131-1)

[4] F. Yonezawa (1980), Numerical study of electron localization for site-diagonal and off-diagonal disorder, *Journal of Non-Crystalline Solids*, **35**, 29 (DOI:10.1016/0022-3093(80)90568-2)

[5] D.E. Logan and P.G. Wolynes (1987), Dephasing and Anderson localization in topologically disordered systems, *Phys. Rev. B*, **36**, 8 (DOI:10.1103/PhysRevB.36.4135)

[6] D.E. Logan and P.G. Wolynes (1986), Anderson localization in topologically disordered systems: The effects of band structure, *Journal of Chem. Phys.*, **85**, 937 (DOI:10.1063/1.451249)

[7] A. D. Mirlin et al. (2007), Transition from localized to extended eigenstates in the ensemble of power-law random banded matrices, *Phys. Rev. E*, **54**, 3221 (DOI: https://doi.org/10.1103/PhysRevE.54.3221)

[8] K.S. Tikhonov, A.D. Mirlin and M.A. Skvortsov (2016), Anderson localization and ergodicity on random regular graphs, *Phys. Rev. B.*, **94**, 220203 (DOI:10.1103/PhysRevB.94.220203)

[9] M. Sonner, K.S. Tikhonov, A.D. Mirlin (2017), Multifractality of wave functions on a Cayley tree: From root to leaves, *Phys. Rev. B.*, **96**, 214204 (DOI:10.1103/PhysRevB.96.214204)

[10] G.H. Zhang and D.R. Nelson (2019), Eigenvalue repulsion and eigenvector localization in sparse non-Hermitian random matrices, *Phys. Rev. B.*, **100**, 052315 (DOI:10.1103/PhysRevE.100.052315)

[11] F. Slanina (2012), Localization of eigenvectors in random graphs, *Euro. Phys. Journal B*, **85**, 1 (DOI:10.1140/epjb/e2012-30338-1)

[12] G.M. Whitesides and R.F. Ismagilov (1999), Complexity in chemistry, *Science*, **284**, 89 (DOI:10.1126/science.284.5411.8)

[13] R. Foote (2007), Mathematics and complex systems, *Science*, **318**, 410 (DOI:10.1126/science.1141754)

[14] J.K. Parrish and L. Edelstein-Keshet (1999), Complexity, pattern, and evolutionary trade-offs in animal aggregation, *Science*, **284**, 99 (DOI:10.1126/science.284.5411.9)

[15] B. J. kim, H. Hong and M. Y. Choi (2003), Quantum and classical diffusion on small-world networks, *Phys. Rev. B*, **68**, 014304 (DOI: /10.1103/PhysRevB.68.014304)

[16] O. Mülken, V. Pernice and A. Blumen (2007), Quantum transport on small-world networks: A continuous-time quantum walk approach, *Phys. Rev. E*, **76**, 051125 (DOI: 10.1103/PhysRevE.76.051125)

[17] M.A.M Aguiar and Y. Bar-Yam (2005), Spectral analysis and the dynamic response of complex networks, *Phys. Rev. E*, **71**, 016106 (DOI: 10.1103/PhysRevE.71.016106)

[18] J. Aguirre, D. Papo and J.M. Buldú (2013), Spectral analysis and the dynamic response of complex networks, *Nat. Phys.*, **9**, 230-234 (DOI: 10.1038/nphys2556)

[19] A. V. Goltsev, S. N. Dorogovtsev, J. G. Oliveira and J. F. Mendes (2015), Localization and spreading of diseases in complex networks, *Phys. Rev. Lett.* , **109**, 128702 (DOI: /10.1103/PhysRevLett.109.128702)

[20] S. Suweis, J. Grilli, J. R. Banavar, S. Allesina and A. Maritan (2015), Effect of localization on the stability of mutualistic ecological networks, *Nature communications*, **6**, 1-7 (DOI: 10.1038/ncomms10179)

[21] J. Moran and J.P. Bouchaud (2019), May's instability in large economies, *Phys. Rev. E*, **100**, 032307 (DOI: 10.1103/PhysRevE.100.032307)

[22] R. Chaudhuri, A. Bernacchia and X.J. Wang (2014), A diversity of localized timescales in network activity, *elife*, **3**, e01239 (DOI: 10.7554/eLife.01239)

[23] B. Barzel and A.L Barabási (2013), Universality in network dynamics, *Nat. Phys.*, **9**, 673-681 (DOI: 10.1038/nphys2741)

[24] E. V. Nimwegen, J.P. Crutchfield and M. Huynen (1999), Neutral evolution of mutational robustness, *Proc. Natl. Acad. Sci. U.S.A.*, **96**, 9716 (DOI:doi.org/10.1073/pnas.96.17.9716)

[25] J. Aguirre, J.M. Buldú and C.S. Manrubia (2009), Evolutionary dynamics on networks of selectively neutral genotypes: Effects of topology and sequence stability, *Phys. Rev. E*, **80**, 066112 (DOI:10.1103/PhysRevE.80.066112)

[26] V. Plerou et. al. (1999), Universal and nonuniversal properties of cross correlations in financial time series, *Phys. Rev. Lett.*, **83**, 1471 (DOI: 10.1103/PhysRevLett.83.1471)

[27] F. Slanina and Z. Konopásek (2010), Eigenvector localization as a tool to study small communities in online social networks, *Advances in Complex Systems*, **13**, 699 (DOI: 10.1142/S0219525910002840)

[28] L. Jahnke, J. W. Kantelhardt, R. Berkovits, and S. Havlin, (2008), Wave localization in complex networks with high clustering, *Phys. Rev. Lett.*, **101**, 175702 (DOI:10.1103/PhysRevLett.101.175702)

[29] M. Sade, T. Kalisky, S. Havlin and R. Berkovits (2005), Localization transition on complex networks via spectral statistics, *Phys. Rev. E*, **72**, 066123 (DOI:10.1103/PhysRevE.72.066123)

[30] R. Albert and A.L. Barabási (2002), Statistical mechanics of complex networks, *Rev. Mod. Phys.*, **74**, 47 (DOI:10.1103/RevModPhys.74.47)

[31] M.E.J Newman (2003), The structure and function of complex networks, *SIAM review*, **45**, 167–256 (DOI:10.1103/PhysRevE.96.012110)

[32] M.E.J. Newman (2002), Assortative mixing in networks, *Phys. Rev. Lett.*, **89**, 208701 (DOI: 10.1103/PhysRevLett.89.208701)

[33] R.B. Bapat (2010), Graphs and matrices, *springer*, **27**, (DOI: https://doi.org/10.1007/978-1-4471-6569-9)

[34] P. Erdos and A. Rényi (1960), On the evolution of random graphs, *Publ. Math. Inst. Hung. Acad. Sci*, **5**, 17–60 (DOI: 10.1.1.348.530)

[35] D. J. Watts and S. H. Strogatz (1998), Collective dynamics of 'small-world'networks, *Nature*, **393**, 440 (DOI: doi.org/10.1038/30918)

[36] S. Milgram (1967), The small world problem *Psychol. Today*, **2**, 60–67 (DOI:10.1137/S003614450342480)

[37] D. S. Bassett and E. Bullmore (2006), Small-world brain networks, *The neuroscientist*, **12**, 512-513 (DOI: 10.1177/1073858406293182)

[38] J. A. Dunne, R. J. Williams and N. D. Martinez (2002), Food-web structure and network theory: the role of connectance and size, *Proc. Natl. Acad. Sci. U.S.A*, **99**, 12917 (DOI: 10.1073/pnas.192407699)

[39] A.-L. Barabási and R. Albert (1999), Emergence of scaling in random networks, *Science*, **286**, 509-512 (DOI: 10.1126/science.286.5439.509)

[40] R. Monasson (1999), Diffusion, localization and dispersion relations on "small-world" lattices, *The European Physical Journal B-Condensed Matter and Complex Systems*, **12**, 555–567 (DOI: 10.1007/s100510051038)

[41] F. Wegner (1980), Inverse participation ratio in $2+\zeta$ dimensions networks, *Zeitschrift für Physik B Condensed Matter*, **209**, 36 (DOI: 10.1007/BF01325284)

[42] M. Schreiber and H. Grussbach (1991), Multifractal wave functions at the anderson transition, *Phys. Rev. Lett.*, **67**, 607 (DOI: 10.1103/PhysRevLett.67.607)

[43] L. Zhang et. al., (2021), Level statistics and Anderson delocalization in two-dimensional granular materials, *Phys. Rev. B*, **103**, 104201 (DOI:10.1103/PhysRevB.103.104201)

[44] V. Oganesyan and D.A. Huse (2007), Localization of interacting fermions at high temperature, *Phys. Rev. B*, **75**, 155111 (DOI:10.1103/PhysRevB.75.155111)

[45] Y.Y. Atas, E.G.O Bogomolny and G. Roux (2013), Distribution of the ratio of consecutive level spacings in random matrix ensembles, *Phys. Rev. Lett.*, **110**, 084101 (DOI:10.1103/PhysRevLett.110.084101)

[46] Billy et al. (2008), Direct observation of anderson localization of matter waves in a controlled disorder, *Nature*, **453**, 891 (DOI: 10.1038/07000)

[47] S. Fishman, D. R. Grempel and R. E. Prange (1982), Chaos, quantum recurrences and anderson localization, *Phys. Rev. Lett.*, **49**, 509 (DOI: 10.1103/PhysRevLett.49.509)

[48] T. Schwartz et al. (2007), Anderson localization of light, *Nature*, **446**, 52 (DOI: 10.1038/nphoton.2013.30)

[49] G. Casati, L. Molinari and F. Izrailev (2007), Scaling properties of band random matrices, *Phys. Rev. Lett.*, **64**, 1851 (DOI: 10.1103/PhysRevLett.64.1851)

[50] U. Buchenau, Y. M. Galperin, V. Gurevich and H. Schober (1991), Anharmonic potentials and vibrational localization in glasses, *Phys. Rev. B*, **43**, 5039 (DOI: 10.1103/PhysRevB.43.5039)

[51] Y. Gefen, D. J. Thouless and Y. Imry (1983), Localization effects near the percolation threshold, *Phys. Rev. B*, **28**, 6677 (DOI: 110.1103/PhysRevB.28.66771)

[52] C. W. Groth et al. (2009), Theory of the topological anderson insulator, *Phys. Rev. Lett.*, **103**, 196805 (DOI: 10.1103/PhysRevLett.103.196805)

[53] D. E. Logan and P. G. Wolynes (1985), Anderson localization in topologically disordered systems, *Phys. Rev. B*, **31**, 2437 (DOI:10.1103/PhysRevB.31.2437)

[54] B. Bollobás (1988), The chromatic number of random graphs, *Combinatorica*, **8**, 49-55 (DOI: 10.1007/BF02122551)

[55] T. A. Witten and L. M. Sander (1983), Scaling properties of band random matrices, *Phys. Rev. B*, **27**, 5686 (DOI: 10.1103/PhysRevLett.64.1851)

[56] D. S. Callaway, M. E. Newman, S. H. Strogatz and D. J. Watts (2000), Network robustness and fragility: Percolation on random graphs, *Phys. Rev. Lett.*, **85**, 5468 (DOI:10.1103/PhysRevLett.85.5468)

[57] I. M. Sokolov, J. Mai and A. Blumen (1997), Paradoxal diffusion in chemical space for nearest-neighbor walks over polymer chains, *Phys. Rev. Lett.*, **79**, 857 (DOI: 10.1103/PhysRevLett.64.1851)

[58] C. P. Zhu and S. J. Xiong (2000), Localization-delocalization transition of electron states in a disordered quantum small-world network, *Phys. Rev. B*, **62**, 14780 (DOI: 10.1103/PhysRevB.62.14780)

[59] R. Pastor-Satorras and C. Castellano (2016), Distinct types of eigenvector localization in networks, *Scientific reports*, **6**, 18847 (DOI: 10.1038/srep18847)

[60] F. de Moura et al. (2005), Localization properties of a one-dimensional tight-binding model with nonrandom long-range intersite interactions, **71**, 174203 (DOI: 10.1103/PhysRevB.71.174203)

[61] T. I. Netoff et al. (2004), Epilepsy in small-world networks, *J. Neurosci.*, **24**, 8075 (DOI:/10.1523/JNEUROSCI.1509-04.2004)

[62] B. B. Mandelbrot (1974), Intermittent turbulence in self-similar cascades: divergence of high moments and dimension of the carrier, *J. Fluid Mech.*, **62**, 331 (DOI: 10.1017/S0022112074000711)

[63] P. Oświe, J. Kwapień and S. Drożdż (2005), Multifractality in the stock market: price increments versus waiting times, *Physica A*, **347**, 626 (DOI: 10.1016/j.physa.2004.08.025)

[64] F. Schmitt, D. Schertzer and S. Lovejoy (1999), Multifractal analysis of foreign exchange data, *Appl. Stoch. Models. Data Anal.*, **15**, 29 (DOI: 10.1002/(SICI)1099-0747(199903)15:1<29::AID−ASM357>3.0.CO;2−Z)

[65] M. S. Movahed et al. (2006), Multifractal detrended fluctuation analysis of sunspot time series, *J. Stat. Mech.*, **95**, P02003 (DOI: 10.1088/1742-5468/2006/02/P02003)

[66] P. Shang, Y. Lu and S. Kamae (2008), Detecting long-range correlations of traffic time series with multifractal detrended fluctuation analysis, *Chaos, Solitons and Fractals*, **36**, 82 (DOI: 10.1016/j.chaos.2006.06.019)

[67] C. K. Lee (2002), Multifractal characteristics in air pollutant concentration time series, *Water, Air, and Soil Pollution*, **135**, 389 (DOI: 10.1023/A:1014768632318)

[68] P. C. Ivanov et al. (1999), Multifractality in human heartbeat dynamics, *Nature*, **399**, 461 (DOI: 10.1038/20924)

[69] I. Garcia-Mata et al. (2017), Scaling theory of the anderson transition in random graphs: ergodicity and universality, *Phys. Rev. Lett.*, **118**, 166801 (DOI: 10.1103/PhysRevLett.118.166801)

[70] L. Jahnke, J. W. Kantelhardt, R. Berkovits and S. Havlin (2008), Wave localization in complex networks with high clustering, *Phys. Rev. Lett.*, **101**, 175702 (DOI: 10.1103/PhysRevLett.101.175702)

[71] G. Celardo, R. Kaiser and F. Borgonovi (2016), Shielding and localization in the presence of long-range hopping, *Phys. Rev. B*, **94**, 144206 (DOI: 10.1103/PhysRevB.94.144206)

[72] C. Sarkar and S. Jalan (2018), Spectral properties of complex networks, *Chaos: An Interdisciplinary Journal of Nonlinear Science*, **28**, 102101 (DOI: 10.1063/1.5040897)

[73] E. G. Kostadinova, C. D. Liaw, L. S. Matthews and T. W. Hyde (2016), Physical interpretation of the spectral approach to delocalization in infinite disordered systems, *Mater. Res. Express*, **3**, 125904 (DOI: 10.1088/2053-1591/3/12/125904)

[74] F. Evers and A. D. Mirlin (2008), Localization and spreading of diseases in complex networks, *Rev. Mod. Phys.*, **80**, 1355 (DOI: 10.1103/PhysRevLett.109.128702)

[75] F. Evers and A. D. Mirlin (2000), Fluctuations of the inverse participation ratio at the anderson transition, *Phys. Rev. Lett.*, **84**, 3690 (DOI: 10.1103/PhysRevLett.84.3690)

[76] A. V. Goltsev, S. N. Dorogovtsev, J. G. Oliveira and J. F. Mendes (2004), The spectra of random graphs with given expected degrees, *Internet Mathematics*, **1**, 257–275 (DOI: 10.1080/15427951.2004.10129089)

[77] I. Varga (2002), Fluctuation of correlation dimension and inverse participation number at the anderson transition, *Phys. Rev. B*, **66**, 094201 (DOI: 10.1103/PhysRevB.66.094201)

[78] M.L. Mehta (2004), *Random matrices*, Elsevier, Amsterdam, (ISBN:9780080474113)

[79] C.E Porter (1965), *Statistical theories of spectra: fluctuations*, Academic Press, (ISBN:9780125623568)

[80] O. Bohigas, M.J. Giannoni and C. Schmit (1984), Characterization of chaotic quantum spectra and universality of level fluctuation laws, *Phys. Rev. Lett.*, **52**, 1 (DOI:10.1103/PhysRevLett.52.1)

[81] B.I Shklovskii, B. Shapiro, B.R Sears, P. Lambrianides and H.B. Shore (1993), Statistics of spectra of disordered systems near the metal-insulator transition, *Phys. Rev. B*, **47**, 11487 (DOI:10.1103/PhysRevB.47.11487)

[82] F.J. Dyson and M.L Mehta (1963), Statistical theory of the energy levels of complex systems. IV, *J. Math. Phys.*, **4**, 701–712 (DOI:10.1063/1.1704008)

[83] T. Brody et al. (1981), Random-matrix physics: spectrum and strength fluctuations, *Rev. Mod. Phys.*, **53**, 385 (DOI:10.1103/RevModPhys.53.385)

[84] I. O. Morales, E. Landa, P. Stránský and A. Frank (2011), Improved unfolding by detrending of statistical fluctuations in quantum spectra, *Phys. Rev. E*, **84**, 016203 (DOI:10.1103/PhysRevE.84.016203)

[85] G. Torres-Vargas, R. Fossion, C. Tapia-Ignacio and J. C. López-Vieyra (2017), Determination of scale invariance in random-matrix spectral fluctuations without unfolding, *Phys. Rev. E*, **96**, 012110 (DOI:10.1103/PhysRevE.96.012110)

[86] C. Kollath1, G. Roux, G. Biroli and A. M Läuchli (2010), Statistical properties of the spectrum of the extended Bose-Hubbard model, *J. Stat. Mech: Theory and Exp.*, **2010**, P08011 (DOI:10.1088/1742-5468/2010/08/P08011)

[87] C.P. Dettmann, O. Georgiou and G. Knight (2017), Spectral statistics of random geometric graphs, *Europhys. Lett.*, **118**, 18003 (DOI:10.1209/0295-5075/118/18003)

[88] V.M Preciado and M.A Rahimian (2017), Moment-based spectral analysis of random graphs with given expected degrees, *IEEE Trans. Netw. Sci. Eng.*, **4**, 215–228 (DOI:10.1109/TNSE.2017.2712064)

[89] L. Alonso, J.A. Méndez-Bermúdez and E. Estrada (2019), Geometrical and spectral study of β-skeleton graphs, *Phys. Rev. E*, **100**, 062309 (DOI:10.1103/PhysRevE.100.062309)

[90] J.A. Méndez-Bermúdez et al., (2015), Universality in the spectral and eigenfunction properties of random networks, *Phys. Rev. E*, **91**, 032122 (DOI:10.1103/PhysRevE.91.032122)

[91] P. Rebentrost et. al. (2009), Environment-assisted quantum transport, *New J. Phys.*, **11**, 033003 (DOI:10.1088/1367-2630/11/3/033003)

[92] J. Adolphs and T. Renger (2006), How proteins trigger excitation energy transfer in the FMO complex of green sulfur bacteria, *Biophys. J.*, **91**, 2778–2797 (DOI:10.1529/biophysj.105.079483)

[93] K. Jang, J. Seogjoo and B. Mennucci (2018), Delocalized excitons in natural light-harvesting complexes, *Rev. Mod. Phys.*, **90**, 035003 (DOI:10.1103/RevModPhys.90.035003)

[94] R. Berkovits (2008), Localisation of optical modes in complex networks, *The Euro. Phys. J. Spec. Top.*, **161**, 259–265 (DOI:10.1140/epjst/e2008-00766-y)

[95] F. Perakis, M. Mattheakis and G P Tsironis (2017), Small-world networks of optical fiber lattices, *J. Opt.*, **16**, 102003 (DOI:10.1088/2040-8978/16/10/102003)

[96] S. Karbasi et. al (2012), Observation of transverse Anderson localization in an optical fiber, *Opt. Lett.*, **37**, 2304–2306 (DOI: 10.1364/OL.37.002304)

[97] J.N. Bandyopadhyay and S. Jalan (2007), Universality in complex networks: Random matrix analysis, *Phys. Rev. E*, **76**, 026109 (DOI:10.1103/PhysRevE.76.026109)

[98] F. Milde, R.A. Römer and M. Schreiber (2000), Energy-level statistics at the metal-insulator transition in anisotropic systems, *Phys. Rev. B*, **61**, 6028 (DOI: 10.1103/PhysRevB.61.6028)

[99] K.S. Tikhonov, A.D. Mirlin and M.A. Skvortsov (2016), Anderson localization and ergodicity on random regular graphs, *Phys. Rev. B*, **94**, 220203 (DOI: 10.1103/PhysRevB.94.220203)

[100] I. Garcia-Mata et. al. (2017), Scaling theory of the Anderson transition in random graphs: ergodicity and universality, *Phys. Rev. Lett.*, **118**, 166801 (DOI: 10.1103/PhysRevLett.118.166801)

[101] R. Mondaini and M. Rigol (2015), Many-body localization and thermalization in disordered Hubbard chains, *Phys. Rev. A*, **92**, 041601 (DOI: 10.1103/PhysRevA.92.041601)

[102] L.C. Bertrand and A.M. García-García (2016), Anomalous thouless energy and critical statistics on the metallic side of the many-body localization transition, *Phys. Rev. B*, **94**, 144201 (DOI: 10.1103/PhysRevB.94.144201)

[103] F. Chung and L. Lu (2003), The average distance in a random graph with given expected degrees, *Internet Math.*, **1**, 91-113 (DOI: /10.1080/15427951.2004.10129081)

[104] D.P. Croft et. al. (2005), Assortative interactions and social networks in fish, *Oecologia*, **143**, 211-219 (DOI: 10.1007/s00442-004-1796-8)

[105] S. Boccaletti et. al. (2006), Complex networks: Structure and dynamics, *Physics Reports*, **424**, 175–308 (DOI: 10.1016/j.physrep.2005.10.009)

[106] R. Xulvi-Brunet and I.M. Sokolov (2004), Reshuffling scale-free networks: From random to assortative, *Phys. Rev. E*, **70**, 066102 (DOI: 10.1103/PhysRevE.70.066102)

[107] S. Jalan and A. Yadav (2015), Assortative and disassortative mixing investigated using the spectra of graphs, *Phys. Rev. E,* **91**, 012813 (DOI:10.1103/PhysRevE.91.012813)

[108] S. Jalan and J.N. Bandyopadhyay (2009), Randomness of random networks: A random matrix analysis, *Europhys. Lett.*, **87**, 48010 (DOI: 10.1209/0295-5075/87/48010)

[109] Z. Burda, J. Duda, J.M. Luck and B. Waclaw (2009), Localization of the maximal entropy random walk, *Phys. Rev. Lett.*, **102**, 160602 (DOI: 10.1103/PhysRevLett.102.160602)

[110] M. Mohseni et. al. (2013), A diversity of localized timescales in network activity, *J. Chem. Phys.*, **138**, 204309 (DOI: 10.1063/1.4807084)

[111] T. Scholak et. al. (2011), Efficient and coherent excitation transfer across disordered molecular networks, *Phys. Rev. E*, **83**, 021912 (DOI: 10.1103/PhysRevE.83.021912)

[112] F. Battiston et.al (2020), Networks beyond pairwise interactions:structure and dynamics, *Physics Reports* **874**, 1-92 (DOI: 10.1016/j.physrep.2020.05.004)

[113] Ghoshal G. et.al (2009), Random hypergraphs and their applications, *Phys. Rev. E* **79**, 066118 (DOI:10.1103/PhysRevE.79.066118)

[114] G. F. de Arruda, M. Tizzani and Y. Moreno (2021), Phase transitions and stability of dynamical processes on hypergraphs, *Commun. Phys.* **4**, 1-9 (DOI:10.1038/s42005-021-00525-3)

[115] T.O. Courtney and G. Bianconi (2016), Generalized network structures: The configuration model and the canonical ensemble of simplicial complexes, *Phys. Rev. E* **93**, 062311 (DOI: 10.1103/PhysRevE.93.062311)

[116] S. Krishnagopal and G. Bianconi (2021), Spectral detection of simplicial communities via Hodge Laplacians, *Phys. Rev. E* **104**, 064303 (DOI: 10.1103/PhysRevE.104.064303)

[117] J.J Torres and G. Bianconi (2020), Simplicial complexes: higher-order spectral dimension and dynamics, *J. Phys. Complexity* **1**, 015002 (DOI:10.1088/2632-072X/ab82f5)

[118] S. Klamt and U. Haus and F. Theis (2009), Hypergraphs and cellular networks, *PLoS computational biology* **5**, e1000385 (DOI:10.1371/journal.pcbi.1000385)

[119] S. Feng et.al (2021), Hypergraph models of biological networks to identify genes critical to pathogenic viral response, *BMC bioinformatics* **22**, 1-21 (DOI:10.1186/s12859-021-04197-2)

[120] V. Zlatić, G. Ghoshal and G. Caldarelli (2009), Hypergraph topological quantities for tagged social networks, *Phys. Rev. E* **80**, 036118 (DOI:0.1103/PhysRevE.80.036118)

[121] J. Zhu (2018), Social influence maximization in hypergraph in social networks, *IEEE Transactions on Network Science and Engineering* **6**, 801-811 (DOI:10.1109/TNSE.2018.2873759)

[122] U. Alvarez-Rodriguez et. al. (2021), Evolutionary dynamics of higher-order interactions in social networks, *J. Phys. Complexity* **5**, 586–595 (DOI:10.1038/s41562-020-01024-1)

[123] G. Burgio et.al (2020), Evolution of cooperation in the presence of higher-order interactions: from networks to hypergraphs, *Entropy* **22**, 744 (DOI:10.3390/e22070744)

[124] B. Mohar, Y.Alavi, G. Chartrand and O. Oellermann (1991), The Laplacian spectrum of graphs, *Graph theory, combinatorics, and applications* **2**, 871-898 (DOI:10.1016/j.camwa.2004.05.005)

[125] M. Barahona and L.M. Pecora (2002), Synchronization in small-world systems, *Phys. Rev. Lett.* **89**, 054101 (DOI:10.1103/PhysRevLett.89.054101)

[126] L.M. Pecora and T.L. Carroll (1998), Master stability functions for synchronized coupled systems, *Phys. Rev. Lett.* **80**, 054101 (DOI:10.1103/PhysRevLett.80.2109)

[127] A. Arenas et.al (2008), The Laplacian spectrum of graphs, *Physics Reports* **469**, 93-153 (DOI:10.1016/j.physrep.2008.09.002)

[128] I. Leyva, I. Sendina-Nadal, J.A. Almendral and M. Sanjuán (1998), Sparse repulsive coupling enhances synchronization in complex networks, *Phys. Rev. E* **74**, 056112 (DOI:10.1103/PhysRevE.74.056112)

[129] A. Arenas, A. Diaz-Guilera and C.J. Pérez-Vicente (2006), Synchronization reveals topological scales in complex networks, *Phys. Rev. Lett.* **96**, 114102 (DOI:10.1103/PhysRevLett.96.114102)

[130] S. Hata, H. Nakao and A.S. Mikhailov (2010), Dispersal-induced destabilization of metapopulations and oscillatory turing patterns in ecological networks , *Sci. Rep.* **4**, 1-9 (DOI:10.1038/srep03585)

[131] H. Nakao and A.S. Mikhailov (2010), Turing patterns in network-organized activator-inhibitor systems, *Nat. Phys.* **6**, 544-550 (DOI:10.1038/srep03585)

[132] T. Carletti et.al (2020), Random walks on hypergraph, *Phys. Rev. E* **101**, 022308 (DOI:10.1103/PhysRevE.101.022308)

[133] G. F. de Arruda, G. Petri and Y. Moreno (2020), Phase transitions and stability of dynamical processes on hypergraphs, *Phys. Rev. Res.* **2**, 023032 (DOI:10.1103/PhysRevResearch.2.023032)

[134] B. Jhun , M. Jo and B. Kahng (2019), Simplicial SIS model in scale-free uniform hypergraph, *Journal of Statistical Mechanics: Theory and Experiment* **2019**, 123207 (DOI:10.1088/1742-5468/ab5367)

[135] T. Carletti et.al(2021), Random walks and community detection in hypergraphs, *J. Phys. Complexity* **2**, 015011 (DOI:10.1088/2632-072X/abe27e)

[136] A. Krawiecki (2014), Chaotic synchronization on complex hypergraphs, *Chaos, Solitons and Fractals* **65**, 44–50 (DOI:10.1016/j.chaos.2014.04.009)

[137] R. Mulas, C. Kuehn and J. Jost (2020), Chaotic synchronization on complex hypergraphs, *Phys. Rev. E* **101**, 062313 (DOI:10.1103/PhysRevE.101.062313)

[138] T. Carletti, D. Fanelli and S. Nicoletti (2020), Dynamical systems on hypergraphs, *Journal of Phys. Complexity* **1**, 035006 (DOI:10.1088/2632-072X/aba8e1)

[139] D. Bollé, R. Heylen and N. S. Skantzos (2006), Thermodynamics of spin systems on small-world hypergraphs, *Phys. Rev. E* **74**, 056111 (DOI: 10.1103/PhysRevE.74.056111)

[140] M.E.J Newman and D.J Watts (1999), Scaling and percolation in the small-world network model, *Phys. Rev. E* **60**, 7332 (DOI: 10.1103/PhysRevE.60.7332)

[141] C Zhan, G Chen and LF Yeung (2010), On the distributions of Laplacian eigenvalues versus node degrees in complex networks, *Physica A* (**389**), 1779-1788 (DOI: 10.1016/j.physa.2009.12.005)

[142] P.N. McGraw and M. Menzinger (2008), Laplacian spectra as a diagnostic tool for network structure and dynamics, *Phys. Rev. E* **77**, 031102 (DOI: 10.1103/PhysRevE.77.031102)

[143] S. De Nigris and X. Leoncini (2015), Crafting networks to achieve, or not achieve, chaotic states, *Phys. Rev. E*, **91**, 042809 (DOI: 10.1103/PhysRevE.91.042809)